
This item was submitted to [Loughborough's Research Repository](#) by the author.
Items in Figshare are protected by copyright, with all rights reserved, unless otherwise indicated.

Measurement of 3D forces at the foot-shoe interface during locomotor activity

PLEASE CITE THE PUBLISHED VERSION

PUBLISHER

© M.J. Forward

LICENCE

CC BY-NC-ND 4.0

REPOSITORY RECORD

Forward, M.J.. 2019. "Measurement of 3D Forces at the Foot-shoe Interface During Locomotor Activity".
figshare. <https://hdl.handle.net/2134/13502>.

This item was submitted to Loughborough University as a PhD thesis by the author and is made available in the Institutional Repository (<https://dspace.lboro.ac.uk/>) under the following Creative Commons Licence conditions.



For the full text of this licence, please go to:
<http://creativecommons.org/licenses/by-nc-nd/2.5/>

Pilkington Library

Author/Filing Title FORWARD, M.J.

Accession/Copy No.

040152562

Vol. No.

Class Mark

ARCHIVES
COPY

FOR REFERENCE ONLY

0401525627



Measurement of 3D forces at the foot-shoe interface during locomotor activity.

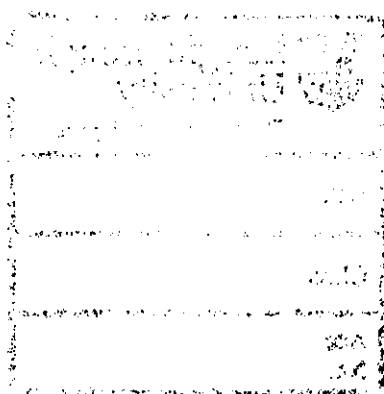
A Doctoral Thesis

by


M. J. Forward

Submitted in partial fulfilment of the requirements for the award of
Doctor of Philosophy of the Loughborough University of Technology

May 1997



© by M J Forward 1997

 Loughborough University Public Library	
Date	Jun 98
Class	
Acc No.	040152562

Dedicated

To the memory of my bother Stephen

A mechanic and practical perfectionist who had no time for academics and was happiest
when at the freedom of the open seas.

On advising on trouble shooting a poorly starting car he once said, "If there is fuel in the
cylinder and an ingnition spark, it will probably start".

A philosophy that may be applied elsewhere I think.

He is sorely missed.

Acknowledgements

This work could not have been carried out without the help and support I have received from a great number of people:

Firstly I am indebted to my supervisor Prof. Roger Goodall for enormous encouragement and help and it is to him and Dr David Pratt (Orthotics & Disability Research Centre, Derbyshire Royal Infirmary) who proposed and sought the initial funding for this research that I owe the opportunity of carrying out this work.

The funding for this work came from the British Diabetic Association, Trent Regional Health Authority (LORS) and Remedi Rehabilitation & Medical Research Trust.

To the Mark Snape and his team for PCB board layout design and production, to the mechanical workshop staff of the Electronic & Electrical Engineering Dept, LUT

To Brain Ward and other workshop staff at the Orthotics & Disability Research Centre, Derbyshire Royal Infirmary.

To the great support and encouragement given me by my friends and colleagues, the team at the Orthotics and Locomotor Assessment Unit, Robert Jones & Agnes Hunt Orthopaedic Hospital, Oswestry, Shropshire where I am currently working, and particularly to John Tait for discussions on electronics and coil theory.

To my other friends and family for encouragement.

However my greatest thanks must go to Kim without whom I would never have completed this thesis. She gave me reason, confidence, encouragement, support, power of expression in the English language alongside offering ferocious proof reading!

ABSTRACT

The origin of this project was the problem of foot ulceration in the diabetic patient. Whilst the principal cause of the susceptibility to foot ulceration in patients with this pathology, and others such as leprosy, is abnormal physiology, there is no doubt the mechanical forces that are applied to the foot surface are a major factor.

Currently several devices are available to measure the perpendicular forces at the foot-shoe interface (i.e. the “pressure” distribution). However the full assessment of tri-axial forces at this interface has largely eluded quantification despite the fact that it has been demonstrated that shear forces may be of equal significance to those of direct pressure.

The purpose of this study was to develop a transducer for the assessment of the three dimensional forces experienced, over a very localised area, at the foot-shoe interface during normal functional locomotor activity.

The application of such a device in the clinical setting will provide valuable information for the medical and orthotic professions and thereby assist them in the treatment of many patients who are at risk of foot ulceration.

The principle for a transducer to be embedded in an insole and utilising electromagnetic induction between air-cored coils was proposed. Coil winding techniques were developed to enable manufacture of coils within constrained sizes. Examination of the inductive coupling possible between the coils and its variation with displacement in space was carried out using a purpose built testing rig. Transducer electronics were designed and manufactured and a data logging system implemented. Various approaches to the derivation of 3D interpretation from the system were implemented in software. An examination of the accuracy of the approach was made. A prototype design and manufacturing method was suggested utilising a specific grade of silicone rubber.

The results indicated that the design proposed could be implemented effectively in a size suited to in-shoe application.

The design offers a relatively low cost method which could be adapted for use in many applications requiring three dimensional displacement or force measurements.

CONTENTS

1. INTRODUCTION.....	1
1.1 MEDICAL MOTIVATION	1
1.2 CONCEPTS OF FORCE ASSESSMENT AT THE FOOT-SHOE INTERFACE.....	2
1.3 OVERVIEW OF RESEARCH	4
1.4 SUMMARY OF ACHIEVMENTS OF THE RESEARCH	5
2. LITERATURE REVIEW OF MEASUREMENT SYSTEMS	6
2.1 HISTORICAL CONTEXT	6
2.2 FLOOR MOUNTED ARRAYS.....	7
2.3 IN-SHOE TRANSDUCERS	10
2.4 OBJECTIVES OF FORCE MEASUREMENTS AT THE FOOT SHOE INTERFACE	16
3. FORMULATION OF THE DESIGN CONCEPT	20
3.1 SPECIFICATION OF DESIGN REQUIREMENTS	20
3.1.1 Initial considerations	20
3.1.2 Transducer size.....	20
3.1.3 Environment	21
3.1.4 Desired range of force transducer.....	21
3.1.5 Summary of design specification.....	21
3.2 REVIEW OF TRANSDUCER TECHNOLOGIES FOR IN-SHOE FORCE MEASUREMENTS....	22
3.3 CHOICE OF TRANSDUCER TECHNOLOGY	23
3.4 MEASUREMENT USING ELECTROMAGNETIC INDUCTION	25
3.5 INVESTIGATION OF THE PRACTICALITY OF USING THE INDUCTIVE TECHNIQUE	26
3.5.1 Size of coils.....	27
3.5.2 Manufacturing of coils	28
3.5.3 Aspects of coil winding	29
3.5.4 Current & frequency limitations	32
3.5.5 Investigation of the shape of the electromagnetic field produced.....	41
3.6 SUMMARY.....	65
4. MATHEMATICAL BASIS FOR 3D MEASUREMENT	66
4.1 PRINCIPLE	66
4.2 SOLUTIONS	67
4.2.1 Planar model.....	67

4.2.2 Look-up table method	71
4.2.3 Hybrid method	73
4.3 CHAPTER SUMMARY	76
5. PROTOTYPE IMPLEMENTATION.....	77
5.1 DEVELOPMENT STRATEGY.....	77
5.2 COIL SET ASSEMBLY.....	77
5.3 ELECTRONIC HARDWARE.....	79
5.3.1 Signal generation stage.....	79
5.3.2 Demodulation.....	82
5.3.3 Data logging hardware.....	86
5.4 TRANSDUCER ORIGIN AND RANGE OF DISPLACEMENTS	86
5.5 GENERAL ASSESSMENT.....	86
5.6 SYSTEMATIC VARIATIONS	95
5.7 STATISTICAL ASSESSMENT.....	95
5.8 ASSESSMENT OF CALIBRATION AND PROCESSING REQUIREMENTS	97
5.9 CHAPTER SUMMARY	98
6. TOWARDS A FORCE TRANSDUCER.....	103
6.1 MATERIAL FOR THE MECHANICAL ELEMENT OF TRANSDUCER	103
6.1.1 General considerations of material selection.....	103
6.1.2 Mechanical properties required.....	104
6.1.3 Material selection.....	107
6.2 FORCE TRANSDUCER ASSEMBLY	107
6.3 FORCE CALIBRATION	108
6.3.1 The problem.....	108
6.3.2 Design objectives	114
6.3.3 Design solution.....	115
7. CONCLUSIONS AND SUGGESTIONS FOR FURTHER WORK	120
7.1 SUMMARY OF ACHIEVEMENTS	121
7.2 SUGGESTIONS FOR FURTHER WORK	123

List of Figures

	Page No
Figure 3-1 Electromagnetic induction.....	26
Figure 3-2 Sectional view of a single coil pair embedded in insole material.....	27
Figure 3-3 Maximum size of the three receiving coils within transducer diameter.....	28
Figure 3-4 Sectional view of coil former	28
Figure 3-5 Cross section of coil.....	30
Figure 3-6 Single layer of winding	30
Figure 3-7 Temperature rise with current at two different frequencies	39
Figure 3-8 In-shoe and bench coil heating tests	40
Figure 3-9 Temperature rise of coils with current	41
Figure 3-10 Current rise with ampere.turns.....	41
Figure 3-11 Basis of calibration rig.....	43
Figure 3-12 Calibration rig	45
Figure 3-13 Current driver circuit.....	46
Figure 3-14 Induced voltage as a function of radial displacement.....	47
Figure 3-15 Direction of flux through receiving coil.....	47
Figure 3-16 Induced voltage v radial displacement (phase inversion represented).....	48
Figure 3-17 Induced voltage as a function of axial separation	48
Figure 3-18 Induced voltage - displacement surface.....	49
Figure 3-19 Range of coil pair relative positions	50
Figure 3-20 Induced voltage as a function of radial displacement.....	51
Figure 3-21 2nd order fit	55
Figure 3-22 4th order fit.....	56
Figure 3-23 6th order fit.....	57
Figure 3-24 SinC fit	58
Figure 3-25 2nd order fit	60
Figure 3-26 3rd order fit	61
Figure 3-27 4th order fit.....	62
Figure 3-28 Inverse function fit.....	63
Figure 3-29 Variation of radius of point of phase inversion.....	64
Figure 3-30 Radial displacement curves at 1,2 and 3 mm axial separation	64
Figure 3-31 Radial displacement curves and scaled fits	65
Figure 4-1 Linear regression over restricted range of displacement	69
Figure 4-2 Relationships of radii to displacement	74
Figure 5-1 Method of attaching lead wires	78
Figure 5-2 Electronic processing scheme.....	80
Figure 5-3 Signal generation stage	81

Figure 5-4 Power amplifier circuit.....	83
Figure 5-5 Phase shift stage.....	84
Figure 5-6 Demodulation (Phase sensitive detection)	85
Figure 5-7 Location of reference origin with respect to the receiving coils	87
Figure 5-8 Planar model.....	88
Figure 5-9 Hybrid model.....	89
Figure 5-10 Look-up table method.....	90
Figure 5-11 R.M.S. errors	91
Figure 5-12 Distribution of errors in x.....	99
Figure 5-13 Distribution of errors in y.....	100
Figure 5-14 Distribution of errors in z.....	101
Figure 5-15 Distribution of errors for 300 random points - Look-up table method.....	102
Figure 6-1 Rubber block under compression.....	105
Figure 6-2 Rubber block under shear	105
Figure 6-3 Mounting of transducer for calibration	109
Figure 6-4 Moulding plates	110
Figure 6-5 Lid with raised sections	111
Figure 6-6 Transducer assembly mould.....	112
Figure 6-7 Removal of assembled transducer from the mould.....	113
Figure 6-8 Force calibration scheme.....	117
Figure 6-9 Force application guidance.....	118
Figure 6-10 Force application and measurement system.....	119

List of Tables

	Page No
Table 3-1 Coil data.....	37
Table 3-2 Results of curve fitting for radial displacement curves.....	53
Table 3-3 Results of curve fitting to the axial displacement characteristics.....	59
Table 5-1 Summary of % errors - systematic tests.....	92
Table 5-2 Accuracy of models.....	93
Table 5-3 Cross talk or models.....	94
Table 5-4 Systematic errors.....	96
Table 6-1 Mechanical properties of rubbers.....	107

Appendices

Appendix 1 Inductance Formulae.....	130
Appendix 2 Displacement Calibration Rig Design.....	132
Appendix 3 Force Calibration Rig Design.....	137
Appendix 4 Publication of research.....	140

1. INTRODUCTION

1.1 MEDICAL MOTIVATION

Skin necrosis is basically due to interference with the skin's blood supply. The blood supply to the skin is from the subcutaneous tissue and any continual force applied to the skin which is sufficient to obstruct the circulation for more than a few hours will lead to tissue necrosis and an ulcer or sore. Other factors are the adequacy of the general circulation, skin temperature, air movement, humidity and the presence of infection.

Pain is a general protection mechanism. However it may not be present in some conditions such as diabetes where peripheral neuropathy is a common side effect of the disease. Thus neuropathy is a risk factor in skin ulceration.

The nature of the forces applied is also a factor. Direct force or pressure can be seen to occlude blood supply (evidenced by the changing colour of the skin following squeezing and releasing a fingertip of a healthy subject) whilst the influence of shear force is perhaps not so obvious. Experiments by Bennet et al. (1979) demonstrated that shear force has a significant influence on blood flow occlusion and Davis (1992) pointed out that it is also important to consider the effects of localised variation of pressure and shear force on skin in terms of the cyclic mechanical stresses and strains to which it is subjected.

The large number of attempts at assessing the mechanical forces on the foot during walking are indicative of the importance placed on these forces by workers faced with the problem of foot ulceration. Whilst not the cause of susceptibility to foot ulceration, mechanical forces can be modified by appropriate footwear and patient vigilance.

The consequence of foot ulceration in diabetic patients is often gangrene and subsequent amputation. To some extent the side effects of the disease are inevitable, however, protective measures can lead to the inevitable being delayed and a near normal quality of life being maintained for much longer.

The need for a tool for mapping the three dimensional forces applied to the foot surface during walking is clear both in a research and in a prescriptive clinical setting.

1.2 CONCEPTS OF FORCE ASSESSMENT AT THE FOOT-SHOE INTERFACE

Perhaps in many ways the study of forces applied to the human foot is an enigma!

Consider:-

The foot is a complex dynamic structure consisting of bone, muscle, connective tissue, and skin. Whilst these “materials” have differing mechanical properties that change with age and pathology we tend, in day-to-day life, to view the foot as an amorphous “blob”, albeit a relatively soft one. Such a simple model should not be retained when viewing results of foot pressure or force studies.

In the clinical setting we are usually looking at problems of pain and/or recurring soft tissue injury when dealing with the foot. Such conditions often arise due abnormal physiology which ultimately leads to foot deformity and abnormal force distribution.

The soft tissues of the body are invariably visco-elastic, having properties of both fluids and solids which are exhibited according to the rate and time of application of mechanical forces or pressures.

Pressure is a concept associated with a gas or a fluid. Pressure always acts perpendicular to any surface to which it is applied. It is easy to visualise that such surfaces might be solid, flexible or simply interfaces between fluids. Forces are vector quantities having magnitude, direction and points of application, and are generally thought of in the context of solid objects.

Rubber and rubber-like polymers apply fluid-like pressures to objects forced into contact with them; that is they act rather like fluids in compression. Many modern shoe insoles are manufactured from rubber or rubber like materials. These invariably have a visco-elastic component and are designed to break the impact on the foot during walking and thus lead to additional comfort.

In attempting to understand and solve foot problems there are, perhaps, two different “viewpoints” chosen. The orthopaedic surgeon may be wishing to understand the effect of foot deformity on the dynamic forces and their distribution over the foot surface during walking. An overview of these forces in the most general condition of barefoot walking is

desired since this picture will be independent of footwear and most dependent, and repeatably so, upon foot structure and dynamic function. The orthotist, on the other hand, seeking to prescribe footwear to alleviate the risk of foot ulceration in diabetic patients needs to be able to measure forces that are applied to the foot surface under variable in-shoe conditions. Ideally the orthotist should also be able to assess the effect of modifying the footwear and using this feedback to obtain an optimum pressure or force distribution for that patient.

To obtain a truly representative picture of pressure or force distribution over the foot surface under any circumstances would require infinitely small transducers. They would need to be extremely thin to enable their arrangement over contoured surfaces and have mechanical properties such that they did not modify the surface over which they lay.

Even if such transducers could be produced questions still may be raised as to the meaning of the results. Soft tissue movement over the bony structures of the foot leads to questions of interpretation and positioning. If the transducers are not adhered to the surface of the foot then it is not possible to determine whether the skin has slipped over the transducers during walking. It is apparent then that the question of what is meant by the results of pressure or force measurement over the foot surface, or indeed over any part of the human body, during everyday activity cannot be easily answered for any given system.

Perhaps it is the difficulty of force definition, together with the widespread use of soft rubber-like polymer in-soles (viewed as exerting hydro-static like compression), that has resulted in the dominance of “pressure” measurement systems in the literature and clinical practice of foot problem assessment. A more likely explanation is the added difficulty of measuring shear or multi-axial forces with high spatial resolution over an area the size and complexity of the typical foot surface. The options for available instrumentation for the assessment of these quantities in this environment have always been limited. It is not surprising then that all too often the question of what is actually meant by “pressure” or “vertical force” or even “shear” is not even addressed.

The results of this research offer an adaptable technique that may be applied to the problem of studying tri-axial forces acting over discrete areas of the body. Its use, alongside

“pressure” measurement techniques, may begin to allow development of a more thorough picture of the static and dynamic forces applied to the body during day to day activity.

In the final analysis, however, we must be clear that we are attempting to measure, in the in-shoe case, the interface forces between visco-elastic “materials” behind which are the “solid” dynamic structures of the foot and shoe.

1.3 OVERVIEW OF RESEARCH

Attempts to quantify the forces applied to the foot during normal activity have been made over many years. A literature review of such methods demonstrates the use of several different measurement techniques and emphasises the problems involved (Section 2). None of the principles behind the techniques previously used appeared to offer a route to in-shoe tri-axial force measurement (Section 3.2).

The motivation for this work was the problem of diabetic foot ulceration. Many diabetic patients who are at risk of foot ulceration are issued with prescription insoles whose upper surface is a compliant rubber like material. Thus a transducer that could be manufactured using a similar material to that used in insoles could be incorporated unobtrusively in an insole. If the mechanical properties of this material were known and repeatable then measurement of the deflection under stress would enable determination of the forces applied. The measurement of the deflection of this material under stress was then the remaining problem. This is, of course, the basis of many force transducers, that of the measurement of the deflection of a central mechanical element under stress. Indeed this approach is not new in in-shoe measurement techniques except in-so-much as here it was proposed to measure three dimensional deflections to enable determination of three dimensional forces.

The principle of electromagnetic induction was proposed as the basis on which to design a three-dimensional force transducer. In progressing towards this an overall design specification was first derived (Section 3.1). This was followed by an investigation of the practicality of utilising an electromagnetic technique (Section 3.4).

The design specification led to physical constraints on the size of any coils used in the inductive technique proposed. The problem of manufacturing of coils of this size was

successfully addressed and enabled investigation of the electromagnetic feasibility of the principal proposed. It was first established that suitable sized coils could be excited with an alternating current such that a significant voltage was induced in a similar sized receiving coil. Following this an investigation of the voltage - displacement characteristics of a coil pair was carried out to enable completion of the investigation of the feasibility of the approach. This was enabled by the design and manufacture of a three dimensional displacement calibration rig (Section 3.5.5).

Having satisfied the basic feasibility question, a methodology for three dimensional displacement measurements was developed (Section 4.1), mathematical solutions proposed (Section 4.2), implemented (Sections 5.1-5.3) and evaluated (Section 5.4-5.8).

The question of transducer core mechanical element was next addressed and a suitable prototype material was selected (Section 6.1). A prototype force transducer assembly procedure was devised and implemented (Section 6.2). A force calibration system was designed and built but demonstrated practical problems. A revised calibration rig design was proposed (Section 6.3).

1.4 SUMMARY OF ACHIEVMENTS OF THE RESEARCH

This thesis describes research which:

- explores the problems of in-shoe force measurement,
- proposes the basis for a tri-axial non-intrusive force measurement system,
- offers mathematical algorithms for utilising the approach,
- provides practical verification of the method,
- describes a viable approach to manufacture of a device,
- examines the problems of calibration, including recommendations on design of a definitive calibration and dynamic testing rig.

The development described could be applied to many other engineering applications requiring three dimensional displacement or force measurement.

2. LITERATURE REVIEW OF MEASUREMENT SYSTEMS

2.1 HISTORICAL CONTEXT

It is perhaps not surprising that man's thoughts on the forces inflicted on his feet go back many generations. Whilst our view of forces and pressure, even cause and effect, has evolved somewhat over history, it is interesting to note that at times, man has faced the same problems and intuitively understood the same phenomena. Galen (131-210 AD) perhaps appreciated the effect of shear forces on the sole of the foot when he wrote "the skin of the foot is closely adherent to all the parts lying beneath it, to prevent it from being easily folded over in any direction.". It is difficult to see what, other than shear, would cause the skin of the foot to "fold". Clearly he also appreciated the hazardous effects of neuropathy. "The foot was not meant to be a common instrument of touch for the whole body but an instrument of their locomotion only, and it therefore has only as much sensation as it needs to avoid being easily injured" (translation by May, 1968). Petrus Camper (1722-1789) postulated that shear and pressure were important mechanical factors in foot pathology. He claimed that there were parts of the foot that "are not calculated to endure much friction" (cited by Davis, 1992).

What was probably the first dynamic multi-point recording of human gait was carried out by Marey (1873) who placed two manometric cells at the bottom of a sandal. This was, perhaps, the first attempt to use technology to map the forces acting over the surface of the human foot during walking. One hundred or so years later, during which has been seen the discovery and evolution of many forms of technology, the search continues for the ultimate force transducer for the mapping of these forces.

There have been essentially two approaches to the problem of mapping these forces, the first using small transducers mounted on the foot or in the shoe between the foot and shoe (either discrete transducers or arrays of transducers), and the second using a regular array of transducers mounted in the floor.

The latter approach is useful only in the assessment of barefoot walking since it provides information on the dynamic foot contact with the flat floor. It tends to have the disadvantage of generally being only possible, in practice, to instrument a small portion of a floor, and thus it must be arranged for the subject to strike this whilst walking "normally".

This can be difficult for subject and operator! Invariably such systems measure only the “pressure” distribution (as opposed to the force distribution) under the barefoot subject.

The stability of shoe, insole or foot mounted transducers is much harder to ensure. The aim is to have the transducers in contact with the foot surface at all times and thus measure the pressure or forces in the local area of the transducer and at the position of contact with the skin of the foot. That is, there is hoped to be no movement of transducer with respect to the skin of the foot. It is perhaps worth noting that this may not be the same situation as that in which the transducer remains stationary with respect to the foot structure. There is generally great difficulty in measuring absolute force rather than dynamic force changes with in-shoe measurements. The recording would have to begin prior to the shoe being placed on the foot and remain until the shoe was removed at the end of the trial. This would thus require extended recording periods over which to maintain manageable drift. This would rule out many capacitive and piezoelectric systems. Also there is often difficulty in differentiating between signal changes due to forces applied to the upper surface (and thus causing stresses within the transducer mechanical element) of a transducer and the stresses induced in a transducer because its base is deformed when the surface onto which the transducer is attached/embedded bends as the subject walks.

2.2 FLOOR MOUNTED ARRAYS

One of the first systems using a floor mounted array of “transducers” was developed by Morton D J (1930) who used a simple technique utilising inked paper. The “Kinetograph” simply comprised a rubber mat with a flat top surface and a rigid inked lower surface. Local pressure of the foot applied to the top surface flattens the triangular ridges against the paper under it and leaves an ink print consisting of parallel lines whose width is proportional to pressure (cited by Lord, 1981).

Elftman H (1934) developed this into a cinematic technique using contoured mats resting on glass plates. The pressure on the upper surface of the rubber forced varying degrees of complete contact of the dimpled under surface with the glass plate. The foot ground sequence was captured on film for analysis. Elftman’s Barograph provided, for the first time, an indication of *instantaneous* foot pressure.

Chodera patented the “Pedobarograph” in 1960 (cited by Lord 1981). This consisted of a flat optically clear glass plate illuminated along two opposing edges. Light introduced into the plate is conducted by a series of internal reflections at the plate/air interface. A thin sheet of deformable material is placed on the top surface of the glass plate. The subject stands on this sheet. Wherever the sheet is pressed into contact with the plate, the condition for internal reflection is destroyed, and the light escapes the plate to illuminate the underside of the sheet. Plantar pressure on the top surface of the sheet will cause a proportional flattening of the underside and thus, viewed from below, a black and white intensity modulated footprint or “pedobarogram” is produced. A video camera can be used to display and record the impression of barefoot pressure. Betts et al. (1978,1980) and Franks et al. (1983) describe enhancements of this system using image processing techniques to provide static and dynamic foot pressure *measurement* systems. Applications to pathologies, such as the ulceration of diabetic feet (Duckworth et al., 1985), from this time on are common. Optical techniques provide very high levels of resolution and with careful selection of the transducer sheet material it is possible to obtain an almost linear relationship between applied pressure and light intensity. Several problems may occur with these materials however. These include adhesion to the glass plate, saturation within the range of interest, material deformation and wear, poor dynamic response time, image intensity and uniformity dependent on surface granularity, the dependence of sensitivity on temperature and static measurement problems due to creep of the surface material (Franks and Betts 1988). Nevertheless, use of the pedobarograph for clinical applications continues to the present day.

Dhanendran et al. (1978) constructed a floor mounted foot pressure system containing 128 strain gauged load cells (“proving rings”) , resulting in a load sensitive surface of 12.5 x 25cm. Each load cell had a surface area 15mm x 15mm and a (vertical) load range of 500 N. Despite the use of strain gauged transducers the system was designed only to measure vertical loads. This provided an accurate, system with a high frequency response, but with rather low spatial resolution.

An alternative to the pedobarograph for high resolution imaging was developed by Rhodes et al. (1988). This consisted of a 500 by 380 x 2.4mm photo-elastic sheet and a polariser bonded to a walkway constructed from 19mm thick transparent acrylic. A thin sheet of

silver sprayed polycarbonate above the photo-elastic sheet acted as a reflector. A photo-elastic plastic is a material that exhibits variable rotation of the plane of polarised light in response to the difference in the strains in (orthogonal) x and y directions (perpendicular axes within its own plane) within the plastic. The load was transmitted to the photo-elastic sheet through a 3mm pitch corrugated plastic indenter to provide a maximum difference in the two orthogonal directions of strain to which the photo-elastic effect is proportional. With increasing load the light transmitted to the photo-elastic sheet is rotated about the axis of propagation and can pass through the polariser to form a parallel line image of the indenter with point intensity proportional to applied force. The image is captured by a camera adjacent to the walkway. To filter out surface irregularities and “simplify interpretation”, pixels were assigned the average intensity value within each 3mm square area. In fact the resolution of this system does not rival that of the pedobarograph (assuming it has a carefully chosen plate covering material). The system also needs to be evaluated in terms of the static, dynamic and temperature dependent properties of the materials of which it is constructed.

Assente et al. (1985) constructed a 580 x 380mm platform using a piezoelectric PVDF (polyvinylidene fluoride) film. An array of transducers was formed with this material as its core. Charge amplifiers sampled the output from each transducer at 100Hz. No details of the performance of the system are given. In all probability this system would not be suitable for static measurements due to the piezoelectric basis of the system. Indeed Cobb and Claremont (1995) give a typical low frequency limit of 0.1Hz on systems using piezoelectric materials.

The Musgrave Park System (Musgrave Systems Ltd, Llangollen, Denbighshire, UK) is a widely used, commercially available, floor mounted foot pressure measurement system. This uses force sensing resistors comprising two polymer sheets one with deposited pectinate electrodes and the other coated with the semi-conducting material molybdenum disulphide. Contact area between the electrodes on the semi-conducting material increases with applied force, resulting in a large change in resistance. The devices are between 0.25mm and 0.75mm thick. The characteristic is logarithmic with precise response dependent on substrate type, conductor geometry and semi-conducting material used. The Musgrave system incorporates a matrix of 2048 3mm x 3mm force sensing resistors, with a

measurement range of 0-4MPa per sensor. The devices can be used within the range 11kPa to 110kPa, giving a typical variation in resistance from 1M Ω to 2k Ω . Above 110kPa a sensor's response to a given load can vary by +/- 2% per loading cycle. Above 1 Mpa, the response of different sensors to the same load can vary by +/- 15%. The temperature coefficient is load dependent, typically around 0.1% per kg. °C⁻¹ (Cobb and Claremont, 1995).

It is interesting to note that in all the approaches to the problem of foot pressure distribution measurement there have been few if any reported attempts to develop floor mounted instrumentation to measure simultaneously the pressure and shear at discrete locations over the foot surface during gait. This is despite the development of the 'force platform' in 1938 (Helenbrandt 1938) which provides tri-axial force measurements, i.e. measures gross shear and vertical forces as the subjects walks over it. This apparent neglect of shear does not occur in the reports of in-shoe transducer development.

2.3 IN-SHOE TRANSDUCERS

Following Marey's (1873) example of discrete in-shoe transducers, Bauman and Brand (1963) utilised a thin transducer, then recently developed, for studying the pressures on the sole of the foot both for walking barefoot and whilst wearing shoes. The device was essentially a capacitor which responded to increased pressure with increasing capacitance. These transducers were 1mm thick and had a pressure sensitive area of 1cm² and had a range of 490kPa. No indication of the dynamic performance is given. The transducer was applied by Bauman et al. (1963) in a study of plantar pressures in trophic ulceration.

Whilst measuring only pressure with their transducer Bauman et al. (1963) recognised they were only obtaining a limited picture - "For a completely objective evaluation actual measurements of intermittent pressure and shear during walking are needed." They felt that "To appreciate the relationship between pressure and plantar ulceration it is necessary to first analyse the forces acting on the sole of the foot. to divide any such force into two components - one parallel and the other perpendicular to the skin."

Applying electromechanical techniques, Rabischong et al. (1967) placed four electrical parallelepiped strain gauge transducers under a selected area of the sole, each of which

measured the vertical and horizontal components of force. Load and shear distributions were recorded on a 16 channel polygraph as the subject walked on a treadmill.

In an attempt to address the question of the effect of shear on tissue, Bennett et al. (1979) studied the relationship between tri-axial force application and blood occlusion on the thenar eminence of the hand. Whilst the instrumentation used is not applicable to in-shoe applications, the results of the study, if they may be extended to the more general case of blood occlusion in tissue certainly are. The results “.. showed the combination of pressure and shear was particularly effective on promoting blood flow occlusion. At a sufficiently high level of applied shear stress (~ 10 kPa) the pressure necessary to produce occlusion was half that required when little shear was present”, confirming Bauman’s hypothesis and vindicating Rabichong’s efforts.

In addressing shear, Tappin et al. (1980) developed a magneto-resistive “uni-axial shear” transducer for in-shoe measurements. The core of this transducer was a centre-tapped magneto-resistor whose resistance varied with the magnetic field in which it was placed. A small magnet was secured onto a deflectable upper plate, constrained to be deflected only along a horizontal groove. As shear was applied along the axis of the groove the magnet deflected and caused an imbalance in the bridge circuit of which, the centre tapped magneto-resistor formed two legs. An elastic self centring force was provided between the two components. The transducer was calibrated to 196 kPa and had a surface area of 2cm². Results are quoted for longitudinal shear force of up to 88 kPa. The overall transducer thickness was 2.7mm and yet barefoot recordings were considered valid. Indeed no mention is made of a recess for the transducer in the in-shoe measurements. The main drawback of this device was the fact that it gives a uni-axial assessment of shear force as opposed to a tri-axial assessment of force. Also there is no indication of assessment of cross talk effects from forces along other axes than that which it is designed to measure. Calibration was carried out by applying static loads along the shear axis only with a fixed vertical loading “equivalent to body weight”.

Attempting pressure measurement only, Soames et al. (1982) describe a strain gauge based transducer - overall size 13mm square by 0.9mm thick having an internal section forming a cantilever (5mm x 3mm) deflected by “pressure” applied to a rubber membrane which was used to cover the transducer. Sixteen transducers were used, each individually calibrated

using a static calibration. "Depending on the calibration factors" the quantisation errors were found to be between 1.84 and 3.32kPa. They claimed errors of between 1-3% depending on the particular transducer. In data presented, of normal and pathological subjects, peak pressures up to 4500kPa were recorded. These transducers were not mounted in recesses when in-shoe measurements were taken but the authors claim no discomfort was felt during these tests indeed "after being worn for a short time, a transducer will embed itself into the surface of the skin and may thus more accurately reflect the local pressure". Despite this "reassurance" it would be informative to see comparative results with a transducer recessed into an insole for in-shoe trials. The active area to total area of transducer is small and this may distort the pressure value or at least may make it incomparable with other work. There is no discussion of dynamic performance, although one may perhaps not have reason to suspect a problem here, depending on the rubber membrane and electronics used. The effect of shear on the transducer itself would probably be negligible but again no evidence is given.

Hennig et al. (1982) developed an in-shoe pressure transducer using a polycrystalline piezoelectric ceramic in a rubber matrix "of appropriate flexibility". They reported deformation of 10^{-4} - $10^{-5}\%$ in response to a stress of 10^5N.m^{-2} . They claimed the transducers were relatively inexpensive and easy to manufacture, that they generated a linear and virtually hysteresis free response to stress with large charge output and lack of sensitivity to humidity and stray electrical disturbances in comparison to the rubber filled capacitor transducers. However they admit they are more sensitive to temperature - they are effectively pyroelectric as well as piezoelectric. The group developed a flexible array of 499 sensors $4.78\text{mm}^2 \times 1.2\text{mm}$ thick. These were lead zirconate titanate transducers embedded in a 3-4mm thick layer of "highly resilient" silicone rubber which was impervious to moisture and electrically insulating. The transducers had silver electrodes bonded to their major surfaces, arranged in a square pattern and had a centre to centre spacing of 6mm on a thin sheet of copper gauze cut to the size of a US size 10 foot. The gauze acted as a common ground and the separate connection of the upper electrode of each transducer was made using a thin annealed copper wire which runs through the silicone rubber to the edge of the array and thence up the leg of the subject. Good evidence of calibration, both static and dynamic, was given, up to 1500kPa peak with 0.5kPa resolution. The temperature effects claimed were such that the relative sensitivity or relative resolution varied less than

1.5% between 10°C and 40°C. Theoretically the effect of shear on the performance of these transducers and of *pure* bending should be negligible. Actual values of pressure recorded are not given. Whilst the bandwidth of this device was not fully defined, as with any piezoelectric method these transducers could only measure dynamic/quasi-static pressures.

Reports of similar piezoelectric (Pedotti et al. 1984, Gross and Bunch, 1988) and capacitive (Nicol and Hennig 1978; Hermans et al., 1986) transducers followed. However “the development of these plantar transducers ran into serious technical difficulties” according to Peruchon et al. (1989). They reported another approach (described by Clot et al. 1975) utilising a (conductive) rubber laid upon base of polyimide on which there was a matrix of small electrodes. They used 2x127 electrodes, covered by a layer of rubber 2mm thick, the overall thickness was 2.5mm. The electrodes consisted of a central electrode surrounded by a circumferential ring. The conduction between the central electrode and the outer ring is dependent on the pressure exerted on the conductive rubber covering. The conductive rubber was designed for pressure ranging up to 600kPa. The full scale output signal was measured at 25% deformation corresponding to a pressure of 300kPa. Linearity was found to be 16% at 75% full scale and 22% at 90% full scale corresponding to a 15% compression of the material. The material deformation speed for these tests was 0.4mm.s⁻¹. The response time was 0.004s and the recovery time 0.015s for a 25% deformation. Under normal conditions of gait, the transducer operated within 50% full scale with a frequency response reaching 100Hz and a lifetime of around 1000 cycles of 25% deformation. Negligible temperature effects were claimed. A film covering over the conductive rubber was used for protection. The transducers were spaced at 1 cm intervals. Dynamic testing was carried out at 1Hz. The non-linear response was corrected with a linearisation table in each transducer. A resolution of 20kPa was obtained. Cross talk was however found between sensors. Mechanical and electrical (conductive) effects were minimised by cutting groves in the underside of the conductive rubber covering. In this way maximum cross talk of 1% was reported. In spite of a series of technical improvements performance of the system was felt limited by the modest electromechanical properties of the conductive rubber. In particular accuracy and response time prevented its application to sports studies. In fact very few specific results were given by the group and these were reported as the composite output of all transducers with emphasis on centre of pressure. It is disappointing that no detailed results of individual transducer output over successive gait cycles is given.

The F-Scan system (Tekscan Inc.) represents a commercially available foot pressure measuring insole utilising force sensing resistors. This uses conductive and resistive links on a mylar substrate to form a matrix of 960 sensors on a disposable, 0.1mm thick insole. Each 5mm² sensing element is formed by depositing a layer of resistive ink between two orthogonal conductors. Aluminium tracks deposited on the external surfaces provide connection to a small instrumentation unit worn at the ankle. The matrix is scanned at 165Hz per sensor with a resolution of +/- 4kPa. Other details of the performance of the system are not given.

The Electrodynogram system (Langer Biomechanics Inc.) provides discrete sensors with a thickness of 0.3mm. These sensors are said to be suitable for both in-shoe and barefoot measurement. Each sensor is an integrated circuit containing a resistive bridge with temperature compensation (New Scientist 1985). The measurement range is 0-1.5MPa with sensitivity of +/- 30kPa. The sensors exhibit non-linearity of 5-10%, a high hysteresis error of 15-20% and drift of 8% after 1 minute. The system has a maximum sampling rate of 200Hz per sensor.

A similar commercial system, the Emed Pedar (Langer Biomechanics inc.), uses an improved version of the capacitive system developed by Nicol and Hennig (1978). This system provides 99 sensors on a 2mm thick insole with individual sensors occupying an area of 17mm². Sensor measurement range is 30kPa - 0.6MPa with sensitivity of 1kPa varying by +/-5% over the temperature range of 10-40°C. Hysteresis of less than 3% is reported together with a frequency response of 50Hz. Mechanical decoupling of the sensing elements allows performance to be maintained when bending forces are applied (Cobb and Claremont, 1995)

Taking a quite different approach Maalej et al. (1988) describe a discrete in-shoe electro-optical force transducer. This was employed as an asymmetric U-shaped steel spring which deflected to occlude transmission of light between an LED and photo-detector. The spring has a lower beam length of 4mm, upper beam length of the 3.5 mm and radius of curvature of 1.5mm. The transducer is encapsulated in silicon rubber to provide even loading and protection against water and dirt. The overall thickness of the transducer was then 8 mm. The load range was 0-50N giving a maximum deflection of 0.11mm; good sensitivity was reported. Figures for non-linearity of +/- 2.5% and hysteresis of 1.5% are stated. Static

calibration was carried out with a 25 mm diameter spherical indenter. No discussion of dynamic performance is given. It is not clear over what area the force transducer measures. At best one can assume the area would be 3.5 x 5mm (spring dimensions). However when the transducer was embedded in rubber it is not clear what the active area actually is, or whether it is in fact a discrete area. The overall thickness of 8mm for the embedded transducer required the use of extra-depth shoes.

Nevill et al. (1991) developed piezoelectric pressure transducers using PVDF copolymer film. The transducers were 10 x 10 x 2.8mm. These were located in recesses cut into a 3mm thick rubberised cork insole. Over the measurement range of 0 to 1 MPa, the transducers were linear to within 1.5% and had a hysteresis error less than 1.5%. Sensitivity was reported as +/- 1kPa within the calibration range. The frequency response extends from 0.008Hz - 250Hz. This was followed up and developed further (Nevill et al. 1995) with a declared aim of "absolute pressure measurement at predetermined sites to within 10%". Calibrated range was 0-100N over an area of 10 x 10mm. The maximum possible frequency response was reduced from 200Hz to 10Hz following experimentation which revealed little additional information in normal walking trials above 10Hz. The low frequency cut-off was 0.01Hz. It is not clear how absolute pressure measurements were achieved without d.c. pressure!

Returning to the problem of shear measurement, Pollard et al. (1983) extended the work of Tappin et al. (1980) using a combination of uni-axial shear transducers and pressure transducers. This did not, however, represent any advance in technology. The assessment of forces was made in three trials per site. One for each shear axis and one for pressure. The results obtained, especially specific values, are not clearly given. The paper does not achieve the objective of an instantaneous assessment of three dimensional forces on the foot surface.

Williams et al. (1992), working in the field of prosthetics, reported a tri-axial force transducer for investigation of the stresses at the stump/socket interface. They utilised two of the transducers developed by Tappin et al. (1980) together with a strain gauged diaphragm. These components were mounted together to form one transducer of 4.9mm x 16mm. The 100N maximum vertical force applied over an area of 200mm² corresponds to a 500 kPa limit with a resolution 0.1N. In shear the 50N upper limit corresponded to 250kPa, with a hysteresis of 4N and resolution 0.2N. The authors do however raise the problem of

creep characteristics during shear. "Large deformations held over a long period result in stress relaxation within rubber. The same process occurs in creep when the rubber continues to deform under a given load. A step load of 30N was applied to the shear axis of the transducer which resulted in typically no more than 5% change in output. Once the load was removed, within a further 30s the output returned to within 1% of its original value, and eventually recovered completely resulting in no permanent deformation of the rubber. For the normal axis creep was practically negligible."

It would appear that this device, initially reported three years after the research in this thesis (results reported 1992, Warren-Forward et al.) began, could be used in addressing the in-shoe measurement problem. Two questions remain unanswered, can the diameter of the device be reduced and, more importantly, what are the values of cross talk between the three axes?

The idea of combining two of Tappin et al.'s transducers into one to obtain a complete picture of shear is again used by Lord et al. (1992), this time in in-shoe measurements. The transducers manufactured were 4mm thick and 16mm in diameter and had a 50N range (250kPa on the area of 200mm²). They were (rather puzzlingly) calibrated over 30N with a 0.1Hz "quasi" static calibration. Further confusion is created by the use of a data capture system using 50Hz sampling, the data then being processed by 250Hz low pass filter, somewhat ignoring the Nyquist theorem. Shear values up to 65kPa were reported. The transducer was recessed into a stiff section of insole such that their surface was flush with the rest of the insole. This system was used in conjunction with a commercial in-shoe foot pressure measurement system utilising an array of piezoelectric transducers in a thin insole, the F Scan system described previously. Despite using a similar approach this implementation does not seem as rigorous as that described in the stump-socket application of Williams et al. (1992)

2.4 OBJECTIVES OF FORCE MEASUREMENTS AT THE FOOT SHOE INTERFACE

In understanding what is being sought of tri-axial force measurements at the foot-shoe interface it is perhaps worth referring to Davis (1992). Presenting an hypothesis on the causes of foot ulceration in respect of shear and vertical forces and apparently unaware of the efforts of Williams et al. (1992), he stated "Unfortunately the studies that have focused

on the nature of shear forces under the feet have had the limitation that instrumentation could detect forces in one direction only. This limitation inevitably results in an underestimate of maximum shear stress since this quantity results from a combination of medio-lateral and anterior-posterior components.It is hypothesised that particular combinations of pressure and shear are more important than others. These hypotheses are not related to the concept of 'vertical shear' inside the tissue, but rather to localised slipping of the external skin surface." (i.e. relative to the underlying tissue)

Davis (1993) uses the concept of coefficient of limiting friction and the variation of shear force areas of adjacent skin to discuss ulceration. Considering localised shear and pressure Davis proposes that three possible scenarios exist:-

A localised area the skin may slip:

- 1) towards
- 2) away from
- 3) parallel to a neighbouring skin region

These lead, respectively, to local wrinkling, tearing or torsion of the skin.

Davis (1993) suggests that results in the literature may support his theory - even where sites of ulcer are at high pressure regions, it may be the change of the coefficient of limiting friction at the edge of such sites that leads to the ulcer, rather than the high pressure. He references Ciercteko et al. (1981) who concluded that the magnitude of vertical force was not the only factor that contributed to the occurrence of diabetic neuropathic ulcers. He also suggests that sports blisters may occur due to a change in the coefficient of limiting friction with perspiration.

Davis concludes that his theory should be examined by future researchers who should give attention to the need to measure simultaneously vertical force and shear at a multitude of locations. As Hennig et al. (1982) suggest "...the information required is the variation throughout the gait cycle of (1) the magnitude, direction and point of application of the resultant force and (2) the way in which this spatially distributed over the plantar surface of the foot."

The problem is, of course, as Pollard et al. (1983) put it: "Concerning human gait assessment, a basic question can be raised, how can a foot ground contact analysing method be designed so that it does not interfere with the walking function? The experimental

procedure must not generate too important physical or psychological constraints which could screen the physiological reality, moreover the measurement device must be chosen or designed so that its mere physical presence does not perturb function itself”.

Clearly the floor mounted transducer array has some advantages here for the assessment of barefoot walking which may be useful depending upon the application “for example barefoot to ground patterns are the most relevant presentation for the orthopaedic surgeon who wishes to evaluate the outcome of foot surgery, whereas shoe to ground or foot to insole prints would be appropriate to reveal the redistribution of loading caused by wearing a particular design of shoe or insole” (Lord, 1981).

Since 1873 then we have seen many approaches to the problem of measurement of the forces applied to the foot during quiet standing and walking. The devices described have been based on many different principles including, manometric, optical, resistive, capacitive, piezoelectric and magneto-resistive. Capacitive, piezoelectric and resistive based transducers have perhaps been the most commonly used for in-shoe measurements. Indeed these techniques are now being utilised in commercial foot pressure measurement systems, for both in-shoe transducer systems and floor mounted arrays. Opinions on the use and validity of such systems clinically varies. In general there is a dearth of comprehensive static and dynamic force calibration evidence. The fundamental questions about what is actually being measured, what is meant by pressure or by vertical and shear force, has in general not dared to have been addressed. Perhaps the main reason for this may have been the lack of available instrumentation to map tri-axial forces acting over the foot surface and thus provide the window needed to answer at least some of the questions.

In attempting development of a tri-axial force transducer for in-shoe measurements it is perhaps particularly worth remembering “In assessing and presenting results from clinical studies involving measurement of plantar pressures, it is important to define and quantify the limitations of the devices used to allow an objective comparison to be made with the findings from other studies. Future development of plantar pressure transducers may include insoles with the capability of simultaneous measurement of vertical and shear forces. Better calibration methods need to be developed to allow the effect of factors such as bending forces and temperature on transducer performance to be assessed. Standardised methods of

evaluating and defining the performance of plantar pressure transducers need to be developed” (Cobb and Claremont, 1995).

It is hoped that what is to follow has made some gains towards these ends.

3. FORMULATION OF THE DESIGN CONCEPT

3.1 SPECIFICATION OF DESIGN REQUIREMENTS

3.1.1 Initial considerations

In beginning the design process, two important requirements of the transducer were identifiable. Primarily, it should be capable of measuring tri-axial forces and secondarily it should be possible for it to be placed unobtrusively within the shoe, at the foot-shoe interface.

It is also essential to be able to record force measurements over a reasonably small area of the foot surface. This will allow the gradual construction of a detailed map of the force distribution over the whole foot. The map could be achieved in one of two ways, either by repeated positioning of the same transducer or, by using an array of transducers. The second of these was considered preferable since simultaneous recording of forces from the array of transducers could then be obtained.

The design focus was initially targeted at the plantar aspect of the foot since many pathological conditions, such as foot ulceration in the diabetic patient are derived from abnormal forces applied to this area. Thus, the transducer was designed so that it could be conveniently situated within an insole in the shoe.

3.1.2 Transducer size

The constraints permitted the design of a transducer of maximal thickness and diameter of 5mm and 10mm respectively. It was considered that anything larger would have created two main problems:

- a) A transducer of larger diameter would diminish resolution. This would result in a cruder force map being produced.
- b) Shoe size would need to be increased in order to accommodate a thicker transducer.

3.1.3 Environment

The transducer should be also capable of coping with the variable temperature and humidity of the shoe environment. Electrical safety within this environment was also taken into account so that in the event of direct contact, between skin and the transducer's active components, errant sources of current would be limited in magnitude to a safe level.

3.1.4 Desired range of force transducer

Values of foot pressures up to 1.4MPa have been reported (Duckworth et al.,1985) and applied shear stress of up to 90kPa (Tappin et al., 1980). Given the experience expressed in the literature of foot pressure measurements and pressure ranges used in commercial systems a figure of 1.5MPa was set as a design target, whereas the applied shear stress range measured by Tappin et al. was given a 100% margin, and thus an applied shear stress range of 180kPa was chosen.

Taking another approach to examine the suitability of these ranges: from established force plate studies (Perry, 1992), vertical forces on the whole of the foot reach approximately 1.1 times body weight during walking in a normal subject. For an average subject of 75kg this might act over 10% of the area of the foot (taken as 150cm^2) giving an average pressure of 540kPa. In the anterior-posterior direction a total force of around 25% maximum is seen, whilst in the medio-lateral direction a maximum of 10 %. Assuming the worst case in which the vector sum of these acts at the same time over 10 % of the foot area of approximately 150cm^2 , then a maximum applied shear stress of the order of 132kPa would be expected.

3.1.5 Summary of design specification

A transducer of 5mm maximum height, 10mm maximum diameter, capable of measuring vertical stress of 1.5MPa and shear stress of 180kPa over a wide range of temperatures and humidity forms a compact summary of the design constraints of the required prototype transducer.

3.2 REVIEW OF TRANSDUCER TECHNOLOGIES FOR IN-SHOE FORCE MEASUREMENTS

Inevitably there are a few basic physical phenomena/principles utilised and essential to the operation of any particular force transducer. Many of these have been seen in the literature review of attempts at measuring the forces applied to the human foot. In general, force transducers may be grouped by whether they are based upon capacitive, inductive, piezo-electric, strain-gauged or resistive effects. These are based on the various principles in that the quantity being measured (the measurand), which is related to the force by some fixed relation, is capacitance, inductance, piezo-electrically derived surface charge or resistance. The resistance based group may be further sub-divided in that the resistance variation could be in strain gauges, potentiometers, magneto-resistors or even between contact electrodes between two surfaces being forced together.

The most common bases for in-shoe *pressure* transducers have been and continue to be capacitive, piezo-electric, and resistive (electrode contact type).

The limited attempts at *shear force* measurement have all been based upon a magneto-resistor. This is a semi-conductor device whose resistance varies according to the magnetic field in which it is placed. Displacement of the magnet, when shear is applied, varies the magnetic field through the magneto-resistor and thus the resistance of the magneto-resistor.

Whilst strain gauged systems are commonly used in general engineering they have seen only occasional use in the field of in-shoe force measurements. This has been to measure either vertical force or direct pressure. In terms of measuring shear force, whilst the strain gauges need only be very small, the mechanical element whose deflection under shear would be used to quantify shear force is likely to require rather too much space for in-shoe measurements.

No references to inductive techniques in foot-force assessment were found. The use of linear variable inductance transducers (LVDT's) in force (and displacement) measurements in general engineering is common. These use the variation of mutual inductance between a primary and secondary coil as the position of the moveable core changes. The core is restrained, but not prevented from moving, by a mechanical element. The linear (uni-axial)

force required for displacement of the core then may be calibrated with the (dependent) mutual inductance between the coils.

3.3 CHOICE OF TRANSDUCER TECHNOLOGY

Any transducer capable of measuring mechanical force should have two fundamental elements, a mechanical element influenced by force and a measure of the mechanical element's change under the force applied. Output from piezo-electric based transducers is often considered a "direct" indication of the force applied in-so-much that the mechanical elements response to stress may be measured, as surface charge, on the mechanical element (the piezo-electric crystal) itself. This contrasts with capacitive based transducers in which the mechanical element is simply the dielectric between the plates of the capacitor. The mechanical element's response to stress is measured indirectly by the change in capacitance due to the change in gap between the plates on either side of the mechanical element. In both cases, however, the mechanical element and a means of measuring its response to stress must be present. Given that the force-response properties of the mechanical element are known, repeatable, reproducible, suitably stable whilst fast enough in response then the force applied may be derived reliably. In most cases the mechanical response measured is one of deformation and hence many of the basic principles used in force measurement are also used in displacement transducers.

One aspect of note is that both in force and displacement measurement systems the degree of complexity rises steeply as two and three dimensional force and displacement measurements are required. This is especially so where space and accessibility are a problem and the solution cannot be to simply use two or three uni-axial transducers. This approach may also produce difficulty in making concurrent measurements at a single point along three axes.

In developing an approach to the problem of in-shoe foot-shoe force measurement, the use of the various basis for the force transducer design were to be examined to identify possible approaches.

The piezo-electric approach has one fundamental limitation, that of the time dependent nature of the output surface charge. This essentially limits the use to dynamic measurements of limited duration (realistically, seconds at most). Long term (e.g. 24 hour) monitoring may

then be ruled out because of the drift problem. The suitability of the transducer for long term monitoring would offer many more opportunities for research into foot ulceration and thus piezo-electric methods were ruled out.

The magneto-resistive principle appears very useful in shear but would require a separate method for measurement of compression. The capacitive techniques for measurement of compression could conceivably be adapted for compression and shear since lateral shift of the top plate with respect to the lower would reduce the effective area of the capacitor. However it is noted that in general, even for pressure measurement systems, capacitive techniques tend to have been superseded by piezo-electric and resistance based transducers. Perhaps this was because of the comparative difficulty in measuring capacitance accurately. It is clear that for a transducer of 10mm diameter and 5mm thick the capacitor formed by applying conductive plates on either surface, even with a mechanical element of high dielectric constant, will be very small ($\sim 10\text{pF}$) and thus it would be difficult to measure small changes and would lead to a very poor signal to noise ratio. This leaves the use of resistive techniques for pressure measurement - in particular the electrode-contact area approach. The concept of using a combination of techniques such as magneto-resistive for shear measurement alongside a resistive (electrode contact) method for pressure seemed unattractive in view of the complexity and space limitations put on the design by the application.

Taking a different approach and considering a suitable mechanical element first; the shoe insole material lent itself as a natural choice. It was anticipated that it might be necessary to isolate an area around the transducer - to have a gap in the insole material around the transducer itself, in order to ensure truly localised force measurement. The advantage of having the insole and transducer manufactured from the same material was that it would ensure a uniformly compliant surface for the foot. Reference to the literature shows clearly that this approach is not new except in-so-much as the three dimensional deformation would indicate the three dimensional forces applied to the foot as opposed to the compression indicating pressure applied to the foot. The problem faced then was to measure and calibrate the tri-axial deformation of the insole material.

Given this situation a new approach was deemed necessary:-

As has already been mentioned, inductive techniques are commonly used in general engineering displacement measurement problems but no record of their use in in-shoe force measurement was found.

The principle then proposed for the transducer was to measure the deflection of the insole using the change in mutual inductance between coils embedded in the upper and lower surfaces of the insole.

It was anticipated that a particular configuration of coils would allow detection of the three dimensional material deformation and that selection of the appropriate coils and combination of coils would ensure suitable transducer sensitivity and range to be obtained.

3.4 MEASUREMENT USING ELECTROMAGNETIC INDUCTION

The design of a transducer based on the phenomenon of electromagnetic induction; that is the induction of electromagnetic force in any conductor moving perpendicularly to a magnetic field, or lying in a time-varying magnetic field was considered. Quantified by Faraday's Law:

The induced e.m.f. in the circuit is numerically equal to the rate of change of the magnetic of flux through it.

and further by Lenz's Law

The direction of an induced current is such as to oppose the cause producing it.

Expressed algebraically,

$$E = -d\phi/dt$$

Where E is the induced field and ϕ the time-varying magnetic flux.

Oersted is attributed the discovery (in 1819) that electric currents produce magnetic fields. A time-varying current will produce a time-varying magnetic flux through a coil of wire placed near it. Thus an alternating current $d(i_1)/dt$ in coil 1 will induce a voltage in a coil placed near it. The quantity Mutual Inductance, M_{12} , between the coils is defined to relate these such that a voltage E_2 is seen in coil 2 near to coil 1 by $E_2 = M_{12}.di_1/dt$.

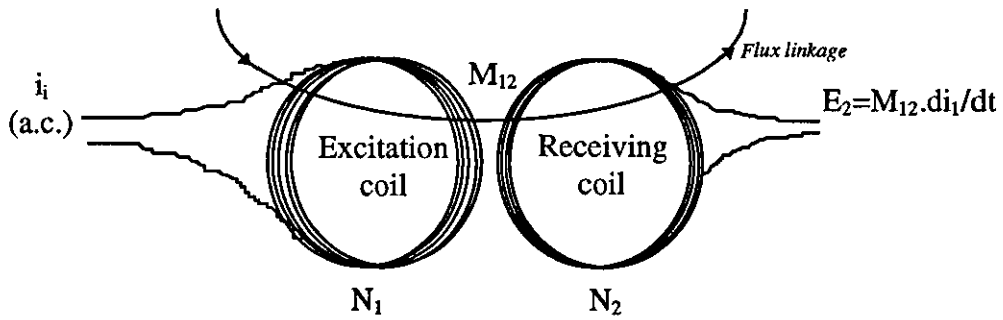


Figure 3-1 Electromagnetic induction

That is, the voltage induced in the second (receiving) coil is proportional to the rate of change of the current in the first (excitation) coil and the mutual inductance. The mutual inductance is dependent on the ratio of the number of turns on each of the coils, the arrangement of the turns within each coil (i.e. the shape of the coil), the media between them and most importantly, in this study, *their relative positions*.

3.5 INVESTIGATION OF THE PRACTICALITY OF USING THE INDUCTIVE TECHNIQUE

The feasibility of the use of the principle proposed in the transducer had now to be investigated. The approach to this may be described in terms of determination of constraints and an evaluation of the effects of those constraints. The constraints arise from the transducer design specification and safety/comfort considerations. Specifically these are:

- a) Coil size - limited by the maximum required size of the transducer and the subsequent difficulty of manufacturing very small coils.
- b) Current & frequency - limited since the dependent heating effects seen in the excitation coil must be minimised for comfort and safety of the subject under whose foot the coils will be placed.

The question then is does the limitation on the size of the coils, the current and frequency used in the excitation coil still allow use of the principle proposed? That is what are:

- a) The level of induced voltages - over the coil separations that are likely to be seen between the coils in the assembled transducer?
- b) The shape of the induced voltage coil separation curves - will a sensitive force transducer be produced?

It should be noted that only the question of voltage induced in a single receiving coil moved with respect to an excitation coil is considered here. The work addressing the problem of three dimensional displacement measurement is addressed in the next section.

3.5.1 Size of coils

The target thickness of the insole was 5mm. Therefore a design compromise between coil size and maximum allowable deflection between the coils embedded in the insole was inevitable.

Any material has fixed elastic limits per unstressed unit volume. For a given coil pair, the mutual inductance change will enable detection of a certain minimum (and maximum) relative displacement of the coils one to another. Therefore the appropriate selection of a combination of suitable material properties, thickness and coil pair for a given transducer specification presented a problem having a large number of possible solutions.

Given the size of the transducer required, within which the coils must fit, it is easy to appreciate that the smaller and thinner the coils are, the more difficult they will be to manufacture. It was found that a 0.5mm coil thickness (axial length) was an achievable goal (see section 3.5.2) leaving 3.8mm of insole material (allowing 0.2mm insole material to cover the upper surface of the ‘insole’). It was considered that this would ensure adequate scope for compression and shear of the material between the coils. Therefore maximum coil dimensions of 0.5mm length and 10mm diameter were chosen (figure 3.2).

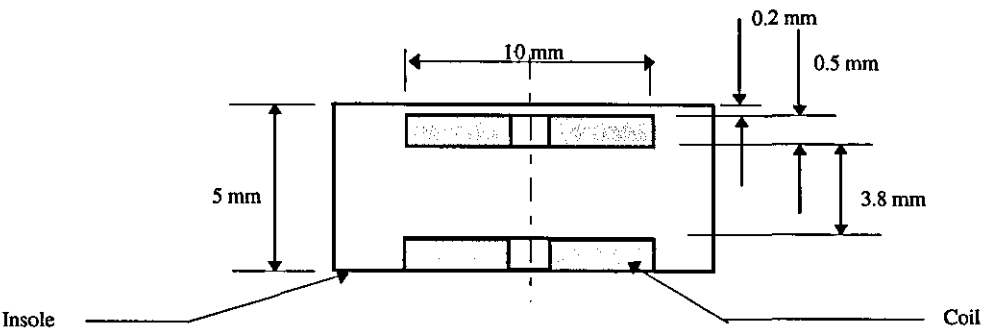


Figure 3-2 Sectional view of a single coil pair embedded in insole material

This of course assumes a single coil on each transducer face, whereas the final design required one excitation coil and three receiving coils. The diameter of the receiving coils has

subsequently to have a smaller diameter than 10 mm, in fact a maximum radius given by (figure 3.3)

$$r = (10 \cdot \sin 60^\circ) / (1 + \sin 60^\circ) = 4.64 \text{ mm} \tag{3.1}$$

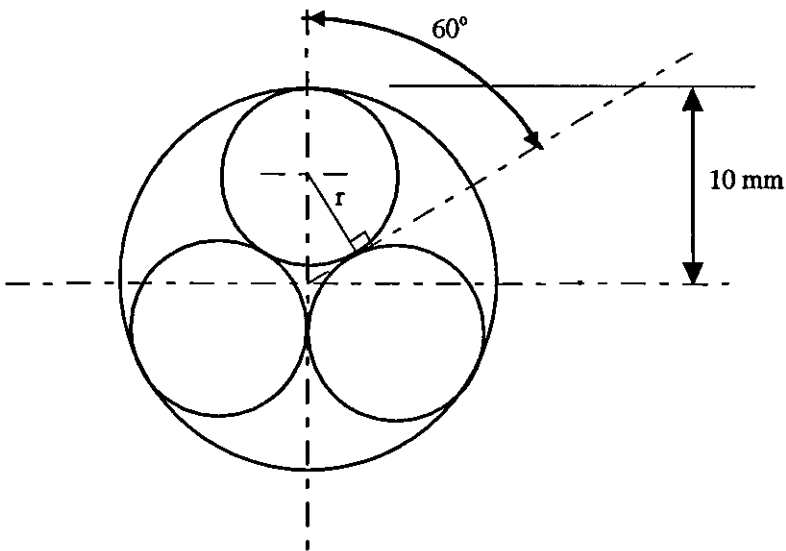


Figure 3-3 Maximum size of the three receiving coils within transducer diameter

3.5.2 Manufacturing of coils

Since no commercially produced coils of the required size could be located*, a coil former was designed and manufactured (figure 3.4).

(*Towards the end of the research a manufacturer willing to wind such coils was identified.)

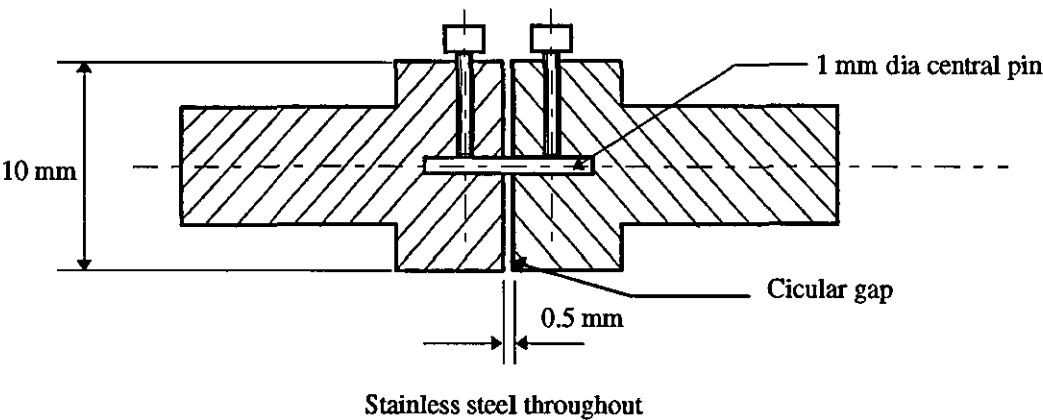


Figure 3-4 Sectional view of coil former

The former consisted of a pin providing the core for the coil mounted between two plates which formed the ends of the mould for the coil. The whole assembly was designed to be mounted in a coil winding machine. The coils were wound using a cyanoacrylate bonding agent to ensure retention of the coil windings and shape. Silicon grease was applied to the faces of the stainless steel former prior to winding to prevent adhesion of the coil to the former.

The aim was to enable the production of a range of “pancake” shaped coils. Various coils were constructed using wires of differing diameter. Each coil fitted within the *constraining* volume of 0.5mm x 10mm diameter (smaller coils were produced), had a 1mm internal diameter and was identified by its size and number of turns

Production of a range of coils enabled investigation of the shape of electromagnetic fields produced when excited and also the flux linkage between pairs of coils. This enabled the eventual selection of appropriate coil pairs for the construction of the final transducer.

3.5.3 Aspects of coil winding

3.5.3.1 *Packing factor*

Is defined as the ratio of copper volume to coil volume, which obviously, for circular wire will always be less than 1 even for perfect winding due to the inevitable gaps.

3.5.3.2 *Total length of wire*

Considering a pancake shaped coils constructed for this work as illustrated in figure 3.5

Assuming the coil is wound as depicted in the diagram we may, for wire of small enough diameter model the total length as a series of layers of concentric circles of wire, summation of which will give an estimate of wire length in the coil.

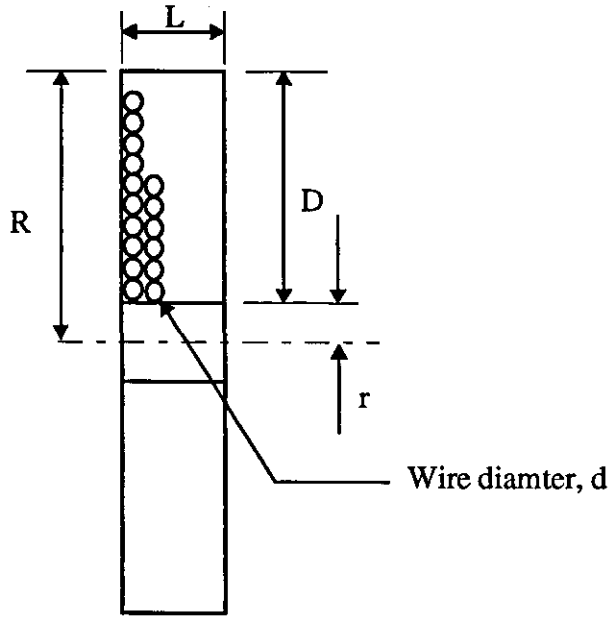


Figure 3-5 Cross section of coil

Considering a single layer of the coil (figure 3.6):

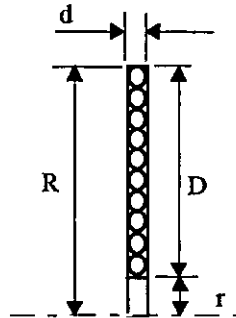


Figure 3-6 Single layer of winding

Then the length of the spiral, l_s will be approximately:-

$$l_s \cong \sum_{x=r+d/2, d}^{R-d/2} 2\pi x \quad (3.2)$$

This is an arithmetic progression with initial term, $r + d/2$ and common difference of d and D/d terms, hence:

$$l_s \cong \frac{2\pi D}{d} \left(r + \frac{D}{2} \right) \quad (3.3)$$

Over the length of the coil L there are L/d layers thus the total length of wire, l , is:

$$l \equiv \frac{2\pi LD}{d^2} \left(r + \frac{D}{2} \right) \quad (3.4)$$

But the total number of turns on the coil, n , would then be given by:

$$n = \frac{D}{d} \cdot \frac{L}{d} \quad (3.5)$$

therefore

$$l \equiv 2\pi n \left(r + \frac{D}{2} \right) \quad (3.6)$$

Further from

$$n = \frac{D}{d} \cdot \frac{L}{d} \quad (3.7)$$

we note that the cross section area of the wire is related to the number of turns for fixed coil dimensions:

$$a = \pi \frac{d^2}{4} \quad (3.8)$$

$$\therefore a = \frac{DL\pi}{4n} \quad (3.9)$$

and thus the volume of copper is given by:

$$a \cdot l \equiv \frac{\pi^2 DL}{2} \left(r + \frac{D}{2} \right) \quad (3.10)$$

which for fixed coil geometry is a constant implying a constant packing factor.

Note that :

$$\left(r + \frac{D}{2} \right) \quad (3.11)$$

is the mean radius of the coil

3.5.4 Current & frequency limitations

3.5.4.1 Heating effects

To ensure electrical stability, shoe comfort and safety, coil heating must be minimal. In order to determine a range of safe currents and excitation frequencies a series of tests were carried out. The objective was to determine a range of currents that resulted in useful levels of induced voltage in a receiving coil without causing a significant heating effect in the excitation coil. The heating effect for a given current is dependent upon the resistance of the coil. The mean power dissipated by this heating effect, P_{mean} is given by:

$$P_{\text{mean}} = I_{\text{rms}}^2 \cdot R_{\text{effective}} \quad (3.12)$$

where I_{rms} is the root mean square current and $R_{\text{effective}}$ the *effective* resistance of the coil - this is the d.c. resistance of the coil modified by any frequency effects that may be seen when an alternating current is passed through the coil (see section 3.5.4.6 for discussion of frequency effects). Ignoring the frequency effects it is worth noting that for a coils of the same packing factor, the energy required to give a specific temperature rise will of course be a constant related to the specific heat of the coil wire. Thus for higher current we require lower resistance for the same temperature rise.

3.5.4.2 DC coil resistance

The d.c. resistance of a metallic conductor is proportional to the resistivity of the metal, the length of the conductor and is inversely proportional to the cross sectional area of the conductor.

That is the resistance of a conductor is given by:

$$R = \rho l / A \quad (3.13)$$

where l is the length of the wire and A its cross sectional area

The resistivity, ρ , of a metal is dependent on temperature and can be represented approximately by:

$$\rho_t = \rho_o [1 + \alpha(t - t_o)] \quad (3.14)$$

where ρ_o is the resistivity at a reference temperature t_o and α is the temperature coefficient of resistivity *G S Ohm (1789-1854)*.

Copper has a resistivity of approximately 1.7×10^{-8} at 293K and α for copper is around $0.00393K^{-1}$.

Decreasing the cross sectional area of the wire will enable more turns per unit volume but will increase the resistance and heating effect for a given current. In fact from section 3.5.3.2 the length of wire was estimated by:

$$l \cong 2\pi n \left(r + \frac{D}{2} \right) \quad (3.15)$$

and the cross section area of the wire was shown to be:

$$a = \frac{DL\pi}{4n} \quad (3.16)$$

and thus the resistance of the coil can be estimated by:

$$R \cong \frac{8n^2 \rho_t}{DL} \left(r + \frac{D}{2} \right) \quad (3.17)$$

thus the resistance is proportional to the square of the number of turns.

3.5.4.3 Coil inductance and mutual inductance

The electromagnetic field produced by current in a conductor induces an e.m.f. opposing any change in that current. Self inductance, like the mutual inductance, quantifies this effect

and is proportional to the number of turns in the coil and is also dependent on the arrangement of turns in space and the media in and around the coil.

The e.m.f. produced, V , by Lenz's Law opposes the current, i , in the coil so that it may be described by:

$$V = -L \cdot di/dt \quad (3.19)$$

where L is the self inductance of the coil and is dependent upon the square of the number of turns and the geometry of the coil.

The mutual inductance between two coils is related to each of their self inductances by:

$$M = k\sqrt{L_1 L_2} \quad (3.20)$$

where M is the mutual inductance between coils 1 and 2 having self inductances L_1 and L_2 respectively. The coefficient of coupling, k , between the coils lies in the range from 0 to 1. Thus the larger the self inductance of the coils the larger the mutual inductance between them.

3.5.4.4 Selection of coil wire

The constraints placed upon the coils are of limitation of dimensions, and limitation of heating in the excitation coil. This leaves only the selection of the wire diameter in question. However:

The induced voltage, V , is given by:

$$V = M \frac{di}{dt} \quad (3.21)$$

where M is the mutual inductance and i , the time varying current. For fixed geometry of coils the mutual inductance is proportional to the square of the number of turns, then for a a.c. current, I , of frequency f :

$$V \propto I \cdot n^2 \cdot f \quad (3.22)$$

But from section 3.5.4.1 the heating constraint leads to a fixed relation of current to coil resistance, R , such that:

$$P_{\text{dissipated}} = I^2 \cdot R = \text{constant} \quad (3.23)$$

where from section 3.5.4.2

$$R \equiv \frac{8n^2 \rho_t}{DL} \left(r + \frac{D}{2} \right) \quad (3.24)$$

Thus

$$I^2 n^2 = \text{constant} \quad (3.25)$$

i.e. that

$$I \propto \frac{1}{n} \quad (3.26)$$

Thus the induced voltage

$$V \propto n \cdot f \quad (3.27)$$

This implies that using finer wire within the constrained volume will increase the induced voltage and the heating effects will be limited being able to reduce the current. Producing perfect winding with increasingly smaller diameter wire however proves more and more difficult and therefore a practical limit exists to the size of the wire that can be used.

3.5.4.5 Coil inductance calculations

As has already been stated coil inductance is dependent on the number of turns and ,in a complex way, on the layout of those turns - the dimensions and relative dimensions of the coil (Grover, 1946). There are a number of approaches to direct calculation of inductance of a given coil. The most direct method is by application of the Biot-Savart law for calculation of magnetic field strength at a point due to local current elements. Integration of such expressions over the area of each loop to the coil reveals the total flux linkage. For a given current the inductance, defined as the flux linkage per unit current, can then be

calculated. Surface and volume integrals are readily encountered which in many problems are not easily evaluated (Lim, 1966).

Another class of methods is based on the concept of magnetic potential vector. Again these approaches involve line, surface and volume integrals whose complexity depends upon the problem at hand. Early texts on calculation of self and mutual inductance offer many formulae used in conjunction with numerous tables and reference plots. These attempt to offer solutions to the problem of inductance and mutual inductance calculations for a myriad of coil shapes and combinations (Grover, 1946; Terman 1955). Murgatroyd (1990) describes a simple method for calculating maximum self inductance obtained from a “given piece of wire” (for a fixed length) for a selection of simple optimum “shapes” of coil. Yu and Han (1987) offer a solution for the calculation of the self inductance of any thick walled circular coil, thin walled solenoid, or disk (pancake) coil which may be carried out “on personal microcomputer”. The approach utilises magnetic vector potential. The derivation in their paper does however seem to contain numerous typographical errors for which corrections have not been obtainable.

Having produced coils of various dimensions, formulae (listed in Appendix 1) from Grover (1946), Terman (1955) and Wheeler (cited by Terman, 1955) for the inductance of short solenoidal forms of coil were applied. Some of the results are listed in Table 3.1.

These measurements and calculations give some indication of the likely mutual inductance between coils of this size since mutual inductance is given by (see section 3.5.4.3):

$$M = k\sqrt{L_1 L_2} \quad (3.28)$$

Thus for the coil 2, coil 5 pair we would expect that M should be no greater than:

$$M_{25} < \sqrt{21 \times 102} \mu\text{H} \quad (3.29)$$

$$M_{25} < 46 \mu\text{H}$$

Coil	Measured Inductance [μH]	Coil length [mm]	Outside diameter [mm]	Internal diameter [mm]	Number of Turns	Grover	Wheeler	Terman
1	92	1.1	8.8	4.1	110	76	75	76
2	≈ 100	0.48	4.5	1.0	100	19	20	21
3	3000	0.42	15.0	1.0	700	1913	1863	1895
4	-	0.4	10.3	1.0	450	830	755	816
5	-	0.48	7.8	1.0	180	93	95	102

Table 3.1 Coil data

Given a 10 kHz excitation current of 30 mA then we can expect a maximum voltage of 87 mV induced in the receiving coil. Thus $k=0.1$ would still result in a voltage large enough to ensure a reasonably good signal to noise ratio. In fact, with these coils and excitation current a maximum voltage of 48 mV was induced in the receiving coil when they were placed touching with their longitudinal axes aligned. This implies a mutual inductance of 24 μH , giving $k = 0.52$.

3.5.4.6 Frequency effects

Whilst the resistance and self inductance of the coils is of primary importance, the induced voltage in any receiving coil is directly proportional to the frequency of excitation for a fixed amplitude excitation current. This encourages the use of higher frequencies.

However there are other changes in the effective impedance of the coils as the frequency is increased. There are two effects, the skin effect and the proximity effect. The skin effect refers to the tendency for the high frequency currents to flow in a shallow “skin” adjacent to the surface of a conductor. Proximity effects are asymmetrical current distributions caused by e.m.f. induced by currents in nearby conductors. Both effects tend to decrease the internal magnetic field of the conductor and hence the inductance. In general the decrease in inductance is insignificant in comparison to the increase in ohmic resistance of the coils due to the inefficient use of the wire’s cross sectional area (Lim, 1966). The effective a.c. to d.c.

resistance ratio increases with frequency, conductivity and the size of the conductor. Thus, at high frequencies, increases in the heating effects of the excitation current are expected. Grover (1946) and Terman (1955) offer various corrective formulae for high frequency effects. The skin depth, δ , in copper at 20 °C is given by:

$$\delta = 66.2/\sqrt{f} \text{ [mm]} \quad (3.30)$$

giving a skin depth of 0.47 mm. The largest diameter conductor used in the coils tested was 0.1 mm in which a 10% reduction in current would be expected at its centre compared to that at its surface. The effective increase in resistance and subsequent heating effect due to this would be small and this was confirmed by heating tests described below.

3.5.4.7 Coil heating tests

In order to measure directly the heating effects in various prototype coils a small thermocouple probe was used to measure the temperature change in coils of various turns and differing wire thicknesses when a.c. excitation was applied.

Receiving coil induced voltage will be directly proportional to frequency hence the desirability of using higher frequencies. Assuming a commercial power amplifier is used for the excitation current then a frequency range up to 10 kHz should easily be obtained. Figure 3.7 show a graph of temperature versus current for the same coil but with two different excitation frequencies.

Whilst there is apparently some rise in temperature with frequency the effect is not large enough to influence the choice of excitation frequencies. This is particularly so in the 0-30mA region where the temperature rises are very small (see insert of figure 3.7). For a difference of perhaps 1°C between the 1 and 10kHz curve we would see a tenfold increase in induced voltage in a receiving coil

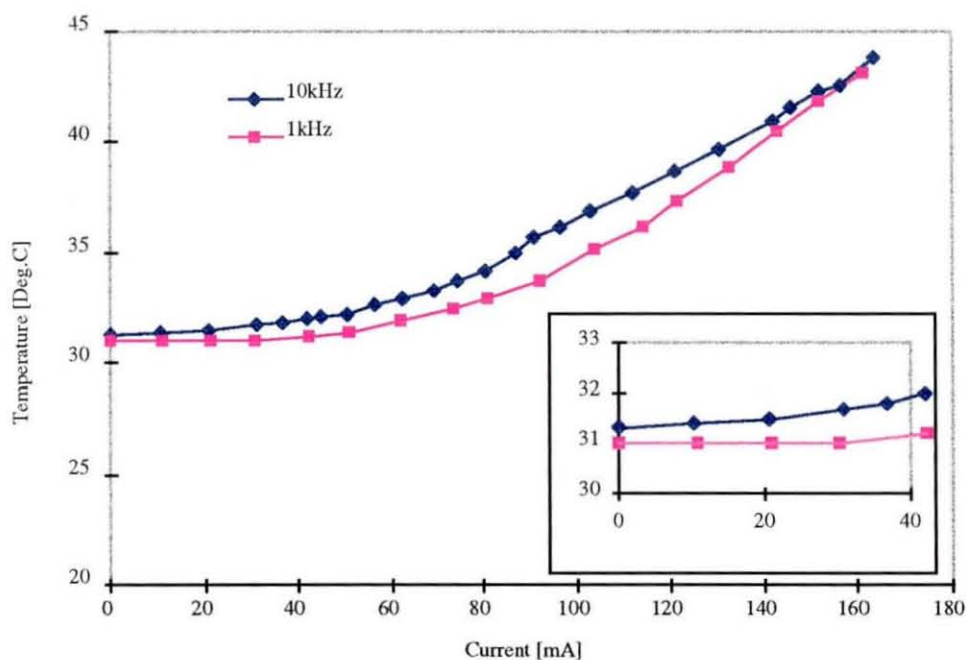


Figure 3-7 Temperature rise with current at two different frequencies

Considering then the effect of magnitude of current on heating with a 10kHz excitation current:

Measurements were carried out under two different conditions: a) with the coils placed upon a bench and with free air flow above the coil and b) in an in-shoe environment under the sole of a foot of a resting subject who was wearing socks. As might be expected the in-shoe tests gave lower temperature rise with current - the direct contact with the foot giving a better thermal conduction path away from the coil than is available in the bench (free air) test. Figure 3.8 illustrates the results from the two tests for the same coil.

In terms of safety, from the point of view of tissue damage, 40°C should be taken as a limit (McArdle et al. 1991), however 40°C under the sole of the foot can cause severe discomfort! Since the bench test proved more sensitive they were used to give a worst case guide of the maximum current that might be utilised in the transducer. A bench test temperature rise of around 3°C translates to an in-shoe temperature rise of around 1-1.5°C which was felt to be acceptable. The heating (bench) test results shown in figure 3.9 are for three different coils. The first coil is a 110 turn coil of 0.1mm diameter wire (dimensions

1.1mm length, 8.8mm outside diameter and 4.13mm internal diameter). The second is a 180 turn coil of 0.04mm diameter wire (dimensions 0.48mm length, 8.1mm outside diameter and 1.0 internal diameter). Finally the third was a (commercially wound) 450 turn coil of 0.03mm diameter wire (dimensions 0.44mm length, 10.29mm outside diameter and 1.0 m inside diameter).

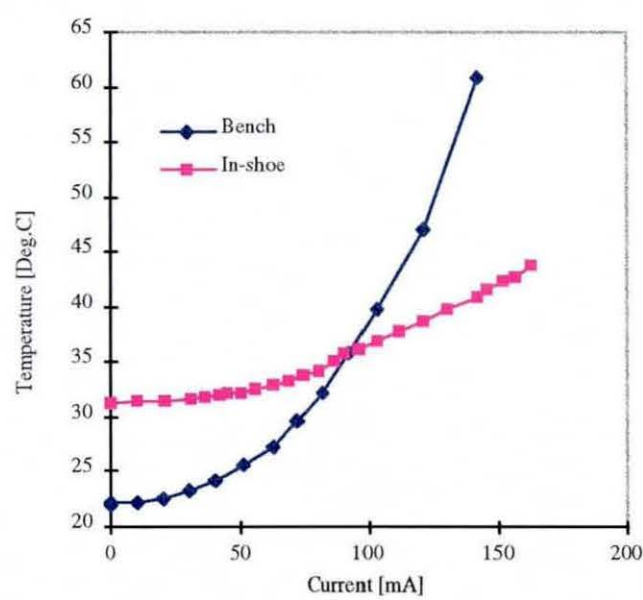


Figure 3-8 In-shoe and bench coil heating tests

Not surprisingly, the higher turn coil of very fine wire exhibits the most pronounced heating effect since it has higher resistance. Expressing the results in plots of Ampere-Turns versus temperature (figure 3.10) it is seen that the commercially wound coil of 450 turns excited with a 15mA drive current is best. This gives approximately the same temperature rise per Ampere-turn, but (neglecting differences in coil shape) requires less current to induce the same voltage in a secondary. Lowering the drive current required reduces the demands on the electronics.

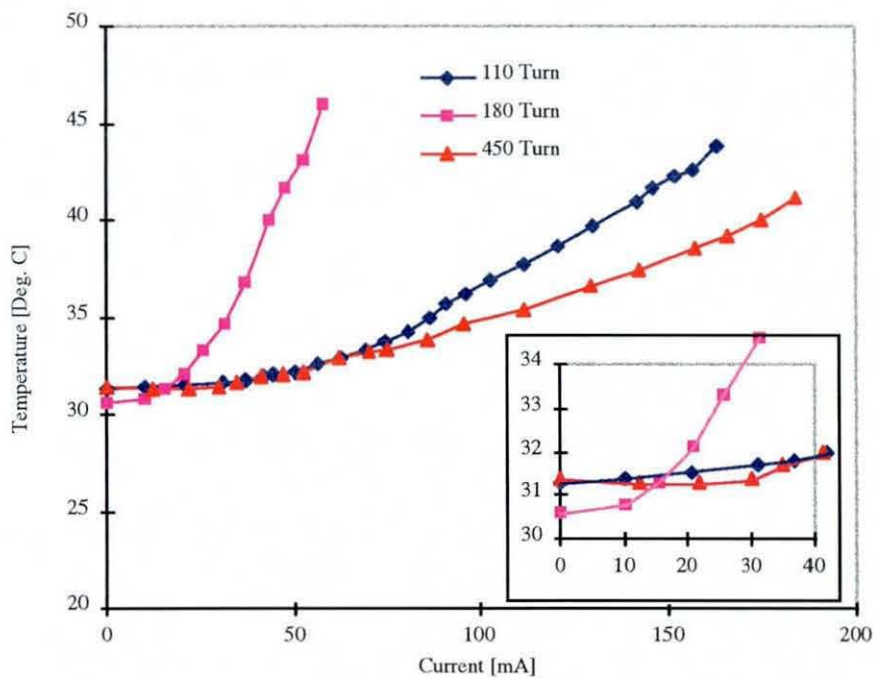


Figure 3-9 Temperature rise of coils with current

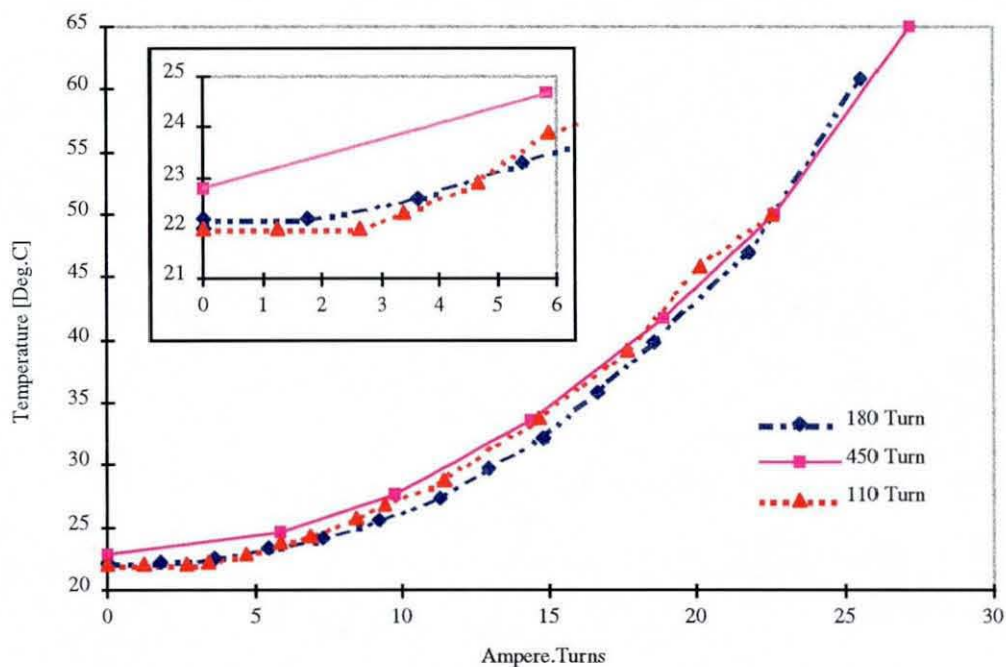


Figure 3-10 Current rise with ampere.turns

3.5.5 Investigation of the shape of the electromagnetic field produced

An investigation of the “shape” of the electromagnetic field produced by the pancake coils with a.c. excitation was carried out, i.e. the variation of the receiving coil’s induced voltage

was measured as its position relative to the excitation coil changed. In particular, measurements were carried out to determine the ranges of motion over which voltage change could be detected and the sensitivity and shape of the voltage to displacement characteristics for different coil pairs. In order to make the measurements a testing rig was designed and manufactured.

3.5.5.1 Test rig design

The design objective was to enable the accurate recording of three dimensional displacements of one coil relative to another. The displacements were to be along each of three orthogonal axes.

The design constraints derived were as follows:

- Maximum displacement along axes:

Vertical separation of coils, $z \geq 10\text{mm}$

Horizontal displacements $\geq x, y \pm 10\text{mm}$

- Minimum resolution of displacement measurement = 0.1mm (representing 1% of 10mm ranges).
- “Cross-talk” between displacements limited to 5%, that is an intended pure displacement along one axis would lead to a maximum magnitude of change of 5% of that displacement along any other axes.
- “Non-magnetic” (only weakly para or diamagnetic) material to surround the coils - coil mounts of magnetic material would artificially increase the induced voltage in the receiving coils.
- Easy mount/dismount of coils.
- Easy access to coil leads.

The design approach allowed each coil to be mounted upon a plate which could be easily removed from the rig. One of these plates would be constrained to move only vertically

when mounted. The other was constrained to move in the horizontal plane when in position on the rig. This motion was made up of a composite of movement along two perpendicular axes representing x and y . Figure 3.11 illustrates the basis of the design for the provision of the motion along each axis. A sliding table mounted upon a sliding table arrangement is used to achieve the x,y motion. Each table is mounted via linear roller bearings such that it has freedom to move along a defined horizontal axes with respect to the rig. One of the coil plates is mounted on the lower of these tables. A piston constrained to move only along an axis perpendicular to the planes in which the sliding tables lie provides the third axis of motion. The second coil plate is mounted on the end of this piston.

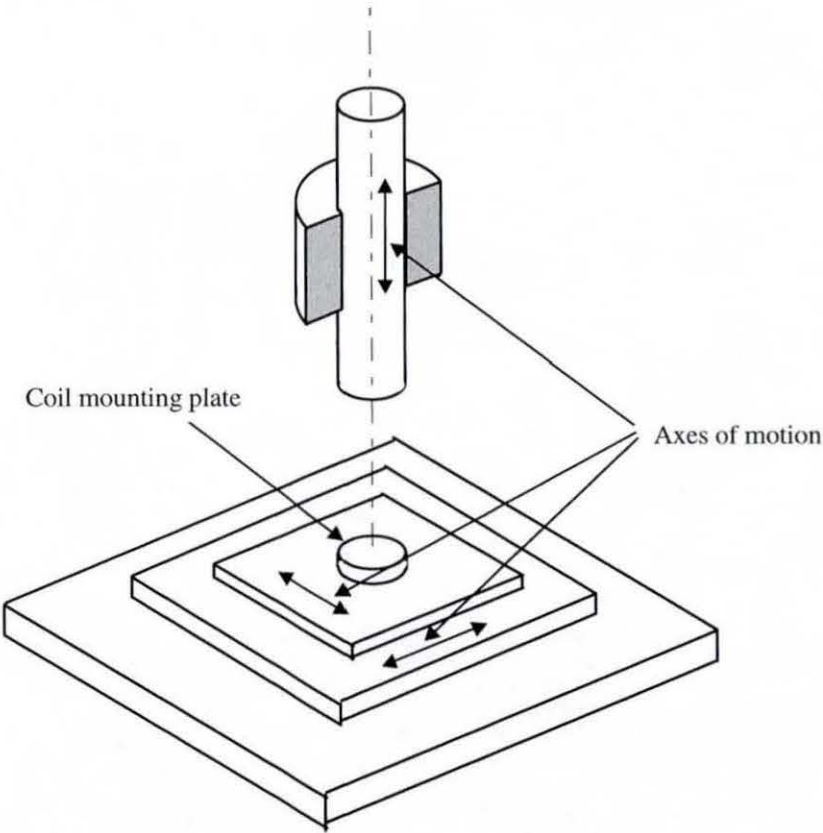


Figure 3-11 Basis of calibration rig

Whilst the rig's primary design objective was to enable controlled displacement measurements, its development into a force calibration rig was borne in mind during the design process.

A force application system was achieved using a cable, pulley and weight system for each of the three directions. This offered an inexpensive method of achieving a method of force application.

The fine control of displacement was achieved using a threaded bar and thumbscrew in opposition to the resistance of the force application system. A threaded bar was attached to each table and the piston. The bar was passed through a locating plate and a knurled nut used to pull the table/piston along its axis of freedom. In each case the adjustment nut was held against its locating plate by resistance from the respective force application systems for each axis. The movement of the tables/piston along each axis was measured using dial gauges positioned appropriately on the rig.

Wherever possible the rig was manufactured from non-metallic materials so there was no influence from the rig on the mutual induction between the coil pairs.

Appendix 2 contains detailed drawings of the rig and figure 3.12 shows a photograph of the device when assembled.

3.5.5.2 Coil characteristics - experimental method

Using the test rig, pairs of coils were mounted on the plates. One of the coils was excited with an a.c. current whilst the voltage induced in the other was measured. Measuring the induced voltage at a set of relative positions produced indications of the "magnetic field" i.e. a map for the coil pair was established in the volume around the excitation coil.

This map was important since it would determine the voltage/displacement properties of the final coil sets.

A sensitive transducer would require a measurable change throughout the likely displacement range of the transducer surfaces. This range would be determined by the force displacement properties of the mechanical element between the excitation and receiving coils. A particular combination of coil pair and mechanical element would provide ideal

force resolution for a selected force range. In this application the coil sizes are limited and thus there was a need to first determine the coil - displacement characteristics, and then select a suitable material for the mechanical element to ensure appropriate sensitivity and resolution over the force range required.

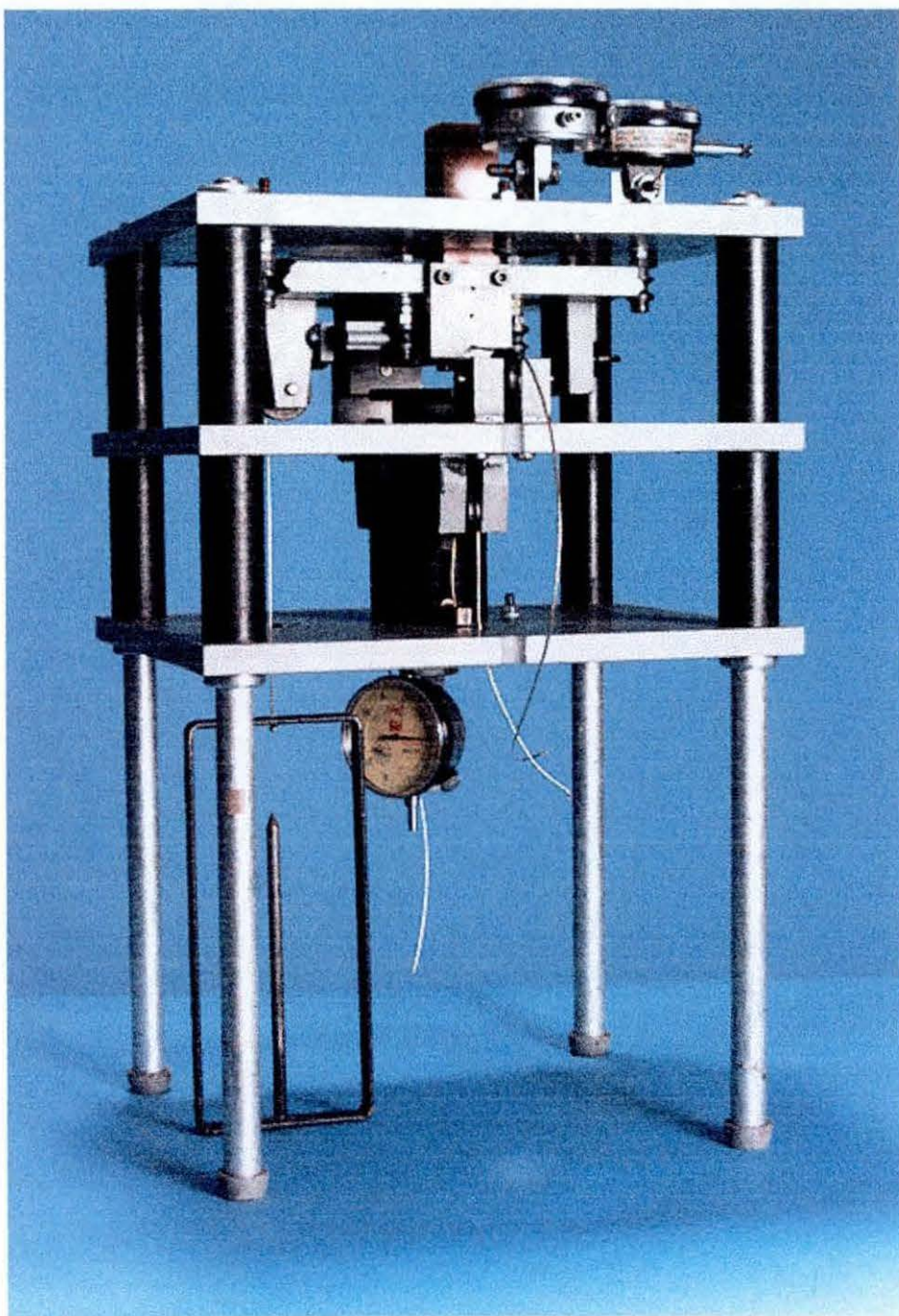


Figure 3-12 Calibration rig

3.5.5.3 Magnetic field characteristics - overview

A typical set of induced voltage versus displacement curves obtained with two "pancake" coils is illustrated in Figure 3.16 and 3.17. These were obtained using a 180 turn excitation coil (outside diameter = 8.11mm, internal diameter = 1.0mm and length = 0.48mm) and a 100 turn receiving coil (outside diameter = 4.54mm, internal diameter = 1.0mm and length = 0.48mm) of 0.04mm diameter wire.

A 30mA, 10kHz excitation current was used to obtain this data. This was derived from the current driver circuit described in figure 3.13. The circuit utilises a power amplifier to provide the current which is given by:

$$I = -\frac{R_f}{R_s \cdot R_{in}} \cdot V_{in} \quad (3.31)$$

provided $R_f \gg R_s$, irrespective of the load impedance (as long as the amplifier can produce enough voltage)

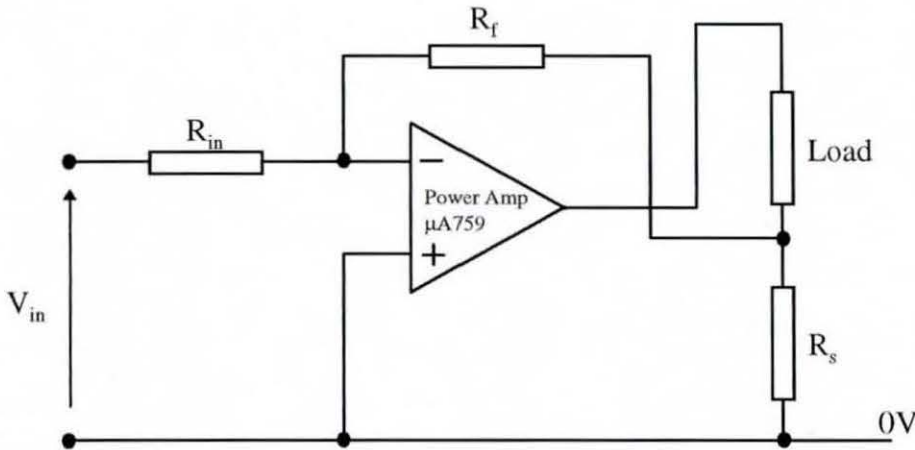


Figure 3-13 Current driver circuit

Figure 3.14 describes the induced voltage as a function of radial displacement at four different vertical displacements.

The coil displacement is such that at the midpoint of the curve both of the coil's longitudinal axes are aligned, i.e. the displacement is a radial displacement along the line of the diameter of both coils. As may be expected the peak of the induced voltage curve occurs as the

longitudinal axes of the two coils are aligned since the flux linkage will then be maximum. Either side of the central peak there is a nominally zero point in the response, with smaller peaks beyond. These represent the region in which the induced flux direction is reversed compared with the central position, as illustrated by figure 3.15.

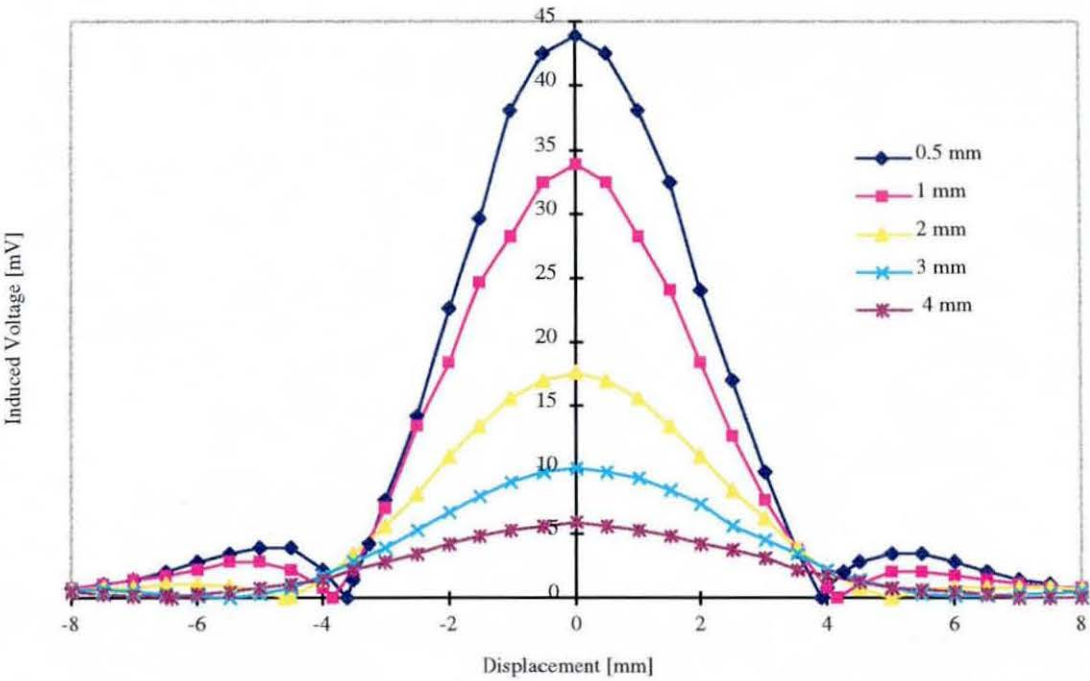


Figure 3-14 Induced voltage as a function of radial displacement

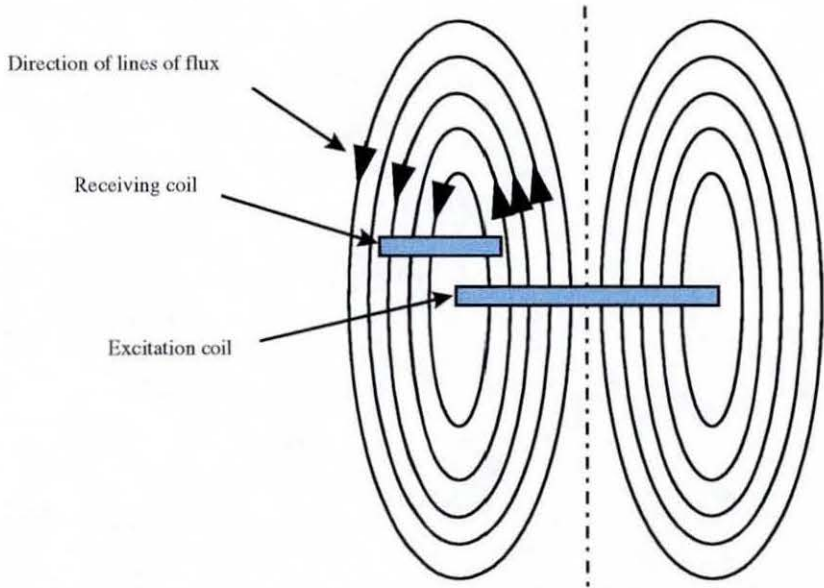


Figure 3-15 Direction of flux through receiving coil

Representing this change of phase as a voltage inversion (from -90 to 90 degrees shift from reference voltage) then we may view a typical curve as that shown in figure 3.16.

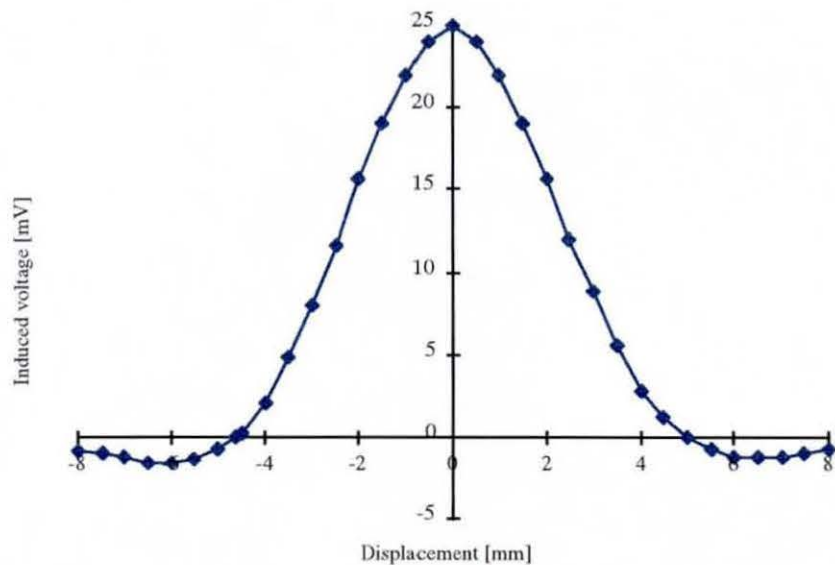


Figure 3-16 Induced voltage v radial displacement (phase inversion represented)

Figure 3.17 describes the induced voltage as a function of separation of the coils along the longitudinal axes of the coils (at a constant radial displacement of zero).

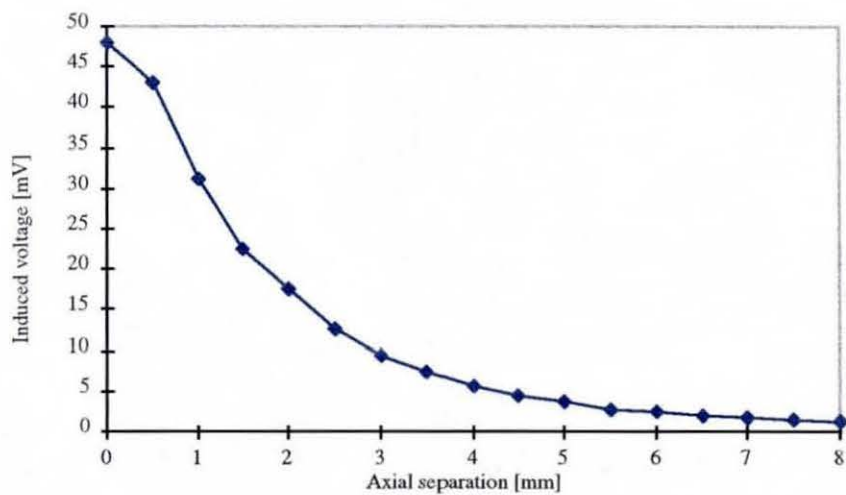


Figure 3-17 Induced voltage as a function of axial separation

Figure 3.18 illustrates the shape of the induced voltage “surface” for displacements in the x-y plane about the central axes of the coils for a vertical displacement, z. This surface was built up by taking measurements of induced voltage at a matrix of (x,y) co-ordinates (0.5 mm steps) lying in a plane perpendicular to the axis of the coils which are separated by a fixed vertical (2 mm) distance. Repeating this at various vertical separations shows that the whole of this surface is scaled up or down as a function of the vertical displacement of the coil pair.

From the induced voltage displacement curves we may derive finite displacements over which the receiving coil may be separated from the excitation coil and still exhibit significant induced voltage. This indicates the need to restrict the range of relative positions of the coil pairs in their use within a position sensor. Limits for the coil pair used in the test are indicated in figure 3.19.

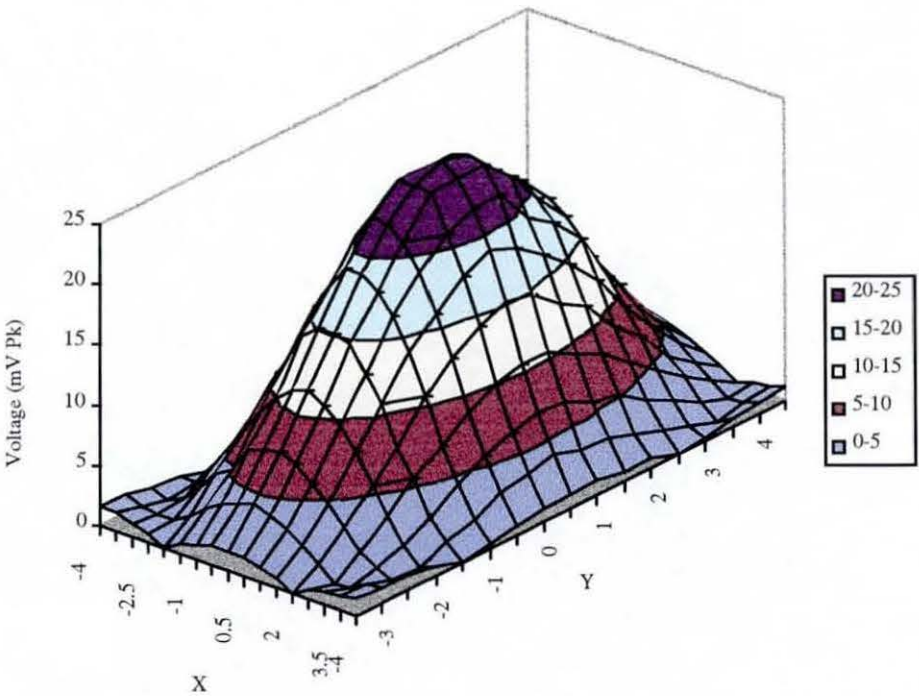


Figure 3-18 Induced voltage - displacement surface

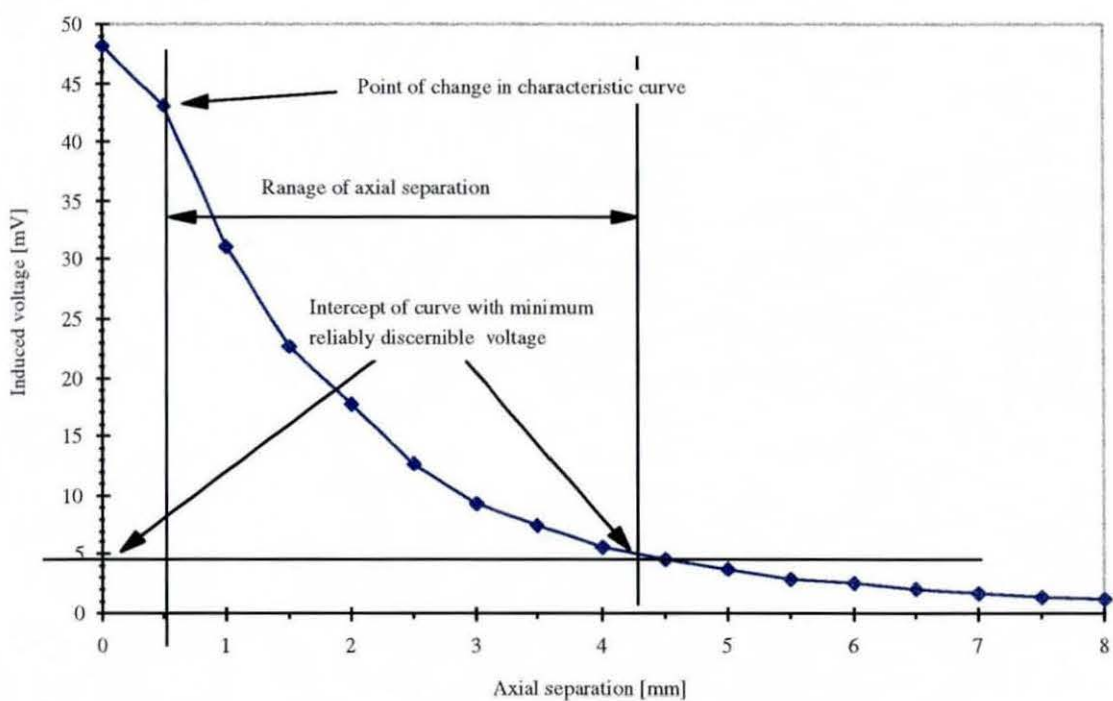
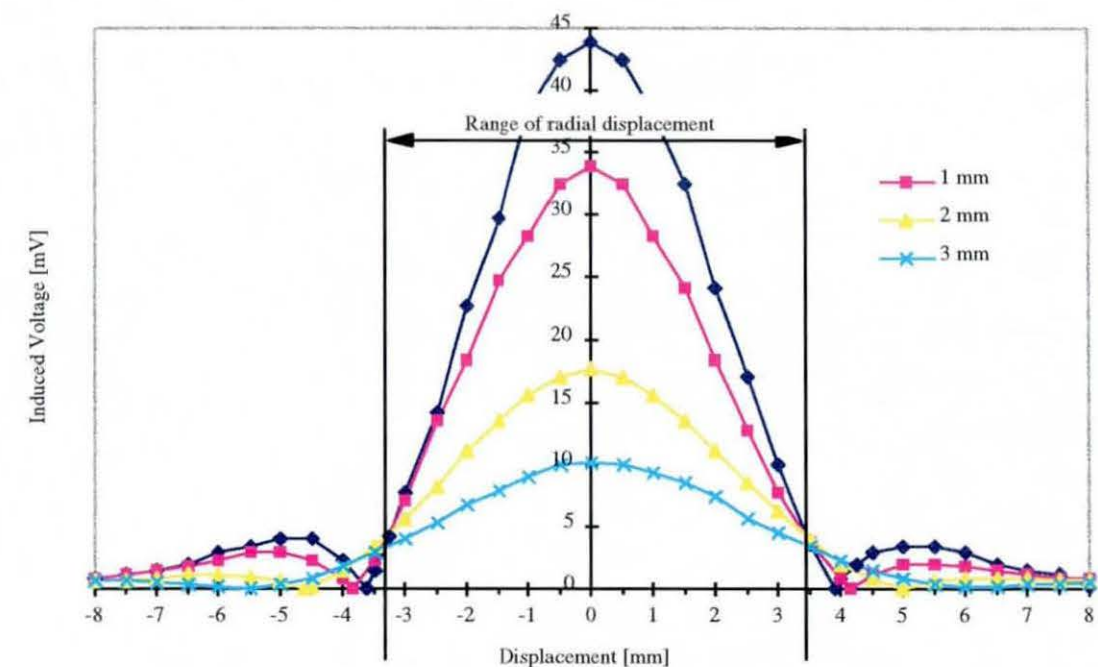


Figure 3-19 Range of coil pair relative positions

In the worst case (at an axial separation of 4mm) this would lead to a change in induced voltage of only 5mV for a radial shift of around 3.5mm. This contrasts with the situation

when the coils are separated by an axial displacement of 1 mm when a radial shift of 3.5 mm would lead to a change in induced voltage of some 40 mV.

Choosing coils with different dimensions will obviously affect the induced voltage-displacement characteristics. Figure 3.20 describes the induced voltage-radial displacement characteristics created using the same receiving coils together with each of two excitation coils. The excitation coils were of 10.25 and 8.11 mm diameter respectively, whilst the receiving coil was 4.55 mm diameter. The axial separation between the receiving coil and the excitation coil was 2 mm in each case.

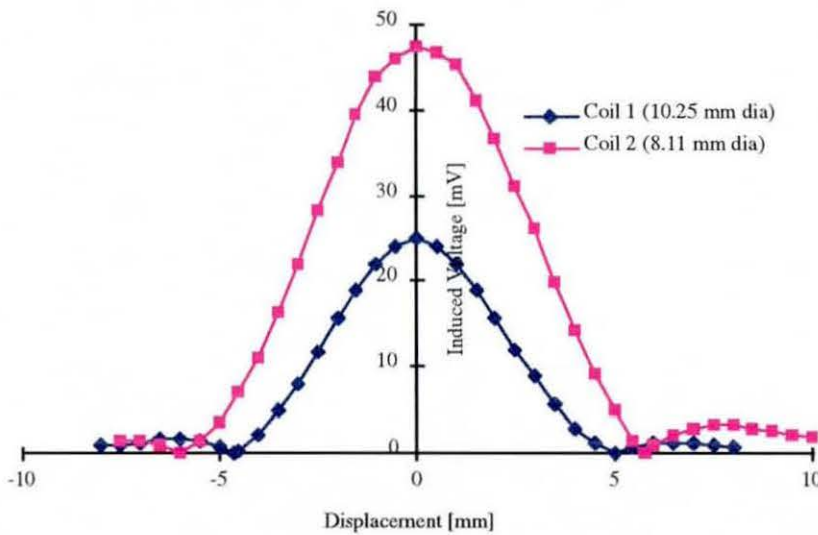


Figure 3-20 Induced voltage as a function of radial displacement

3.5.5.4 Magnetic field characteristics - analysis

In seeking a formal mathematical description of the induced voltage - displacement characteristics various models were proposed and examined. The radial displacement curves were examined separately from the axial displacement curves in the first instance. The curve fitting that was attempted was focused on obtaining the best fit over a limited range of displacements. For the coils used here, the ranges used were +/- 3mm of radial displacement and 1-4mm of axial separation.

Since the radial displacement curve is clearly an even function polynomial fits of order 2,4 and 6 were tested.

For a polynomial fit of degree N to a curve f(x) we need N+1 points on f(x) such that

$$\begin{aligned}
 a_0 + a_1x_0 + a_1x_0^2 + a_1x_0^3 +.....+ a_1x_0^{N-1} + a_1x_0^N &= f_0 \\
 a_1 + a_1x_1 + a_1x_1^2 + a_1x_1^3 +.....+ a_1x_1^{N-1} + a_1x_1^N &= f_1 \\
 &\vdots \\
 &\vdots \\
 a_0 + a_1x_N + a_1x_N^2 + a_1x_N^3 +.....+ a_1x_N^{N-1} + a_1x_N^N &= f_N
 \end{aligned}
 \tag{3.32}$$

Or writing these equations in matrix form:

where

$$\mathbf{V} = \begin{bmatrix} 1, x_0, x_0^2, x_0^3, \dots, x_0^N \\ 1, x_1, x_1^2, x_1^3, \dots, x_1^N \\ 1, x_2, x_2^2, x_2^3, \dots, x_2^N \\ \vdots \\ \vdots \\ \vdots \\ 1, x_N, x_N^2, x_N^3, \dots, x_N^N \end{bmatrix}, \mathbf{a} = \begin{bmatrix} a_0 \\ a_1 \\ a_2 \\ \vdots \\ \vdots \\ \vdots \\ a_N \end{bmatrix} \text{ and } \mathbf{f} = \begin{bmatrix} f_0 \\ f_1 \\ f_2 \\ \vdots \\ \vdots \\ \vdots \\ f_N \end{bmatrix}
 \tag{3.33}$$

Such that

$$\mathbf{V}.\mathbf{a} = \mathbf{f}
 \tag{3.34}$$

Then

$$\mathbf{a} = \mathbf{V}^{-1}.\mathbf{f}
 \tag{3.35}$$

provides the solution.

It was also noted that if the phase inversion was represented as a negative induced voltage as in figure 3.16 then the curve bears some resemblance to the sinC function, that is

$$\text{sinC } x = (\sin (\pi.x))/ (\pi.x)
 \tag{3.36}$$

(used with the assumption that $(\sin x)/x \rightarrow 1$ as $x \rightarrow 0$)

The results of the curve fitting were assessed in terms of mean and maximum absolute percentage error i.e.

$$\% \text{ error} = \text{absolute}(100.[\text{actual} - \text{predicted}]/\text{actual}) \tag{3.37}$$

over the restricted range of displacements of +/- 3mm radial displacement and 1-4mm axial separation. The table below gives a summary of the results for the four methods and figures 3.21-3.24 show the curves, curve fits, error and per cent error plots.

Radial displacements	Power 2	Power 4	Power 6	SinC
Mean absolute error	1.43	0.48	0.35	0.40
Maximum absolute error	3.11	1.23	0.68	1.03
Mean absolute % error	8.84	2.32	1.26	2.22
Max. absolute % error	16.08	5.46	3.01	4.31

Table 3.2 Results of curve fitting for radial displacement curves

In the same way polynomial fits of order 2, 3 and 4 were attempted for the axial displacement induced voltage curves. The typical curve also has the appearance of a inverse function such as

$$f(z) = 1/(1 + x^n) \text{ for } 2 > n > 1 \tag{3.38}$$

The errors produced by this model were evaluated to identify a value for n of 1.55.

The results of these models are listed in table 3.25 and the various curves shown in figures 3.26-3.28.

From the results we can see that for an error of around +/- 6 % (over the restricted ranges of motion) we require at least a 4th order fit to the radial displacement curves and at least a

2nd order fit to the axial displacement curves. The $\sin C$ function fit to the radial displacement curve provides an interesting alternative whose base and amplitude can be determined relatively quickly. The base, can in fact, even be estimated from the coil dimensions since it is close to the radial displacement at which phase inversion occurs, which itself is related to the coil dimensions as described in figure 3.16. As would be expected from the inevitable divergence of the magnetic flux at the end of the excitation coil, the radius at which phase inversion occurs varies with axial displacement (figure 3.29). The insert shows the radius of the point of phase inversion occurring from 3.5mm to 6.5mm as the axial displacement is increased from 0.5mm to 4mm

To some extent this brings into question the approach to modelling the 3 dimensional displacement-voltage relationship as a product of functions fitting the axial and radial displacement curves. That is, can a single radial displacement function scaled by an axial function model the relationship? However if the ranges of displacement are carefully chosen, such an approach, can provide a reasonable description. Figure 3.30 shows a series of 4th order curves modelling the actual radial displacement curves at 1, 2 and 3mm axial separation. Clearly these curves have, to a good approximation, a common point of intersection. Taking this into account figure 3.31 demonstrates that simple scaling of the radial displacement model for the 2 mm axial separation curve gives a good approximation ($\pm 5\%$) to the actual radial displacement at 1 and 3 mm axial separations (over ± 1.5 mm radial displacement).

Whilst it is clear that accurate modelling of the displacement-induced voltage relationship in the space over which discernible induced voltages occur would require extremely complex functions. It has been shown that over limited ranges relatively simple functions can be used to describe the relationship of three dimensional displacements of a “pancake” excitation coil relative to a “pancake” receiving coil to the voltage induced in the receiving coil.

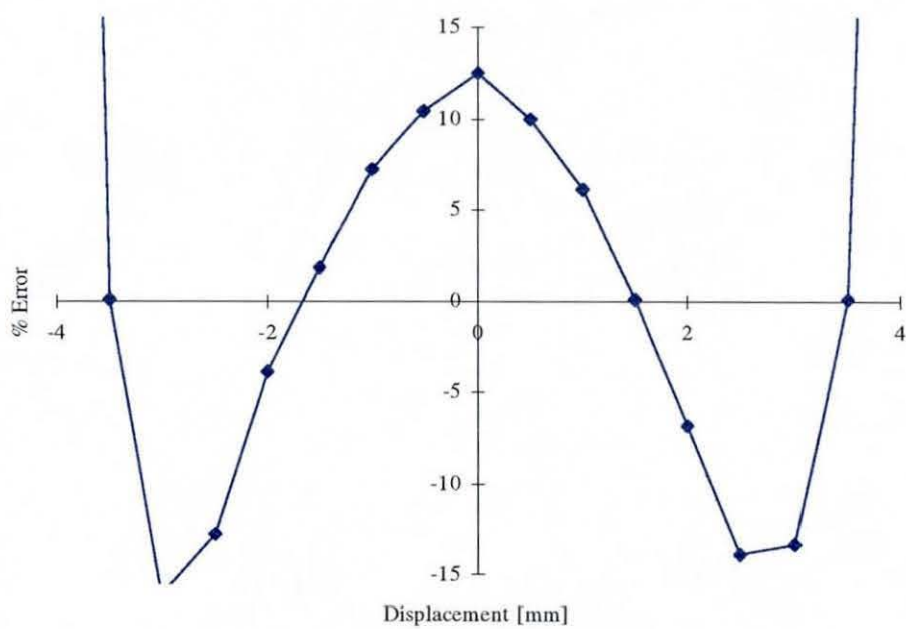
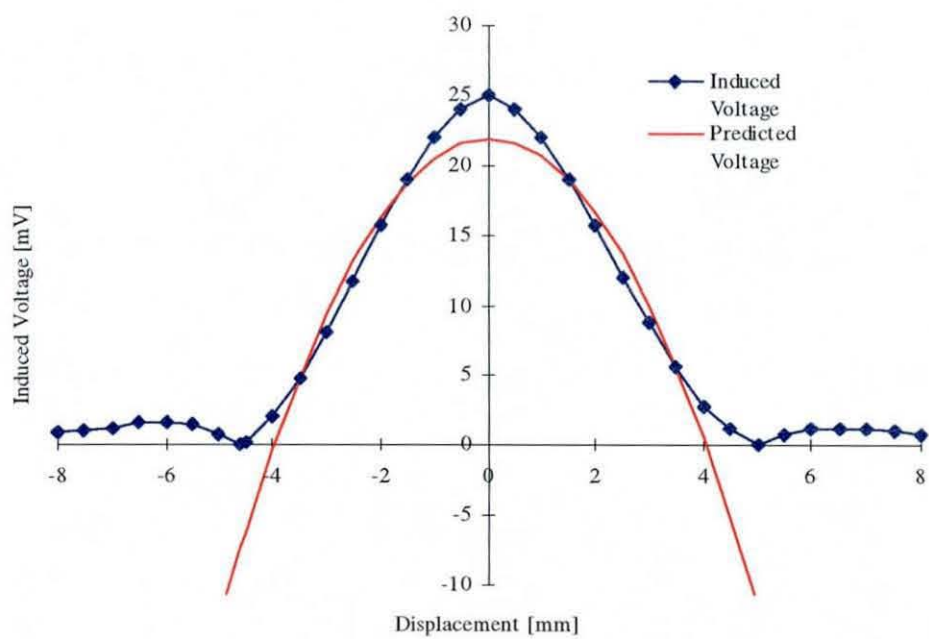


Figure 3-21 2nd order fit

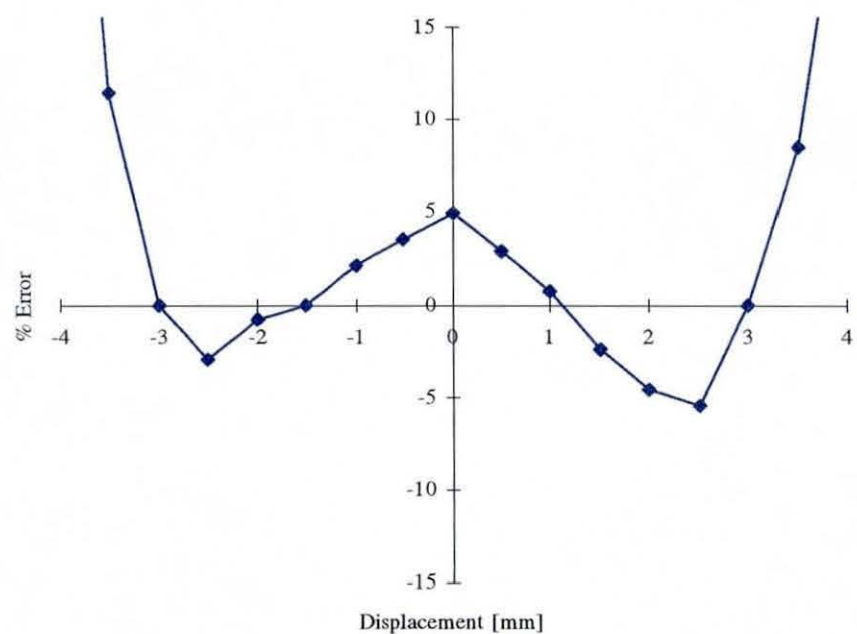
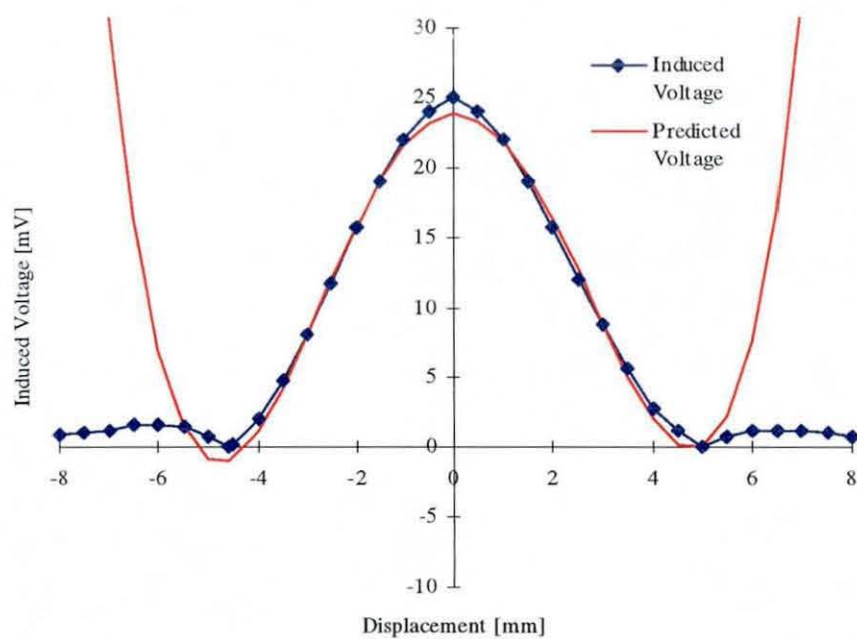


Figure 3-22 4th order fit

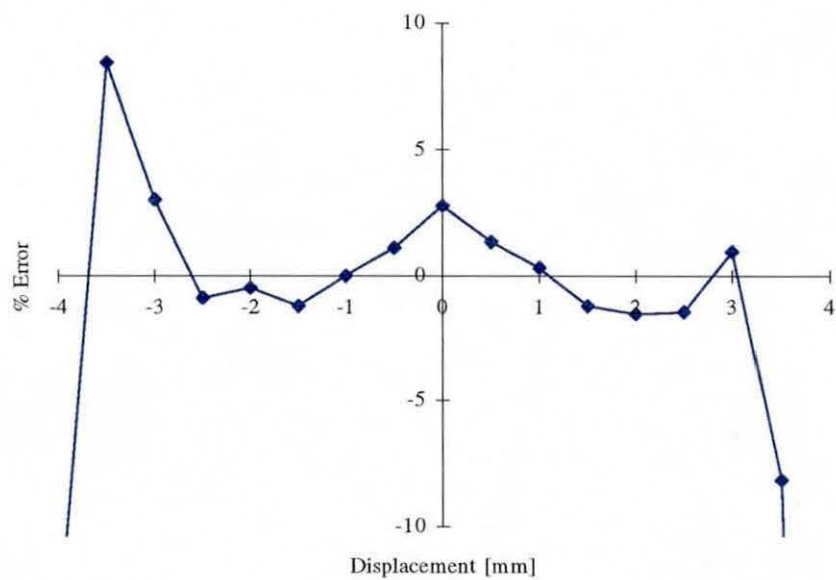
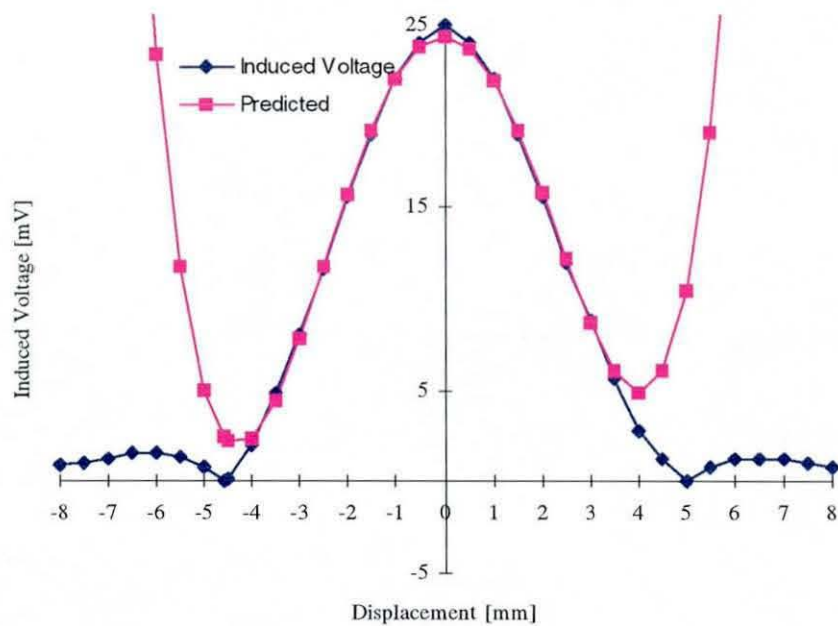


Figure 3-23 6th order fit

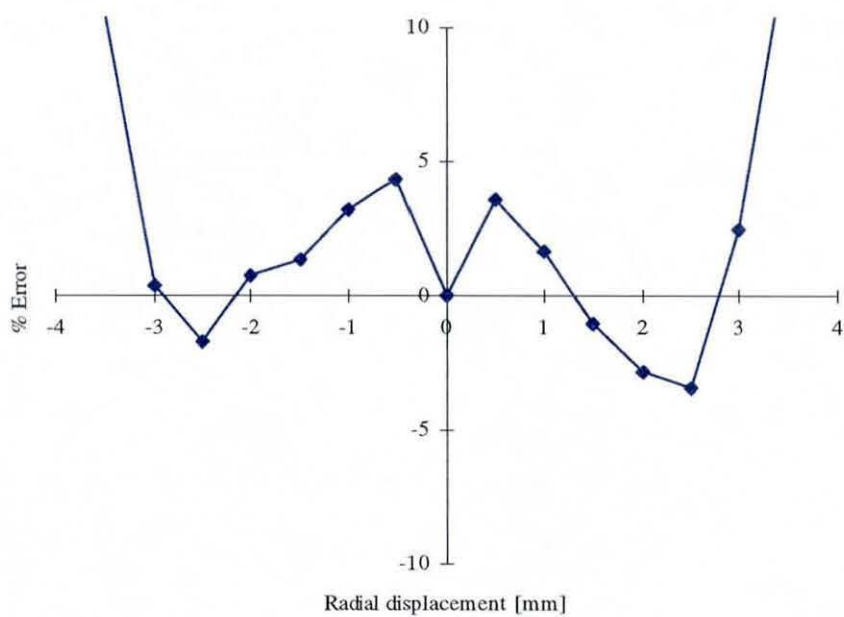
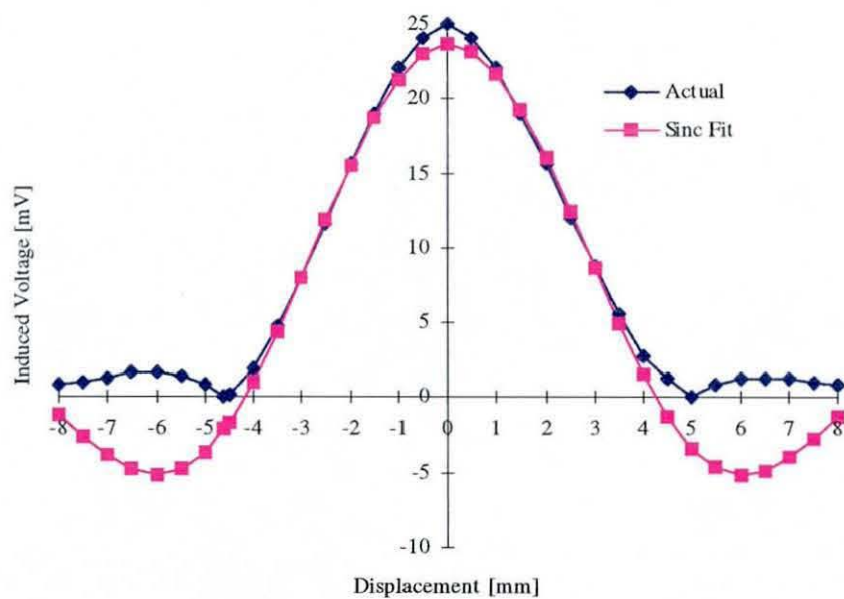


Figure 3-24 SinC fit

Axial displacements	Power 2	Power 3	Power 4	$A/(1 + x^{1.55})$
Mean absolute error	0.29	0.41	0.19	0.40
Maximum absolute error	1.24	1.07	0.54	1.03
Mean absolute % error	2.07	2.56	1.29	2.22
Maximum absolute % error	6.25	6.06	2.88	4.31

Table 3.3 Results of curve fitting to the axial displacement characteristics

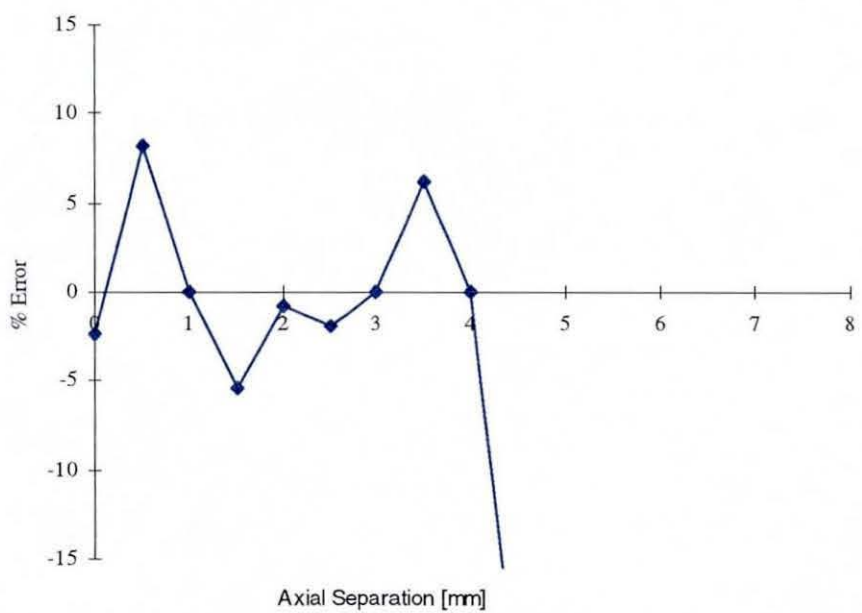
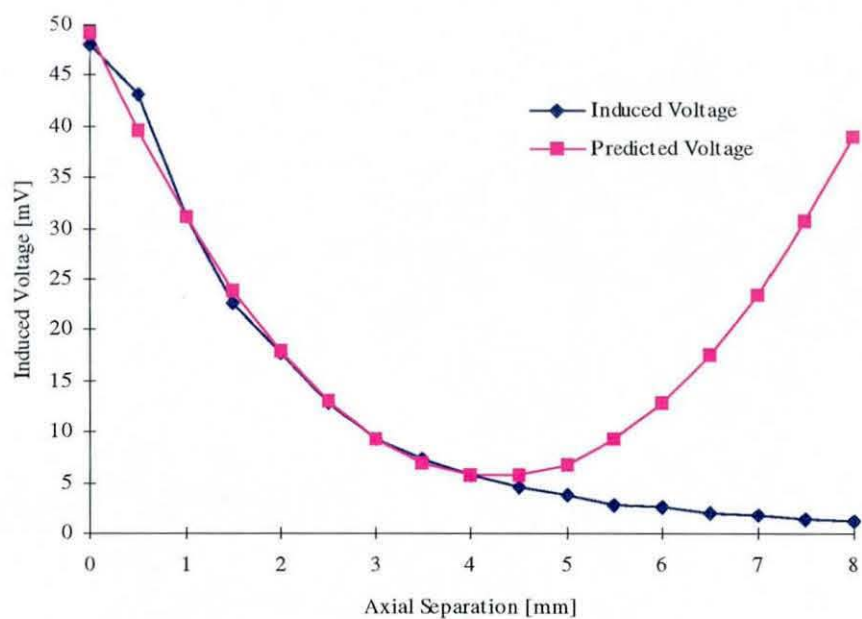


Figure 3-25 2nd order fit

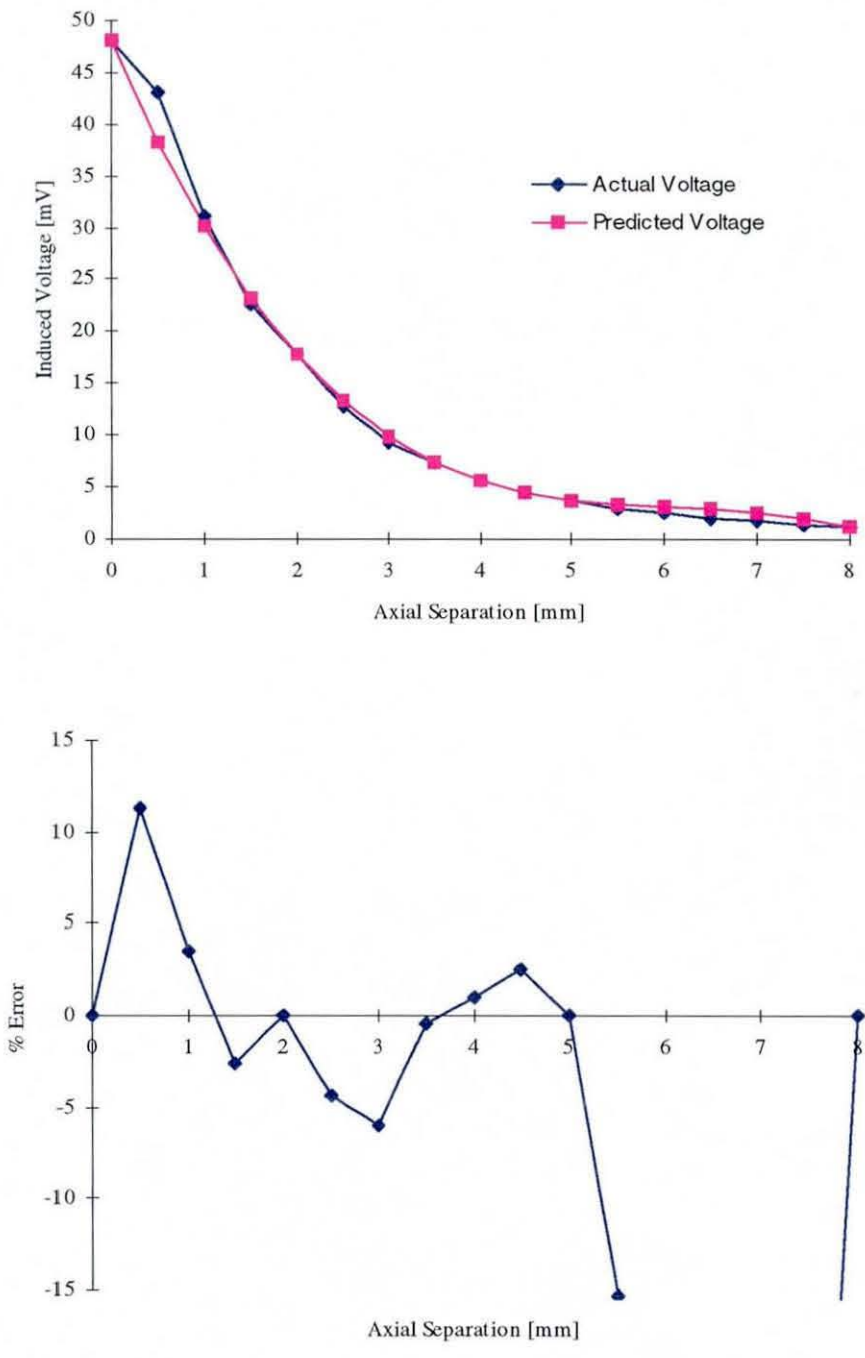


Figure 3-26 3rd order fit

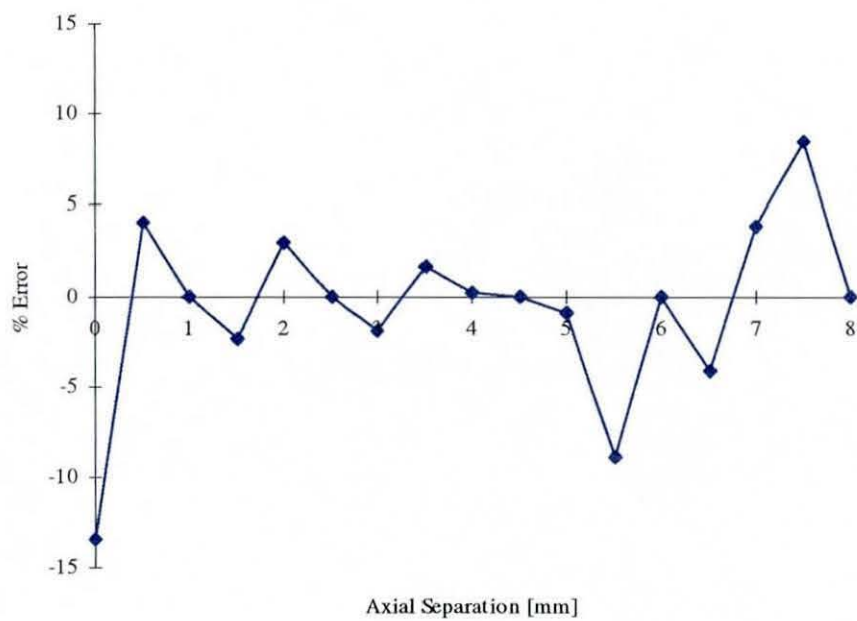
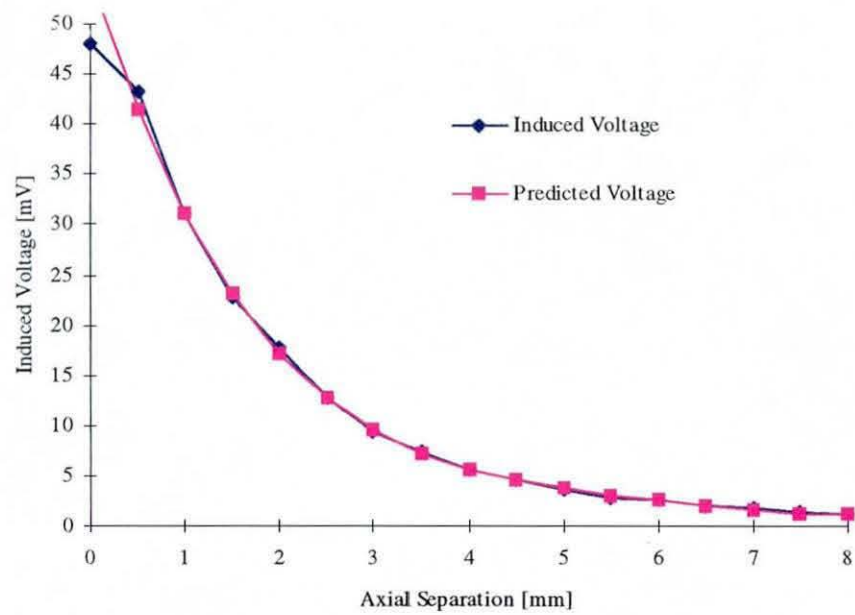


Figure 3-27 4th order fit

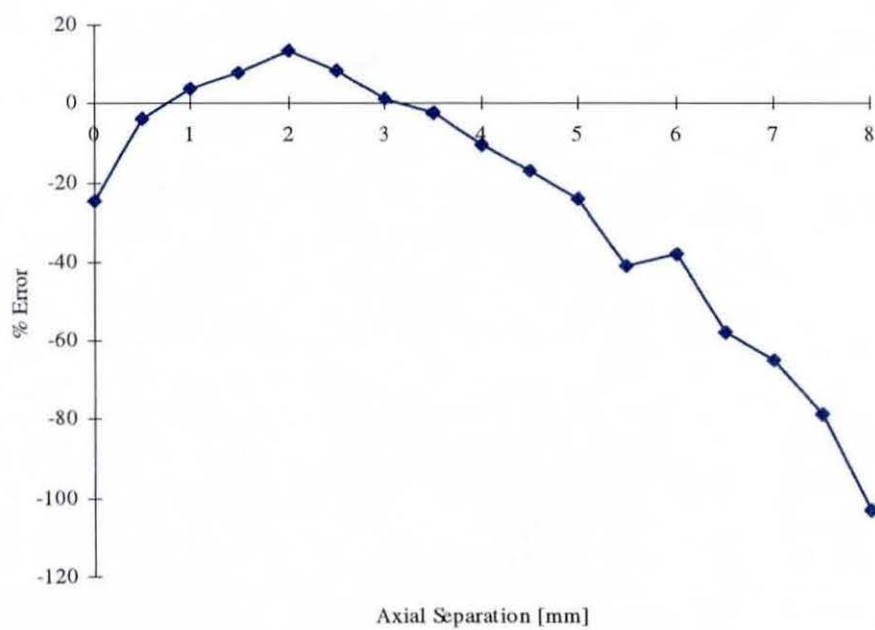
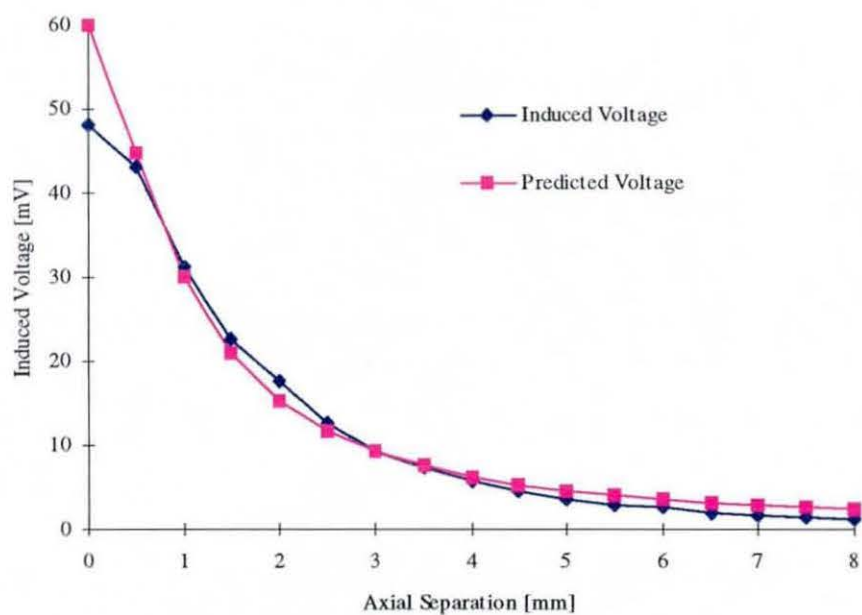


Figure 3-28 Inverse function fit

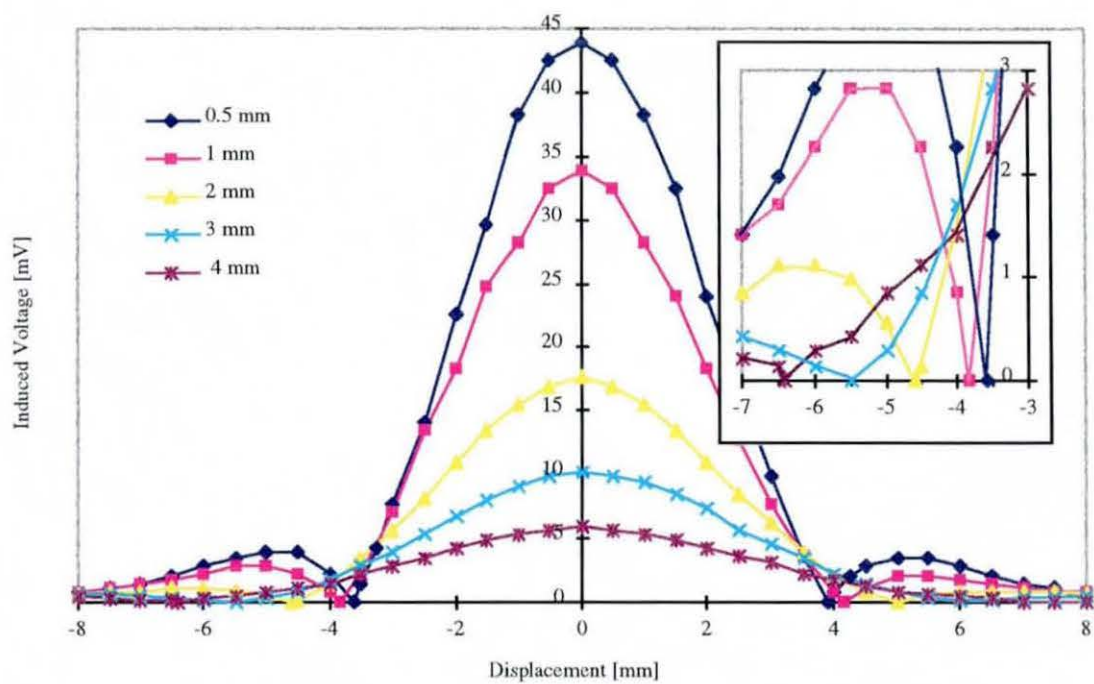


Figure 3-29 Variation of radius of point of phase inversion

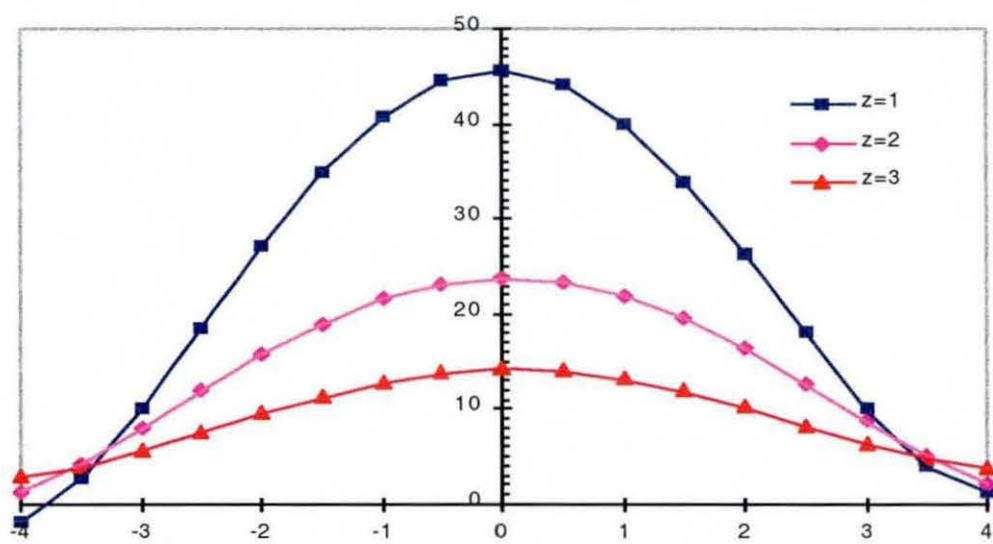


Figure 3-30 Radial displacement curves at 1, 2 and 3 mm axial separation

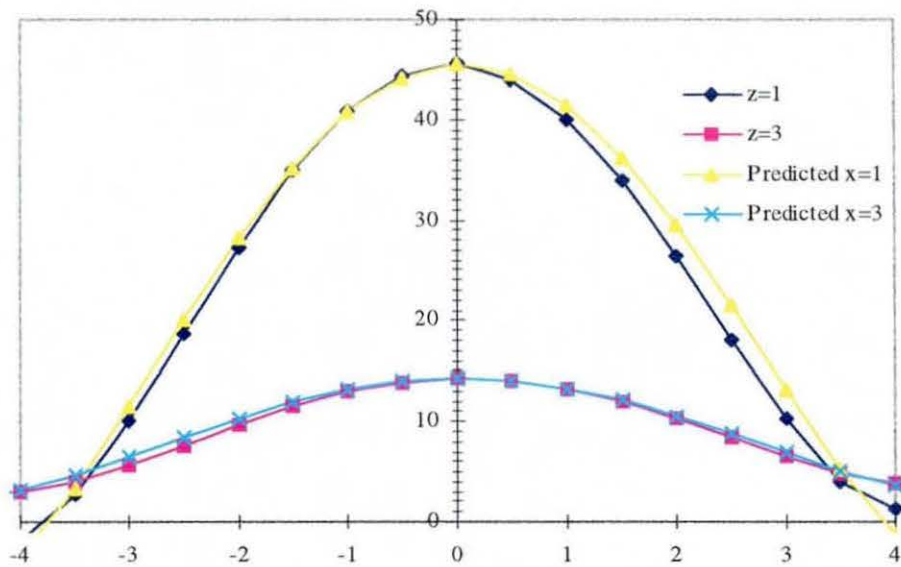


Figure 3-31 Radial displacement curves and scaled fits

3.6 SUMMARY

- The use of electromagnetic induction as a basis for the transducer has been proposed
- The design constraints have been used to identify maximum coil dimensions
- Coils have been manufactured and tested
- The results indicate that the induced voltage levels are sufficiently large and sensitive to be suitable for the design proposed.
- The induced voltage - 3 dimensional displacement relationship has been explored and various models examined.

4. MATHEMATICAL BASIS FOR 3D MEASUREMENT

4.1 PRINCIPLE

Description of the three dimensional displacements requires a minimum of three parameters, one for each dimension of space. An orthogonal axis system, x,y,z is typically used to describe movements in three dimensional space.

For a given separation of excitation and receiving coil the induced voltage in the receiving coil is a function of its position with respect to the exciting coil, although this is not uniquely so. An example as can be seen in figure 3.18 (page 54) which shows the voltage-radial displacement surface of a particular coil pair. A particular voltage V_{xy} would be a result of the displacement of the receiving coil by some radius r_{xy} from the central axis of the excitation coil. However this leaves an infinite number of solutions for x and y constrained (in the ideal case of circular coils of uniform winding) only by the limitation that:

$$r_{xy}^2 = x^2 + y^2 \quad (4.1)$$

Intuitively, given an excitation coil in one plane and a group of three non co-linear receiving coils in any parallel plane, displacements of the group of coils from the excitation coil would be able to be derived from knowledge of the changes in voltages induced in (all three of) them.

This approach is based on the fact that the minimum of three parameters required to reflect the three dimensions of spatial displacement (x,y,z) would be provided by the three voltages. That is, whilst the x,y position at a certain coil separation z was not unique for a single coil pair, the use of three receiving coils would resolve this indeterminacy.

Two approaches to extraction of the position (x,y,z) of the three receiving coils with respect to the excitation coil were examined. The first attempted to use an analytically derived mathematical description of the electromagnetic field whilst, the second, relied entirely on a calibration and look-up table approach.

4.2 SOLUTIONS

4.2.1 Planar model

From the previous chapter it has been established that the voltage induced in a coil is a non-linear function of both its radial displacement from the axis of the excitation coil in a plane perpendicular to it and of the axial separation between the coils. From the results expressed in figure 3.35 we expect to be able to describe the full relationship as the product of two functions (albeit over a limited range of motion), one a function of radial displacement, the other a function of vertical displacement. Mathematically:

$$V(r,z) = J(z).F(r) \quad (4.2)$$

in which V is the induced voltage, r is the radial displacement from the central axis, z the vertical distance between coils;

$J(z)$ and $F(r)$ represent unknown general functions which might, for instance, be suitably approximated by polynomial expressions as shown in chapter 3.

Using only one coil pair, the uniqueness of any induced voltage is not assured unless movement is restricted to an axis perpendicular to the planes in which both coils lie (the z axis) since the function $J(z)$, appears to have unique solutions for all z (in fact for all positive z less than some maximum). The displacement of the receiving coil from the other side of the excitation coil, negative z , would of course produce a similar function to the function $J(z)$ postulated for positive z .

Intuitively, the addition of two or more receiving coils at suitable positions should enable unique position determination in three dimensions. Each receiving coil would form a coil pair with the same single excitation coil. Referring to the voltage displacement surface of figure 3.18, valid at a particular separation, z , it can be seen that each receiving coil's axis will be located over a point on this surface. This will be represented by a voltage in each of the receiving coils. This voltage, together with the fixed geometric arrangement of the receiving coils, results in the necessary and sufficient independent variables with which to solve for the three unknowns (x,y,z), the position co-ordinates, of the centroid of the

receiving coil set relative to the excitation coil. Thus the problem becomes one of solving three equations of the form:

$$V_i(x,y,z) = J(z).F_i(x,y) \quad \text{for } i=1 \text{ to } 3 \quad (4.3)$$

The analysis of the voltage-displacement characteristics described in chapter 3. concentrated on describing the overall characteristics over relatively large displacements (compared with the excitation coil diameter). Given the proposed grouping of three receiving coils positioned centrally above the excitation coil, curve fitting may be considered over a much more restricted range of displacements. For instance given the situation depicted in figure 3.3 the maximum receiving coil diameter was shown to be 4.64mm. The undisturbed position of the coil would then be at a radius of 7.68mm with respect to the excitation coil centre. Keeping the centre of the receiving coil inside the outer diameter of the excitation coil to avoid the phase inversion point (see figure 3.17) will restrict the radial displacement of the coils to within at most $\pm 2.32\text{mm}$ of their reference positions. Clearly, the reduced range of motion allows much simpler modelling of the characteristics. Figure 4.1 illustrates an example of a set of characteristics curves over a restricted radial displacement. For this example, a linear approximation to the curves at each axial separation proves accurate to within $\pm 5\%$.

Given this situation where the radial displacements are small, and the coils spaced such that the displacement occurs on a linear portion of the radial displacement-voltage characteristic, and further that the tangential displacement to the radius is small, then the voltage-horizontal displacement characteristic may be considered a flat plane in (x,y,voltage) co-ordinates, one plane for each coil. Such planes would be described by:-

$$d = l.x + m.y + n.(voltage) \quad (4.4)$$

where l,m and n are the direction cosines of a normal to the plane, and d is the distance from the origin. F(x,y), this then, may be expressed as:

$$F(x,y) = a.x + b.y + c \quad (4.5)$$

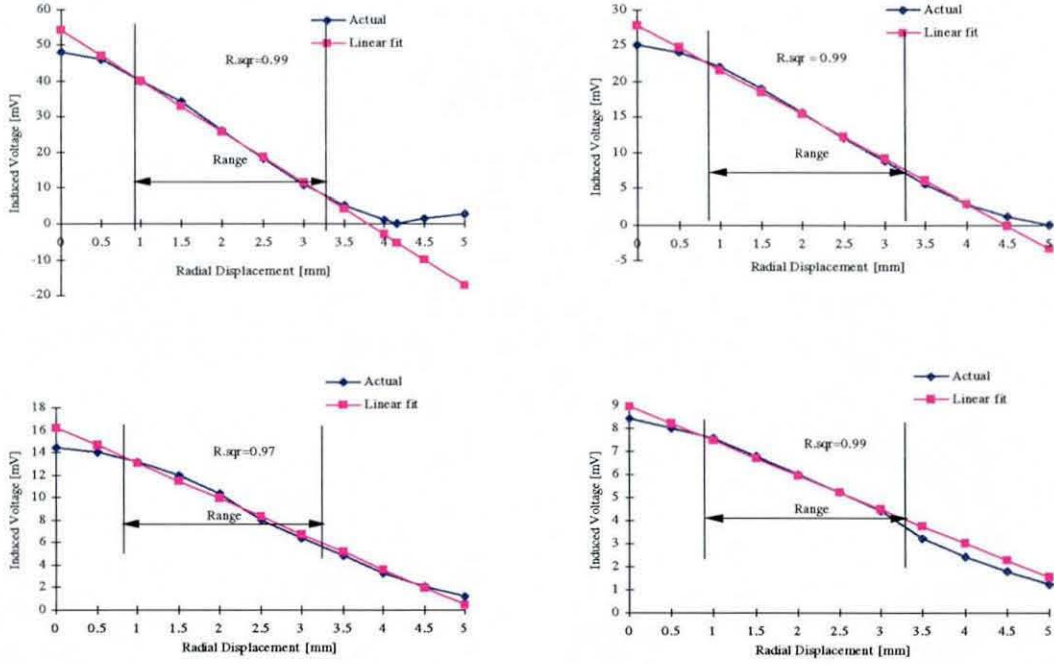


Figure 4-1 Linear regression over restricted range of displacement

Then in terms of the Cartesian co-ordinates x, y, z , noting how the height of the voltage-displacement surface is scaled as a function of z , the voltage at x, y, z may be expressed by:

$$V(x, y, z) = J(z) \cdot F(x, y) = J(z) \cdot (a \cdot x + b \cdot y + c) \quad (4.6)$$

Then using a quadratic approximation for $J(z)$, for coils 1 to 3:

$$V_1(x, y, z) = J(z) \cdot [c_1 + a_1 \cdot x_1 + b_1 \cdot y_1]$$

$$V_2(x, y, z) = J(z) \cdot [c_2 + a_2 \cdot x_2 + b_2 \cdot y_2] \quad (4.7)$$

$$V_3(x, y, z) = J(z) \cdot [c_3 + a_3 \cdot x_3 + b_3 \cdot y_3]$$

where:

$$J(z) = 1 + k_1 \cdot z + k_2 \cdot z^2 \quad (4.8)$$

If the three coils are conveniently placed at the corners of an equilateral triangle lying in the horizontal (x, y) plane then, the coils may be seen either to lie in the same horizontal plane but at different x, y co-ordinates, or they may be represented by three different co-ordinate systems. The co-ordinate systems of the coils are identical except that the horizontal x, y

plane of each coil's co-ordinate system is rotated by 120° to match the corner of the equilateral triangle at which the coil lies. Now for systems with axes x,y,z and x',y',z in which x',y',z is obtained from x,y,z by a rotation of ϕ° of the x,y plane about the z axis, the transformation required to translate co-ordinates in system x',y',z to express them in system x,y,z is:

$$\begin{bmatrix} x \\ y \end{bmatrix} = \begin{bmatrix} \cos \phi & -\sin \phi \\ \sin \phi & \cos \phi \end{bmatrix} \begin{bmatrix} x' \\ y' \end{bmatrix} \quad (4.9)$$

Thus if we make the axes of coil 1 the reference, and those of coils 2 and 3 obtained by rotations of $+120^\circ$ and -120° respectively then

$$x_1 = x$$

$$y_1 = y$$

$$x_2 = -x/2 - (\sqrt{3}/2).y$$

$$y_2 = (\sqrt{3}/2).x - y/2 \quad (4.10)$$

$$x_3 = -x/2 + (\sqrt{3}/2).y$$

$$y_3 = -(\sqrt{3}/2).x - y/2$$

Assuming that the coefficients a_i and b_i for each of the coils are the same, we can see that the sum of the three voltages will be independent of x and y and dependent only upon the initial voltages at the reference origin, and of course on the function $J(z)$. That is:

$$\sum_1^3 V_i(x, y, z) = J(z). \sum_1^3 V_i(0, 0, 0) \quad (4.10)$$

Thus the process of calibrating the coil set consists of choosing an origin, bearing in mind the coil pair characteristics, and selecting convenient calibration points to enable solution of the coefficients in equations (4.8) and (4.10). For instance, voltages at the points $(0,0,1)$ and $(0,0,-1)$ will enable k_1 and k_2 in $J(z)$ to be determined (equations (4.8), (4.10) and (4.7)). Strictly the voltages at the point $(1,0,0)$ may be used in equations (4.7) to determine

a_1 , a_2 and a_3 , although in practice an average from (1,0,0) and (-1,0,0) was used. Similarly the points (0,1,0) and (0,-1,0) for coefficients b_1 , b_2 and b_3 .

The converse process of converting a set of voltages into x,y and z is as follows:

First calculate

$$J(z) = \frac{\sum_{i=1}^3 V_i(x, y, z)}{\sum_{i=1}^3 V_i(0, 0, 0)} \quad (4.12)$$

This enables us immediately to solve the quadratic equation (4.8) to give z (one solution can readily be eliminated on the basis of being out of range i.e. the wrong side of the excitation coil). We can also substitute the value for J(z) into equations (4.7), and solve for x and y using the relationships given in equations (4.10).

The essential requirements for accuracy of this method are reasonably apparent: Throughout the range of operation the assumed functions are representative (linear for x and y, quadratic for z), and also that the coefficients of x , y and J(z) in the above expressions are the same for each coil and that coils are positioned accurately. Additionally the planes in which the coils lie must be kept parallel.

4.2.2 Look-up table method

Whilst four coils are again used with this method, the precise positioning of the three receiving coils is not fundamental to the approach. The only requirement is that they remain a fixed distance apart. The first stage involves the collection (by means of calibration) of three, 3-dimensional matrices containing the induced voltages at a network of positions in 3-dimensional space . The converse process of extraction of the position (x,y,z) from the actual voltages (V_{1a} , V_{2a} , V_{3a}) then involves location of the nearest point in the matrices, followed by linear interpolation about that point, as follows:

Select the nearest point P from the matrices for which

$$[(V_{1a} - V_{1n}) + (V_{2a} - V_{2n}) + (V_{3a} - V_{4n})] \text{ is minimum} \quad (4.13)$$

where (V_{1n}, V_{2n}, V_{3n}) are the voltages at point P in the matrix. Now if we write the exact functions which give the voltage versus position for each coil as functions f where

$$V_i = f_i(x, y, z) \text{ for } i = 1 \text{ to } 3 \quad (4.14)$$

Now at any point x, y, z , a small change in V_i may expressed as

$$\delta V_i = (\partial f_i / \partial x) \delta x + (\partial f_i / \partial y) \delta y + (\partial f_i / \partial z) \delta z \quad (4.15)$$

$$\begin{bmatrix} \delta V_1 \\ \delta V_2 \\ \delta V_3 \end{bmatrix} = \begin{bmatrix} \partial V_1 / \partial x, \partial V_1 / \partial y, \partial V_1 / \partial z \\ \partial V_2 / \partial x, \partial V_2 / \partial y, \partial V_2 / \partial z \\ \partial V_3 / \partial x, \partial V_3 / \partial y, \partial V_3 / \partial z \end{bmatrix} \begin{bmatrix} \delta x \\ \delta y \\ \delta z \end{bmatrix} \quad (4.16)$$

or

$$\delta \mathbf{V} = \Delta \mathbf{V} \delta \mathbf{P} \quad (4.17)$$

and so

$$\delta \mathbf{P} = (\Delta \mathbf{V}^{-1}) \delta \mathbf{V} \quad (4.18)$$

$\delta \mathbf{V}$ can be calculated by taking the nearest voltages \mathbf{V}_n from the actual voltages

$$\delta \mathbf{V} = \mathbf{V}_a - \mathbf{V}_n \quad (4.19)$$

$\delta \mathbf{P}$ can now be calculated from equation 4.17 using $(\Delta \mathbf{V})^{-1}$ and the actual position is

$$\mathbf{P}_a = \mathbf{P}_n + \delta \mathbf{P} \quad (4.20)$$

in which \mathbf{P}_n are the values of x, y and z for the nearest point identified in equation 4.10.

From each (of the three) 3-dimensional matrices of voltages it is possible to determine the range of voltages induced in each of the receiving coils respectively throughout the entire volume of possible positions. Each of these voltage ranges may then be subdivided into suitably fine steps and each combination of $(V_{1sub}, V_{2sub}, V_{3sub})$ may be processed to calculate the corresponding (x, y, z) co-ordinates for each $(V_{1sub}, V_{2sub}, V_{3sub})$ combination. This process is performed off-line to produce matrices of positions x, y and z at evenly spaced voltages (V_1, V_2, V_3) over the defined range.

This data may then be used for rapid position determination from any given (V_1, V_2, V_3)

So for a set of voltages, V_a , the nearest set of voltages, V_b , in the matrix, is found to identify the co-ordinates (x, y, z) as a first approximation to the actual position.

The partial derivatives in three dimensions can readily be deduced from the adjacent values in the matrices. We can then interpolate linearly between the evenly spaced voltages:

$$\begin{bmatrix} \delta x \\ \delta y \\ \delta z \end{bmatrix} = \begin{bmatrix} \partial x / \partial V_1, \partial x / \partial V_2, \partial x / \partial V_3 \\ \partial y / \partial V_1, \partial y / \partial V_2, \partial y / \partial V_3 \\ \partial z / \partial V_1, \partial z / \partial V_2, \partial z / \partial V_3 \end{bmatrix} \begin{bmatrix} \delta V_1 \\ \delta V_2 \\ \delta V_3 \end{bmatrix} \quad (4.21)$$

The maximum range of displacements detectable with this approach is limited only by the range over which a reasonable level of induced voltage is achieved. The accuracy obtainable is dependent upon the number of points used in the calibration table and the non-linearity of the induced voltage-displacement characteristics. For the results presented below a matrix of $13 \times 13 \times 7$ points in x, y and z respectively was used, resulting in 1183 calibration points for each of V_1, V_2 and V_3 .

4.2.3 Hybrid method

The first method in practice was found to be quite inaccurate. The limitation with the model occurs in representing the function $F(r)$ as a linear function of (x, y) since strictly it is a function of the radial displacement between the central axes of the excitation and receiving coils. The plane which is represented by the linear function in (x, y) will be tangential to the actual surface of the characteristic surface. This means that the greater the movement away from the central point, expressed as a fraction of the pitch circle of the centres of the coils, the greater will be the error. This radius is quite small in this application since the outside diameter of the transducer must be less than 10mm. Obviously for the same fractional error, the tangential displacement would need to be reduced as the radius of the excitation coil is reduced.

More complex expressions for $J(z)$ and $F(r)$ were required. Strictly for the conic model:

$$V_i(x, y, z) = J(z) \cdot [q_0 - q_1 \cdot r_i] \quad (4.22)$$

where

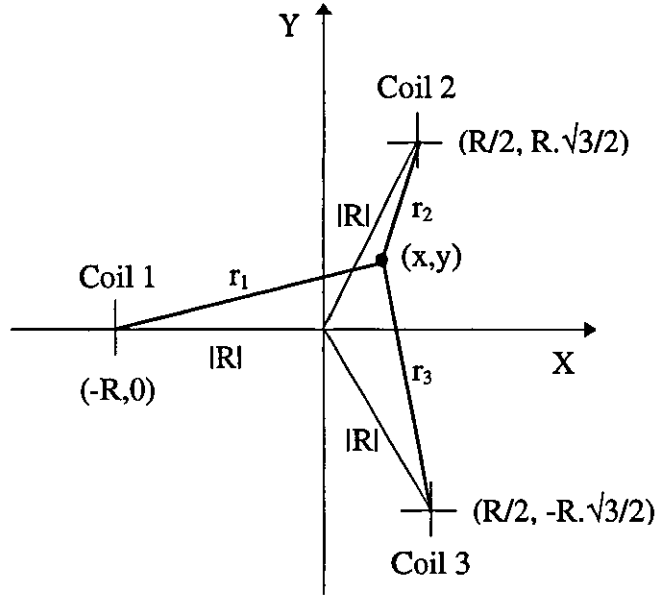


Figure 4-2 Relationships of radii to displacement

$$\begin{aligned}
 r_1 &= \sqrt{(y^2 + (x + R)^2)} \\
 r_2 &= \sqrt{(y - R \cdot \sqrt{3}/2)^2 + (x - R/2)^2} \\
 r_3 &= \sqrt{(y + R \cdot \sqrt{3}/2)^2 + (x - R/2)^2}
 \end{aligned} \tag{4.23}$$

giving

$$\begin{aligned}
 V_1(x,y,z) &= J(z) \cdot [q_0 - q_1 \cdot \sqrt{(y^2 + (x + R)^2)}] \\
 V_2(x,y,z) &= J(z) \cdot [q_0 - q_1 \cdot \sqrt{(y - R \cdot \sqrt{3}/2)^2 + (x - R/2)^2}] \\
 V_3(x,y,z) &= J(z) \cdot [q_0 - q_1 \cdot \sqrt{(y + R \cdot \sqrt{3}/2)^2 + (x - R/2)^2}]
 \end{aligned} \tag{4.24}$$

where $J(z)$ is still described by

$$J(z) = 1 + k_1 \cdot z + k_2 \cdot z^2 \tag{4.25}$$

Thus we have three equations in three unknowns, although the solutions (if they exist) are far from obvious. In any case, this of course assumes that the values of k_1, k_2, q_0 and q_1 are the same for each receiving coil/excitation coil combination. Additionally the excitation coil winding is perfectly symmetrical. These conditions are difficult to achieve in practice. In fact for a wider range of movement it was shown in Chapter 3. that higher order equations are needed. Solutions of higher order equations posses even more difficulty. However an alternative approach may be used. Given that the look-up table method described above avoids the necessity of solving high order polynomials, a hybrid combination of the approaches of the mathematical model involving limited calibration (and thus limited time and high order polynomial approximations) together with the look-up table technique using data generated by such a model was developed.

A series of radial sweeps passing through the longitudinal axis of each receiving coil in turn were made at different vertical separations (of receiving and excitation coils) i.e. a series of characteristics such as that those in figure 3.14 were collected. A fourth order (in radius) approximation was made to each of these (using least squares) and then in turn a third order (in vertical separation) approximation was made to each of the coefficients of the radial functions. In this way a model of the form:

$$V(x,y,z) = J(z).F(r) \text{ where } r^2 = x^2 + y^2 \quad (4.26)$$

was calculated using a limited calibration. This model was used to generate a set of data representing V_1, V_2, V_3 at a series of (x,y,z) which could then be used with the look-up table method described above. Thus high order polynomials could be used to model the induced voltage characteristics without the need for solution of these in order to extract position data from the induced voltages. The results of this approach are presented in the next chapter.

4.3 CHAPTER SUMMARY

- The concept of using three receiving coils to enable determination of 3 dimensional displacements of the group of three coils from the excitation coil has been presented
- Three different methods for the determination of the position from the voltages induced in the receiving coil have been put forward.

5. PROTOTYPE IMPLEMENTATION

5.1 DEVELOPMENT STRATEGY

The analysis methods described in the previous chapter are based on the relationship of the displacement of receiving coils relative to the excitation coil. The extension to force assessment, as has discussed previously, is made by inserting the mechanical restraining element - the rubber or rubber like insole material. This will effectively superimpose the force - displacement characteristics on top of the voltage-displacement characteristics of the coil sets to produce the final force-voltage relationships. In order to efficiently evaluate the analysis methods proposed, it was decided to evaluate the transducer concept without the mechanical element in place so as to evaluate what was effectively a three dimensional displacement transducer. The rig built for the coil pair tests was modified such that groups of coils could be mounted on one face and an excitation coil could be mounted on the other face. This enabled calibrated relative motion of the excitation coils with respect to the receiving coils.

5.2 COIL SET ASSEMBLY

Having derived the theoretical basis for a transducer, it was clearly necessary, in order to implement it, to develop methods of bringing robust leads off from the very fine wire of the coils and also of securing the three receiving coils together.

Various methods were attempted with varying degrees of success observed when the arrangements were subjected to mechanical wear and tear. Use of a common neutral for each of the receiving coils reduced the number of leads to be brought off. Figure 5.1 illustrates the method adopted for both the receiving and excitation coils. Cyanoacrylate was used as both the coil bonding agent during coil winding and for bonding the lead wires to the edges of the coils/coil arrays. A jig was manufactured to aid the assembly process and this helped position the centre of each coil at the corner of an equilateral triangle.

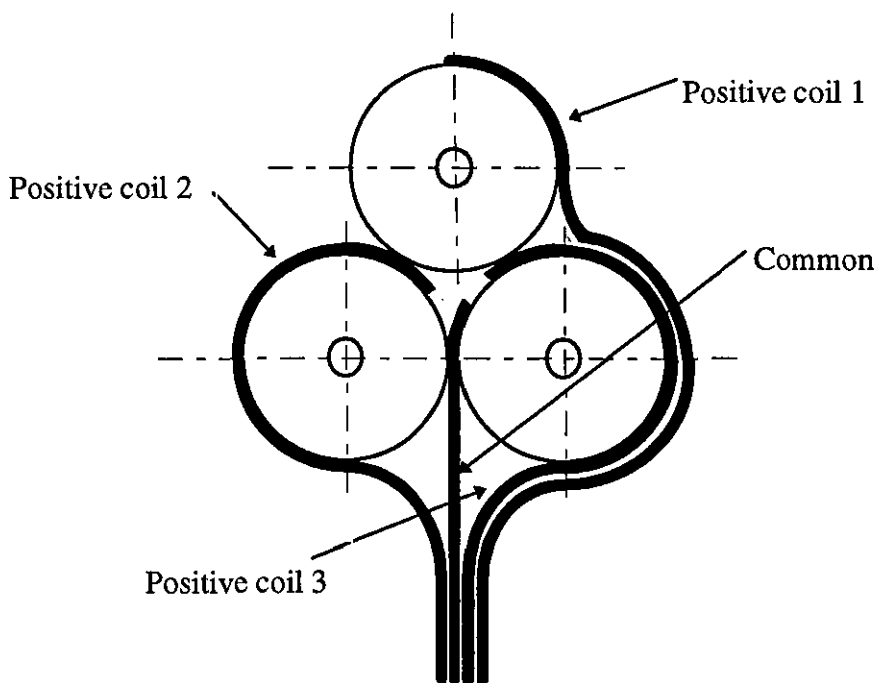
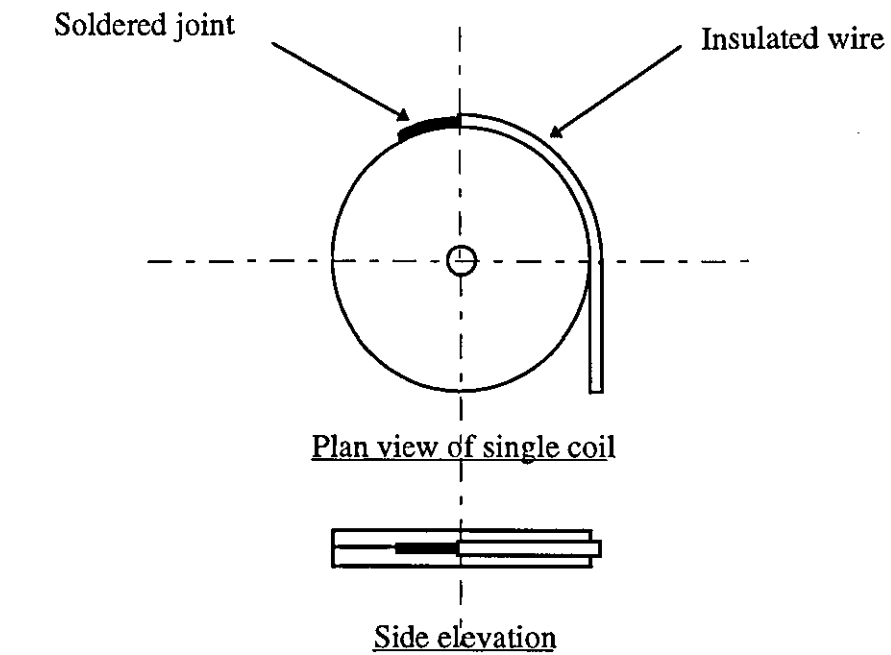


Figure 5-1 Method of attaching lead wires

The configuration of the three receiving coils had implications for both the maximum diameter of the these coils and the diameter of the transducer as a whole. If the excitation coil is used as the upper surface of the transducer (at the foot-shoe interface) then, its diameter will determine the area over which force assessment is made. The receiving coil sets could then be allowed diameters such that their edges are contained within an area larger than the excitation coil. This has implications for the minimum spacing of an array of such transducers. Other factors constraining this will be the wiring “lead-off” problem and interference due to movements of surrounding coils (that is, in changes in magnetic media surrounding the coils of a particular transducer).

5.3 ELECTRONIC HARDWARE

The electronic hardware required for the transducer was designed and manufactured specifically for the project. The system may be conveniently divided into signal generation, coil excitation, detection and recording stages.

The methods of excitation and detection are particularly important to the success of the transducer.

Figure 5.2 is a schematic of the system for signal generation, detection and recording. The signal source is a 20kHz sinusoidal wave. This frequency was arrived at as a compromise being high enough to result in sufficiently large enough induced voltage. Higher frequencies produce larger induced voltages per unit peak current but require higher specification electronics to process them without degradation of signal. The main features of the overall system are:

5.3.1 Signal generation stage

Figure 5.3 shows the simple circuit enabling utilisation of a commercial signal generation chip.

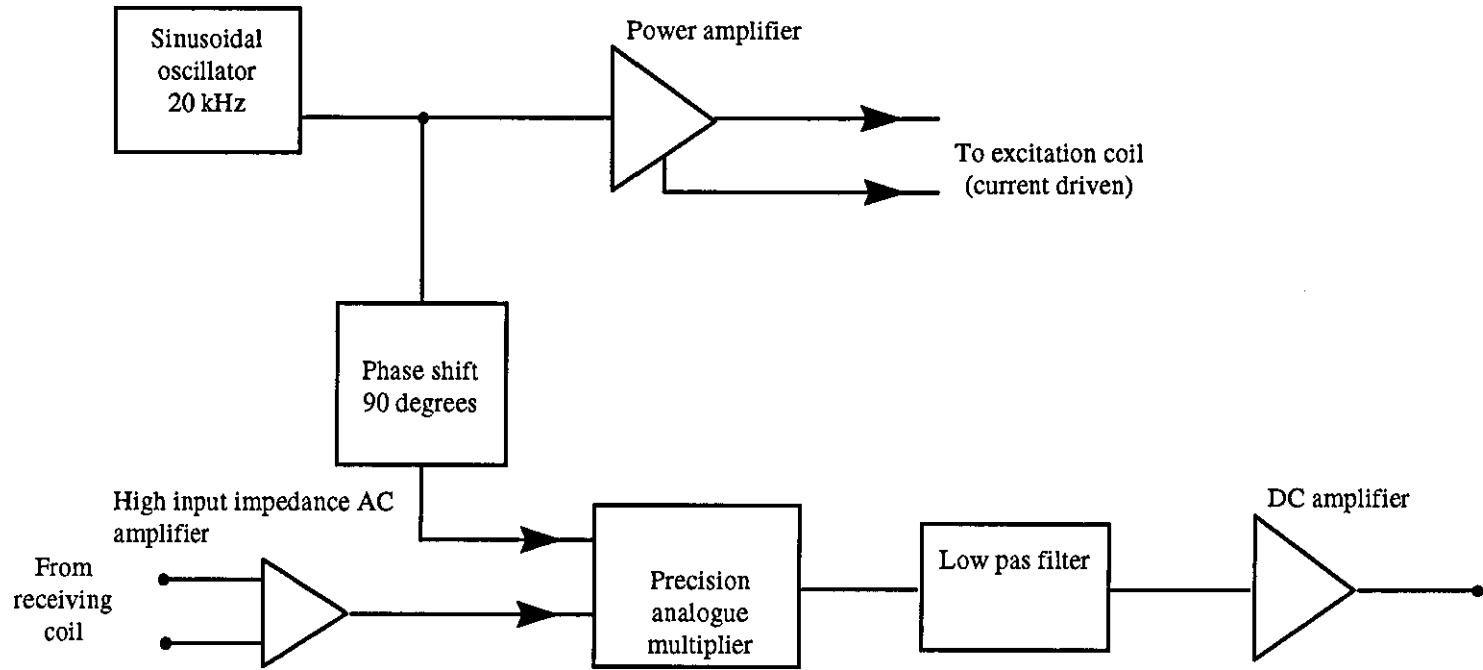


Figure 5-2 Electronic processing scheme

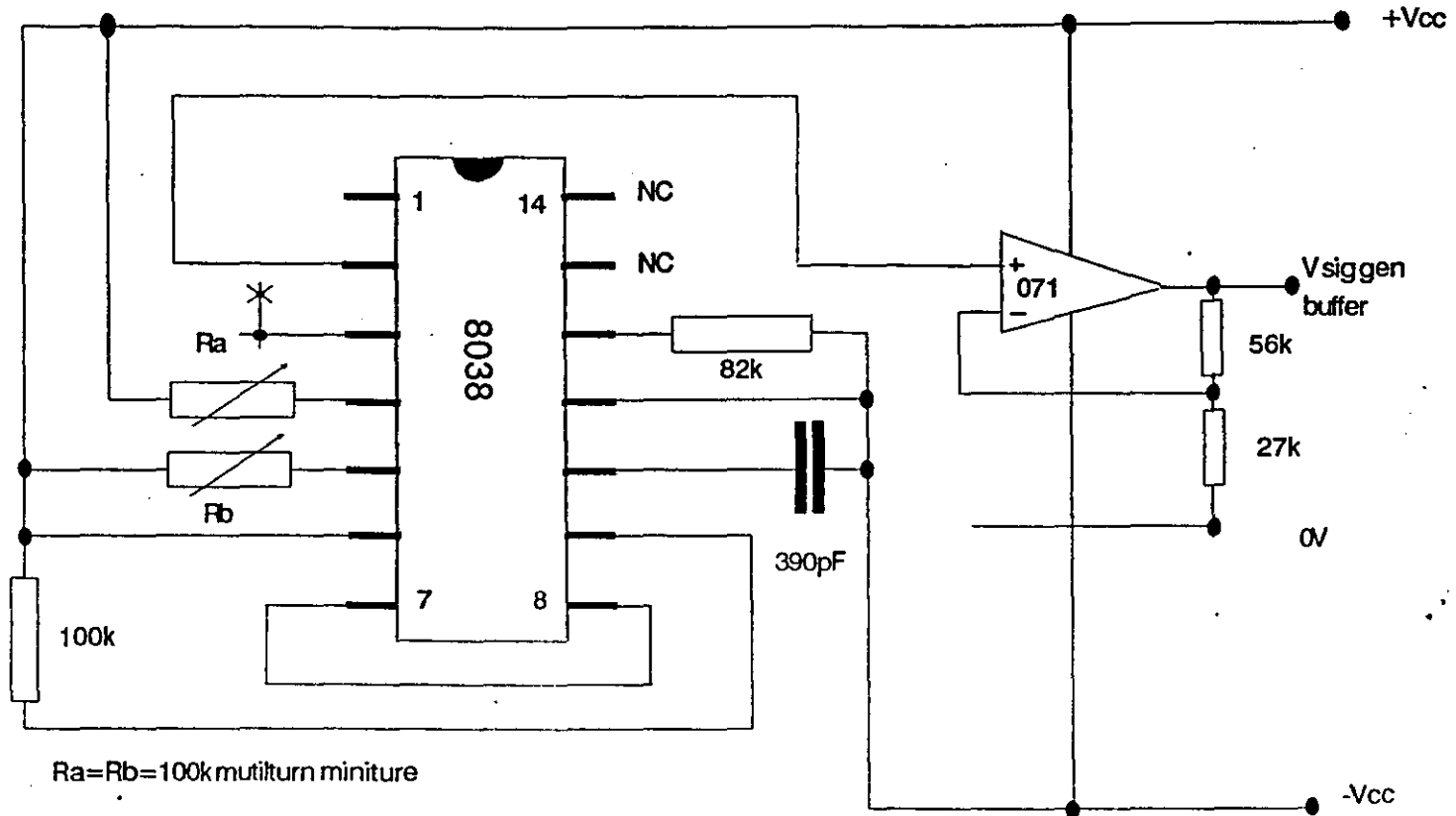


Figure 5-3 Signal generation stage

Current driven excitation

An a.c. current source is required since the induced voltage is directly proportional to the current in the excitation coil. Variations in this will introduce errors in the output voltages. The coil resistance is also a function of temperature and this variation would lead to variation in current were the coil to be voltage driven. Current limitation is also required on safety grounds in case of insulation failure and direct contact with skin. Figure 5.4 shows the excitation coil driving circuit.

5.3.2 Demodulation

A phase sensitive detection or synchronous demodulation circuit was used to extract the induced voltage signal from any background noise signal. Figure 5.5. Shows a schematic of the circuit. Referring to this figure and:

Given some excitation current:

$$I_e = A \cdot \sin(\omega t) \quad (5.1)$$

This will induce a voltage in the receiving coil of:

$$V_i = K \cdot \frac{d(A \cdot \sin(\omega t))}{dt} = K \cdot A \cdot \cos(\omega t) \quad (5.2)$$

If this voltage is multiplied by a voltage, V_r which is 90° phase shifted from the excitation current (figure 5.5) then:

$$V_i \cdot V_r = K \cdot A \cdot \cos(\omega t) \cdot A_r \cdot \cos(\omega t) \quad (5.3)$$

Using the trigonometric identity $\cos^2(x) = (1 + \cos(2x))/2$ this becomes:

$$V_i \cdot V_r = K \cdot A \cdot A_r \cdot (1 + \cos(2\omega t))/2 \quad (5.4)$$

If the double frequency ($2\omega t$) is filtered out, the d.c. voltage that is left provides a convenient direct indicator of the voltage induced in the coil.

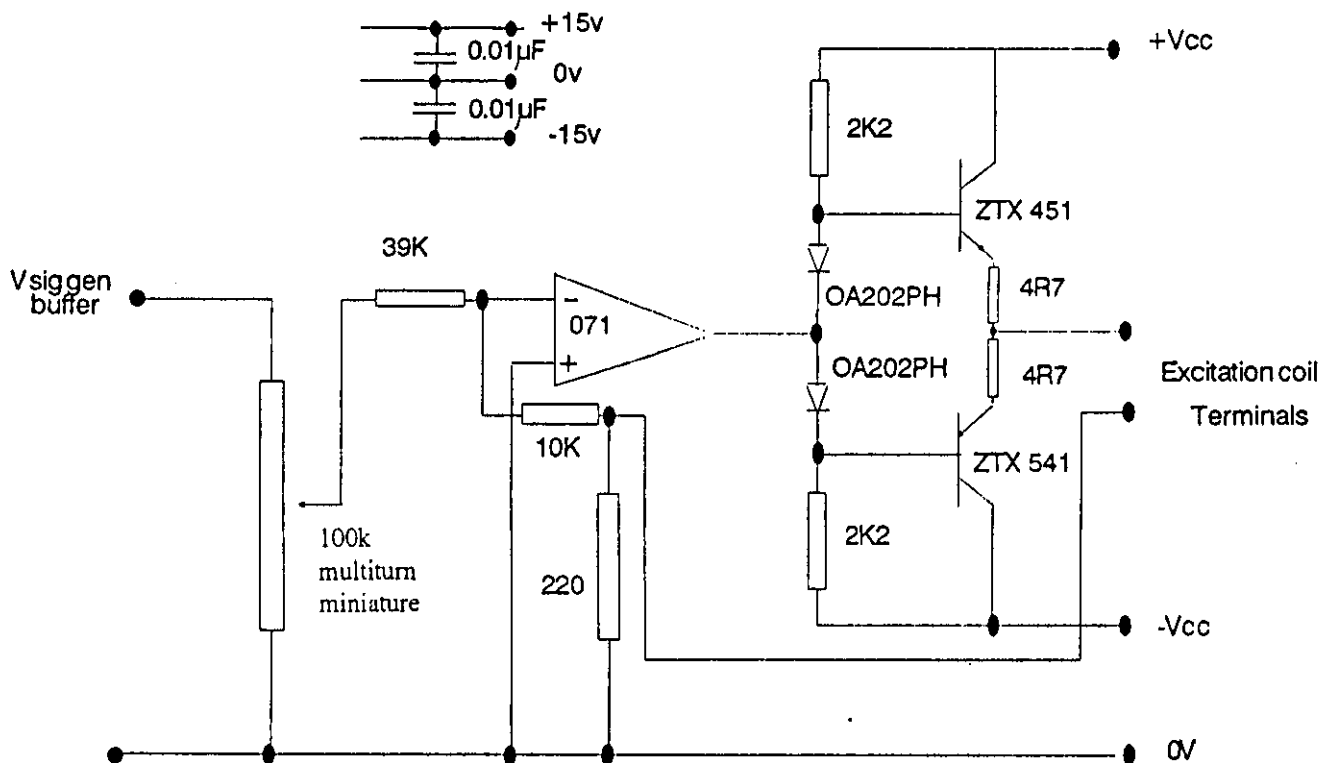
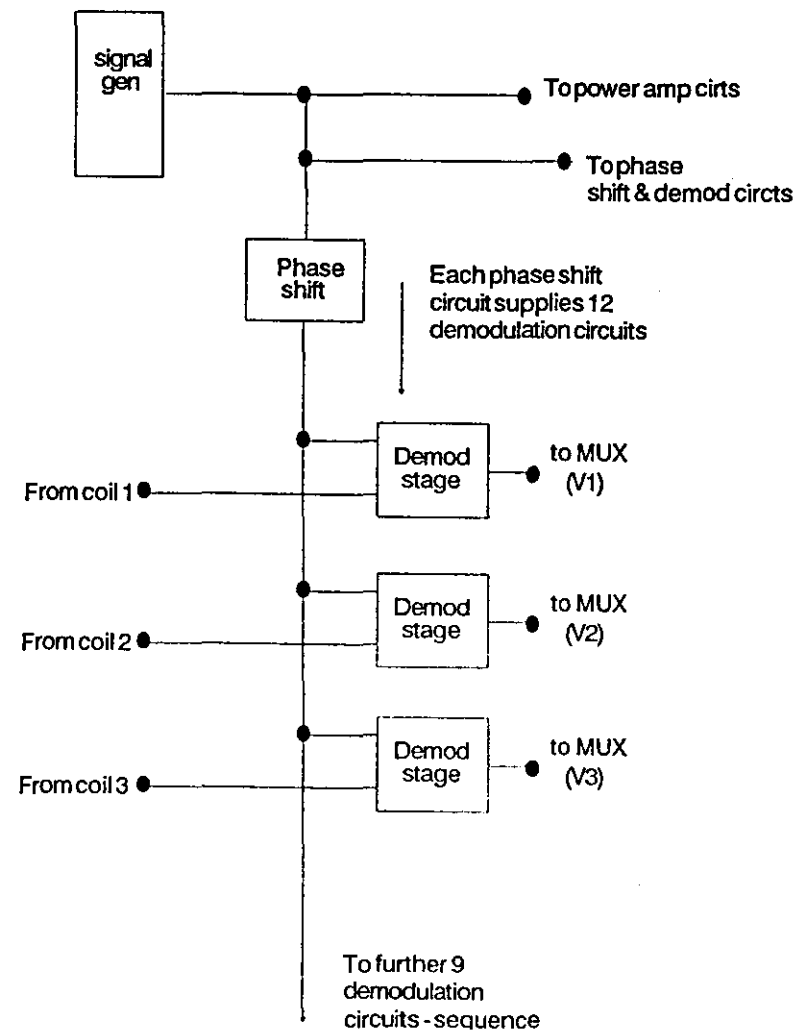
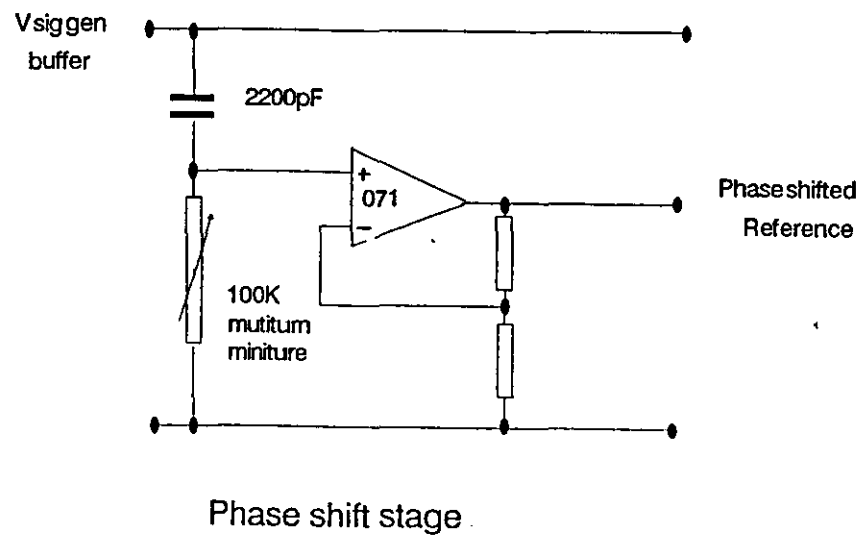


Figure 5-5 Phase shift stage



The process tends to filter out other frequencies of induced voltage that may be generated by pick-up from spurious magnetic field in the vicinity of the receiving coil. The multiplication of these with the reference signal does not produce d.c. components and thus they do not contribute to the d.c. voltage indicating the level of induced voltage in the receiving coil.

5.3.3 Data logging hardware

The filtered d.c. voltages from the demodulation circuit are passed to an analogue to digital converter within a PC used for data logging. The digital to analogue conversion and data storage is controlled with purpose written software.

5.4 TRANSDUCER ORIGIN AND RANGE OF DISPLACEMENTS

Having calibrated a set of coils using both methods described in Chapter 4., the results in Table 5.1 demonstrate the accuracy and range of displacements over which they are obtainable. The results are presented in terms of displacements in the (x,y,z) co-ordinate system, with the origin set at a point 3.5mm from the receiving coils along the central axes of the equilateral triangle upon which the receiving coils are located (see figure 5.7). The movements are of the excitation coil relative to this origin.

Displacements of ± 3 mm in x,y and ± 1.5 mm in z are taken as the maximum imposed by the coil's induced voltage-displacement characteristics. A minimum (vertical) distance of 2.0 mm between the excitation and receiving coils was maintained throughout the tests and calibration. In the force transducer this gap corresponds to the gap at maximum compression of the rubber element.

5.5 GENERAL ASSESSMENT

In order to carry out a systematic evaluation of each of the models used, recordings of the induced voltage were made as displacements were made along each of the axes in turn. For each series of displacements, the non-varying co-ordinates remained at zero. For example x was varied from -3 to + 3mm, whilst y and z were kept at 0mm. The data collected was used to calculate $(x_{est}, y_{est}, z_{est})$ at each (V_1, V_2, V_3) . All three models were used so that a total of three estimated positions were obtained. The error in estimating x,y and z was then

calculated for each method. The errors each of the models produced when predicting actual measurements (expressed as per cent of half range of displacement) whilst varying the displacement along each of the co-ordinate axes in turn are shown in Figures 5.8-5.10. These figures reveal both accuracy and cross talk. Figures 5.11a-5.11c demonstrate the magnitude of the error in determining the position in space, i.e. the length of the vector joining the predicted position and the actual position for the variations along the respective axes. These errors are expressed as a percentage of the maximum vector displacement (i.e. $\sqrt{((x_{\max})^2 + (y_{\max})^2 + (z_{\max})^2)}$). Table 5.1 summarises these results.

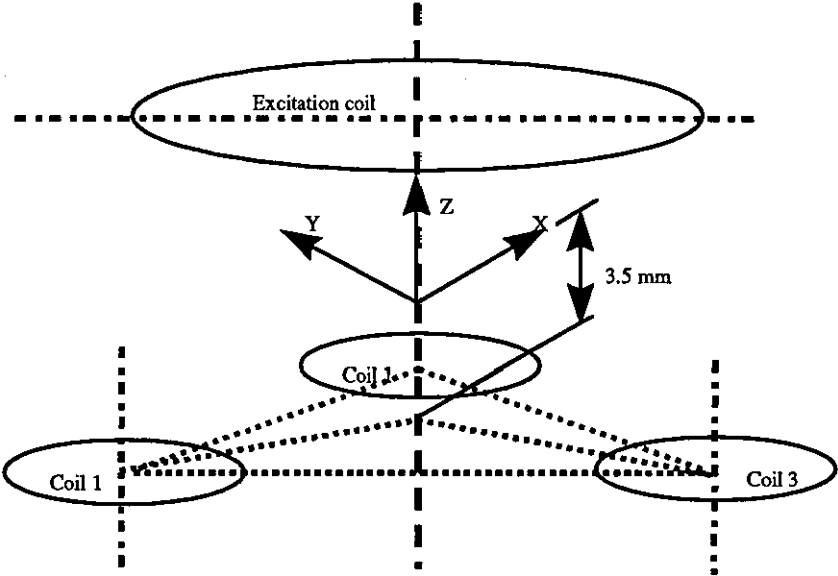


Figure 5-7 Location of reference origin with respect to the receiving coils

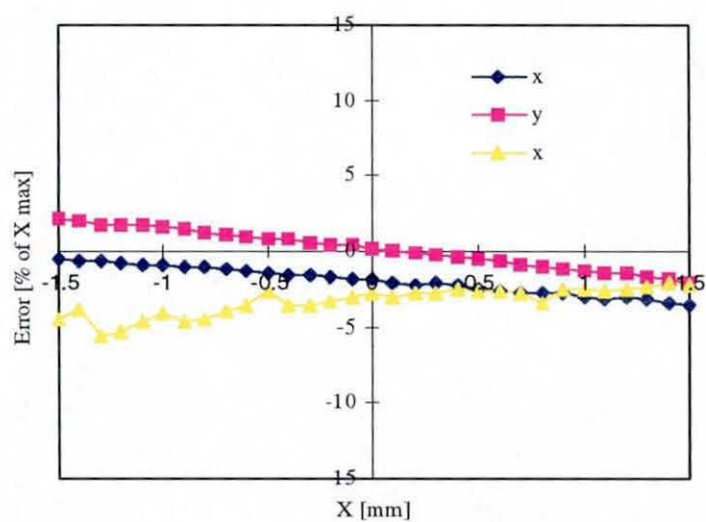
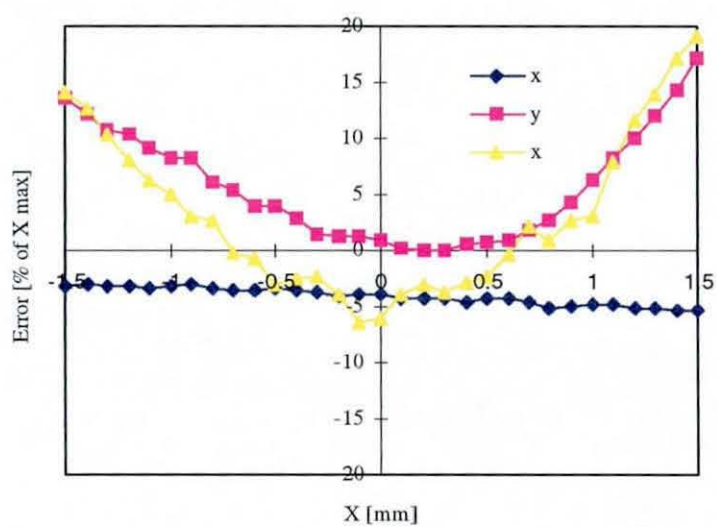
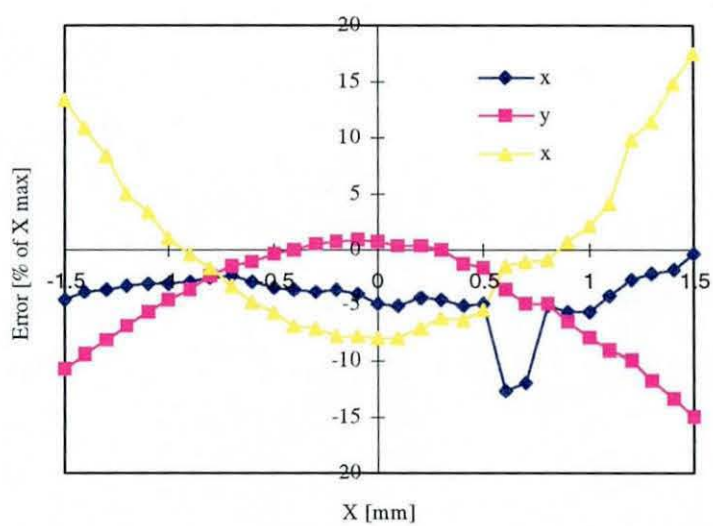


Figure 5-8 Planar model

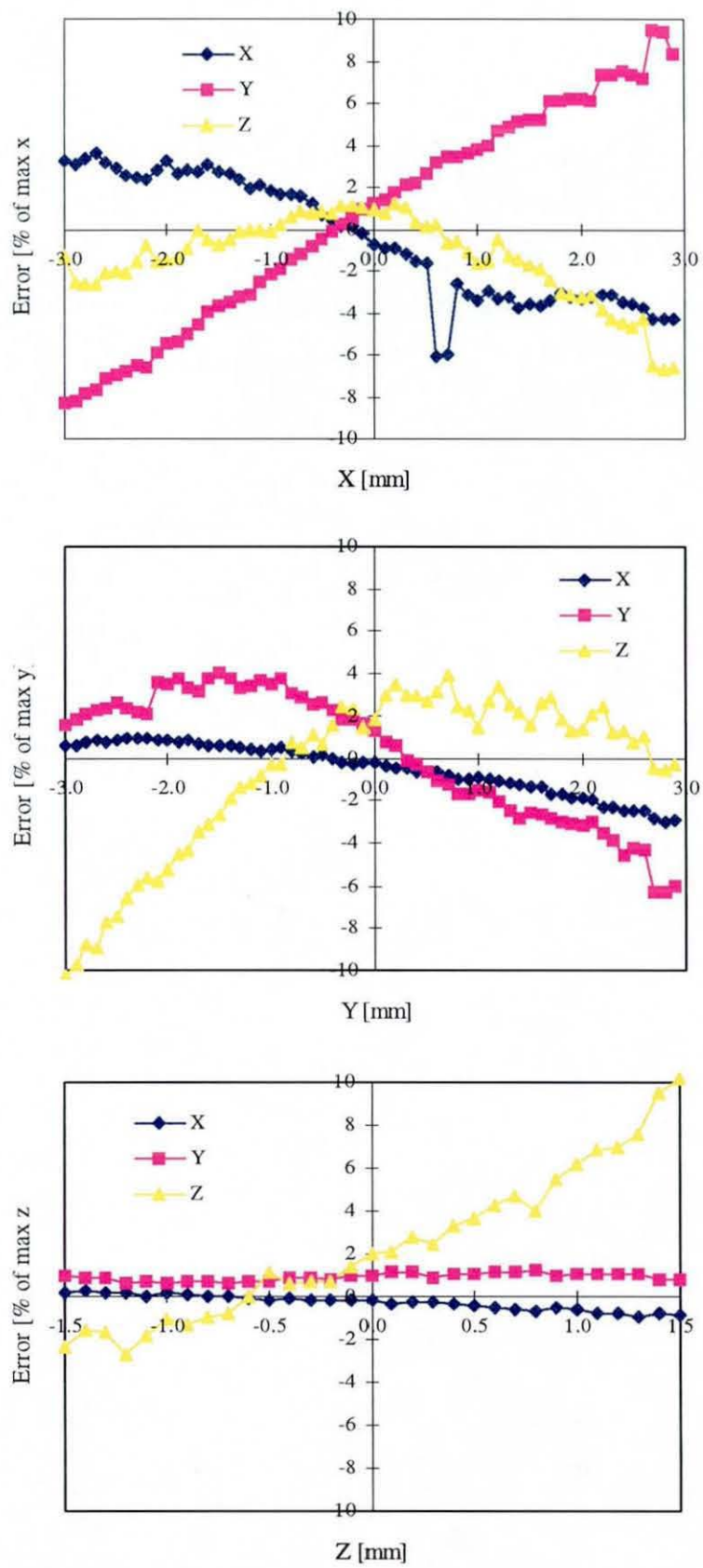


Figure 5-9 Hybrid model

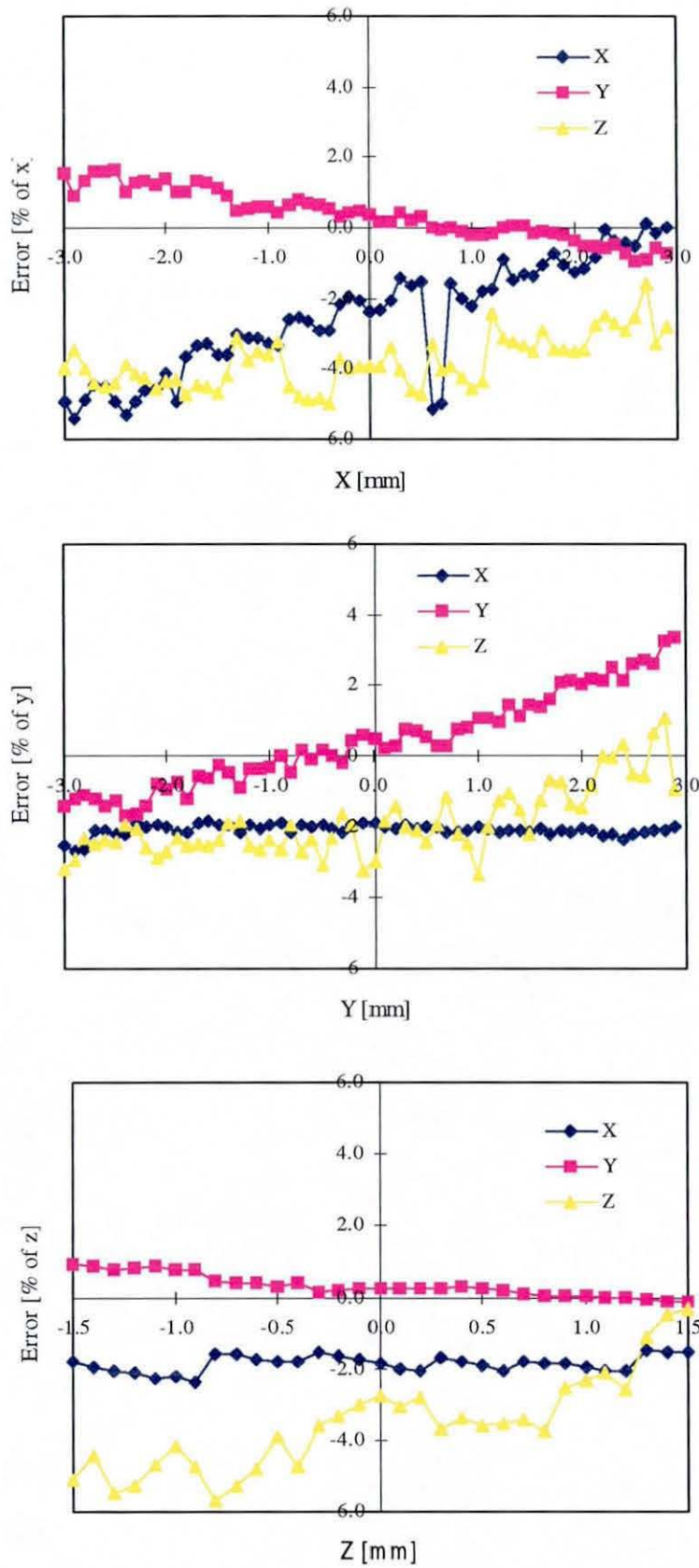


Figure 5-10 Look-up table method

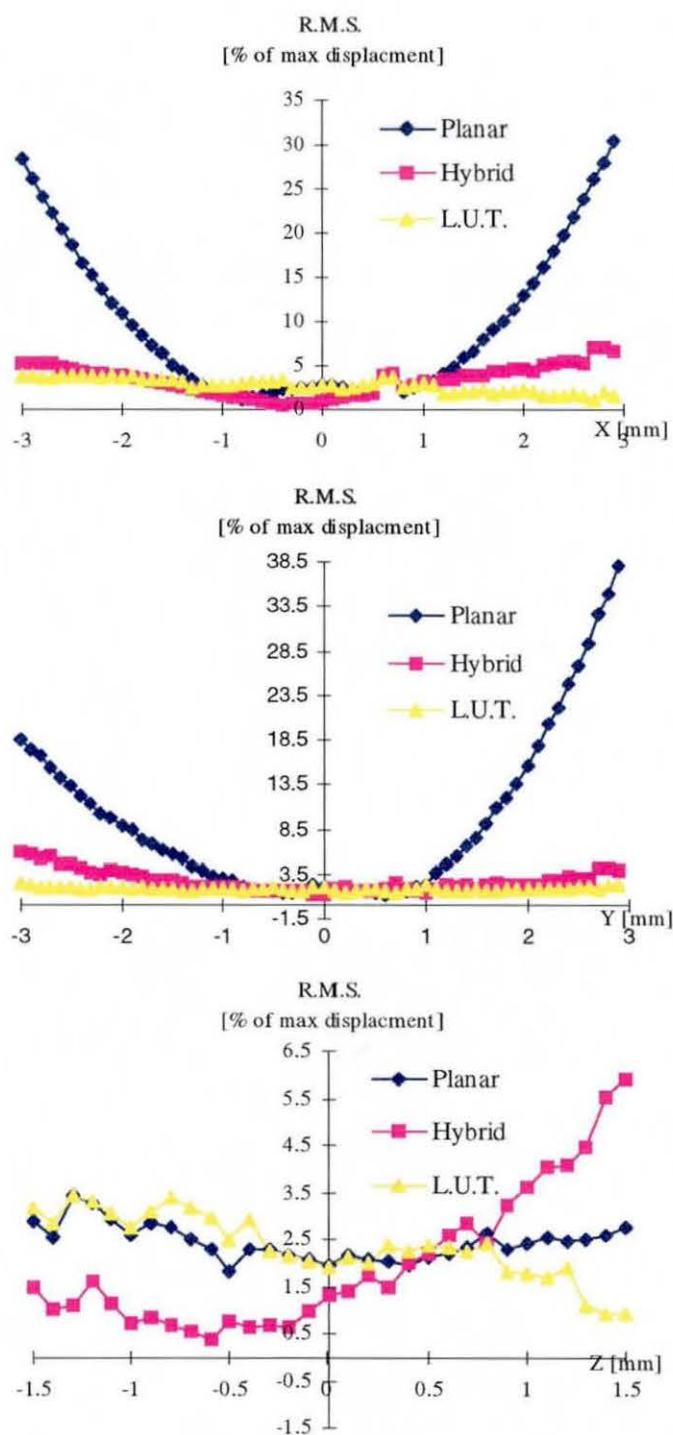


Figure 5-11 R.M.S. errors

Planar	Error range	Mean Error	Median Error	Stdev Error
x(x)	31.3	-1.5	-1.9	6.1
y(x)	23.2	-8.0	-6.3	6.9
z(x)	48.7	11.9	8.1	14.6
r(x)	29.2	9.7	6.0	8.6
x(y)	2.3	-2.3	-2.1	0.7
y(y)	37.5	8.7	7.0	9.0
z(y)	57.4	12.6	8.2	14.6
r(y)	36.8	9.6	6.4	9.3
x(z)	3.1	-2.0	-1.9	0.9
y(z)	4.2	0.1	0.2	1.3
z(z)	3.5	-3.3	-3.1	0.9
r(z)	1.6	2.4	2.4	0.4

Hybrid	Error range	Mean Error	Median Error	Stdev Error
x(x)	9.7	-0.5	-0.5	2.9
y(x)	17.8	0.6	1.1	5.2
z(x)	7.8	-1.4	-1.2	2.0
r(x)	6.6	3.3	3.5	1.7
x(y)	3.9	-0.5	-0.3	1.2
y(y)	10.4	0.2	1.4	3.1
z(y)	14.2	-0.6	1.1	3.8
r(y)	4.7	2.7	2.3	1.1
x(z)	1.2	-0.3	-0.2	0.4
y(z)	0.6	0.9	0.9	0.2
z(z)	12.9	2.3	2.0	3.5
r(z)	5.5	2.0	1.5	1.5

L.U.T.	Error range	Mean Error	Median Error	Stdev Error
x(x)	5.5	-2.6	-2.4	1.6
y(x)	2.6	0.4	0.4	0.7
z(x)	3.4	-3.8	-3.9	0.7
r(x)	2.9	2.8	2.7	0.8
x(y)	0.8	-2.1	-2.1	0.2
y(y)	5.0	0.4	0.3	1.3
z(y)	4.4	-1.9	-2.1	1.0
r(y)	1.1	1.9	1.9	0.2
x(z)	0.9	-1.9	-1.8	0.2
y(z)	1.0	0.3	0.2	0.3
z(z)	5.3	-3.5	-3.6	1.4
r(z)	2.5	2.4	2.4	0.7

Note
 x(x) denotes statistics for the errors in x as x is varied from the origin, y and z being held at the origin.
 r is the magnitude of the error vector i.e. ($\hat{r} = x^2 + y^2$)
 All values are quoted as a percent of the magnitude of the maximum displacements (for x and y this is 3 mm, for z 1.5 mm and for r, $\sqrt{(3^2 + 3^2 + 1.5^2)}$ mm)

Table 5.1 Summary of % errors - systematic tests

In the first instance the range (of x,y and z) is of most interest since half the range will give a worst case % error - assuming the distribution is symmetrical (not skewed).

The success of each model in predicting the changing displacement is illustrated in table 5.2 below:

Model	Dynamic variable	Variable error is in	Error Range
Planar	x	x	31
Planar	y	y	38
Planar	z	z	4
Hybrid	x	x	10
Hybrid	y	y	10
Hybrid	z	z	13
L.U.T.	x	x	6
L.U.T.	y	y	5
L.U.T.	z	z	5

Table 5.2 Accuracy of models

Thus we might expect +/- 19% accuracy with the planar model, +/- 7% with the hybrid and +/- 3% with the look-up table method. However, after examining the range of cross-talk (table 5.3) it can be seen that more realistic figures are +/- 3% for the look-up table method, +/- 9% for the hybrid and +/- 29% for the planar model. These errors may be compared to the magnitude of the vector errors given in figure 5.12 which reveals maximum values of 37% for the planar model, 7% for the hybrid and 3% for the look-up table method. Clearly the planar model appears to have failed over this range of displacements. However, examination of figure 5.15 reveals that if the range of displacements is reduced, the method might be used to resolve to an accuracy of +/- 20% (30% by magnitude of vector error). Similar improvements are not seen in the hybrid model when the displacement range is reduced. Reducing the displacements to +/- 2.5 mm in x,y and +/- 1.125 in z the range of errors still indicate a possible accuracy of the order of +/-9% (6% by magnitude of vector error). No increase in accuracy would be expected by reducing the range of displacements when using the pure look-up table approach unless the number of points in the look-up table was kept the same. That is if a finer 3D mesh of points was used.

Model	Dynamic variable	Variable error is in	Range of % error
Planar	x	y	23
Planar	y	x	2
Planar	x	z	49
Planar	y	z	57
Planar	z	x	3
Planar	z	y	4
Hybrid	x	y	18
Hybrid	y	x	4
Hybrid	x	z	8
Hybrid	y	z	14
Hybrid	z	x	1
Hybrid	z	y	1
L.U.T.	x	y	3
L.U.T.	y	x	1
L.U.T.	x	z	3
L.U.T.	y	z	4
L.U.T.	z	x	1
L.U.T.	z	y	1

Key:

Planar - Planar model
Hybrid - Hybrid method
L.U.T. - Look-up table method

Table 5.3 Cross talk or models

5.6 SYSTEMATIC VARIATIONS

Figures 5.8-5.10 were examined for systematic errors, more specifically for linear systematic errors. Due to its obvious inaccuracies over the full range of displacements, the planar model was only analysed over a limited range of ± 1 mm in x, y and z . Each set of values of errors in x, y and z was examined to identify trends with displacement in the dynamic variable. This was done by carrying out linear regression on the errors in x, y and z respectively for each of the charts. Table 5.4 contains a tabulated summary of this analysis. The table reveals some clear trends of the errors that confirm systematic the inaccuracies with each model. Of note are the variations of errors in x and y with z for the planar model. This would indicate an error in the estimation of $J(z)$ (equation 3 section 4.2.1). Also, for the hybrid model, a clear relation exists between the error in y as x is varied. This may be due to an asymmetry in the field produced by the excitation coil - i.e. the field (indeed the coil) is not circular but elliptical in the plane perpendicular to the coils longitudinal axis. The variation of the error in z with the hybrid model as z is varied also indicates a poor fit to $J(z)$. Since we are modelling the induced voltage-displacement field with simplified functions, we may expect systematic errors with both the planar and the hybrid models. However it is more surprising to see trends, in the errors occurring when the look-up table method is used. Whilst the "cross-talk" errors between x, y and z show much weaker trends, significant trends are seen in the errors produced in calculating x as x is varied, in calculating y as y is varied and in calculating z as z is varied. The look-up table approach does however utilise linear interpolation between points and perhaps this introduces these systematic errors. Use of a finer mesh of points for the look-up table should reduce these trends.

5.7 STATISTICAL ASSESSMENT

In an attempt to assess the accuracy of each technique away from the x, y, z axes, a number of random points (x, y, z) were generated and displacements made to these points. The predicted positions were calculated using each method and the predicted and actual positions compared. In order to compare the methods the random points used lay within the reduced volume of ± 2.5 mm in x, y and ± 1.125 mm in z , the resultant errors in x, y and z being expressed as a percentage of these full scale deflections (figure 5.15-5.17).

Regression carried out on error in 'a' as 'b' is varied for each model : Listed as "Model a-b"	Correlation coefficient	Coefficient of determination - r^2	p value	Confidence level
Planar x-x	-0.25	0.03	3.30E-01	-
Planar x-y	-1.04	0.16	3.00E-02	-
Planar x-z	1.10	0.07	1.60E-01	-
Planar y-x	-0.42	0.96	9.64E-21	99
Planar y-y	0.10	0.001	8.40E-01	-
Planar y-z	0.88	0.05	2.40E-01	-
Planar z-x	-1.01	0.99	9.21E-33	99
Planar z-y	-1.39	0.99	4.12E-41	99
Planar z-z	0.89	0.75	3.22E-10	99
Hybrid x-x	-1.56	0.87	4.39E-27	99
Hybrid x-y	2.99	0.99	5.39E-65	99
Hybrid x-z	-0.54	0.23	1.00E-04	99
Hybrid y-x	-0.66	0.94	1.26E-36	99
Hybrid y-y	-1.58	0.82	3.00E-23	99
Hybrid y-z	1.71	0.60	3.10E-13	99
Hybrid z-x	-0.38	0.97	4.99E-23	99
Hybrid z-y	0.10	0.28	2.00E-03	-
Hybrid z-z	3.80	0.95	2.75E-20	99
L.U.T. x-x	0.81	0.81	8.68E-23	99
L.U.T. x-y	-0.34	0.93	2.66E-35	99
L.U.T. x-z	0.26	0.39	1.06E-07	99
L.U.T. y-x	0.01	0.003	6.90E-01	-
L.U.T. y-y	0.74	0.95	1.52E-38	99
L.U.T. y-z	0.41	0.55	1.01E-11	99
L.U.T. z-x	0.08	0.11	6.90E-02	-
L.U.T. z-y	-0.33	0.89	3.10E-15	99
L.U.T. z-z	1.31	0.76	2.28E-10	99

Table 5.4 Systematic errors

It is apparent that over this displacement range, the planar model technique fails completely whilst the hybrid approach enjoys rather more success showing a range of error of not larger than 20% (giving a potential accuracy of $\pm 10\%$) which compares with a maximum range of 8% (potential accuracy of $\pm 4\%$) obtained with the look-up table method. Given that the hybrid method requires rather less calibration time, and that the calibration process may reduce to coil calibration as opposed to transducer calibration (with the subsequent effect on system assembly), it is felt worthwhile reserving judgement upon this calibration method particularly until confirmation that the transition to force measurement has been made.

It is clear that the look-up table approach allows calibration over a much larger range and in order to emphasise this the random point exercise was repeated using points over displacement ranges of ± 3 mm in x and y and ± 1.5 mm in z. Three hundred random points (x,y,z) were used. The distribution of errors using only the look-up table methods are shown in Figure 5.18 and confirm an accuracy of around $\pm 5\%$ in determining x,y and z.

5.8 ASSESSMENT OF CALIBRATION AND PROCESSING REQUIREMENTS

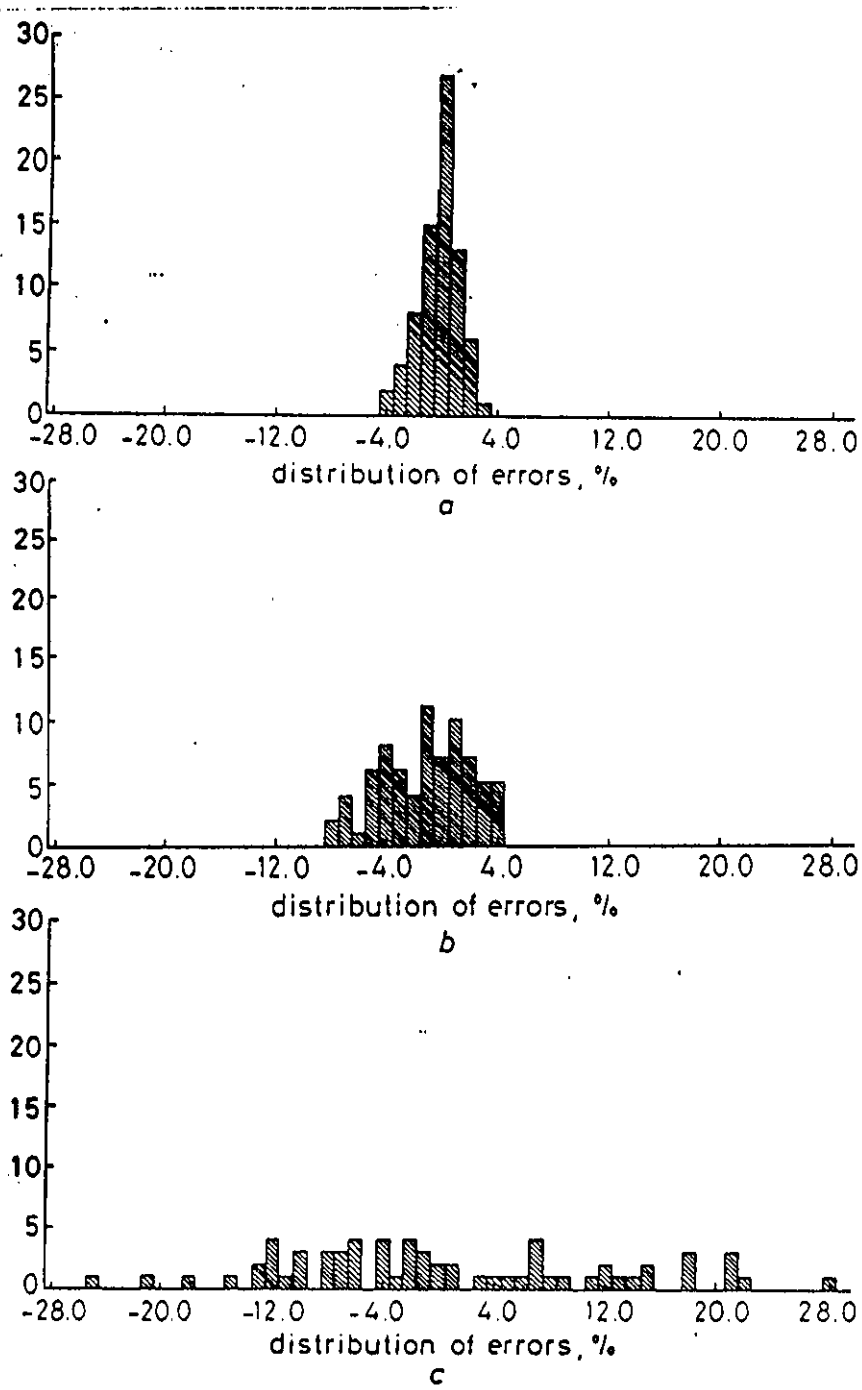
The planar mathematical model technique proved relatively unsuccessful and will not be considered here. The hybrid method utilised 20 points, obtained at five positions (for solution of a fourth order equation) across the range of radial displacement at each of four different axial separations (for a third order equation). The look-up table method, when used in obtaining the above results, required 1183 calibration points (and the accuracy obtained is obviously directly related to the number of points in the table for a given x-y-z space).

Where the hybrid model is used, greater care must be taken in manufacturing the coils to ensure accurate positioning of well matched (identical) coils. Also, characteristics for the combination of excitation and receiving coils need to be examined to judge the best spacing of the coils (size of the equilateral triangle) and calibration points for a given range of movements. Whilst intelligent coil matching and spacing are required for the look-up table method it is by no means as critical. In terms of the hardware processing requirements, there is little to separate the hybrid and look-up table methods since the core of both methods is

the matrix manipulation described in section 4.2.2. The real time processing involved in each method is thus identical.

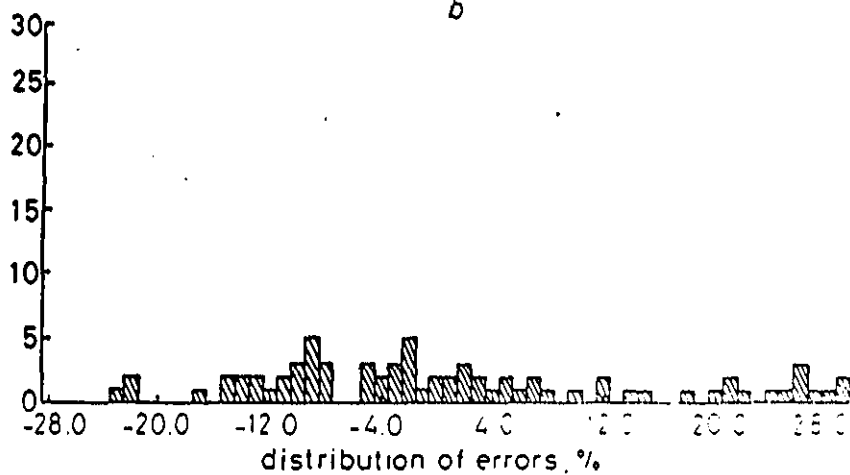
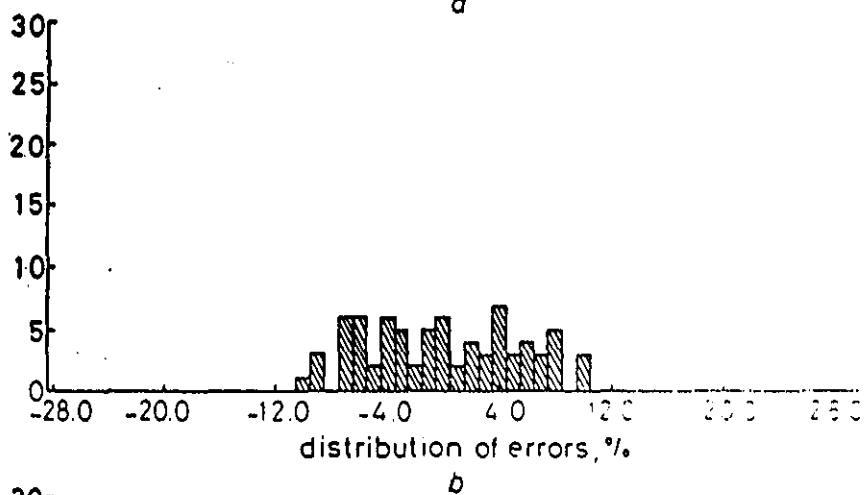
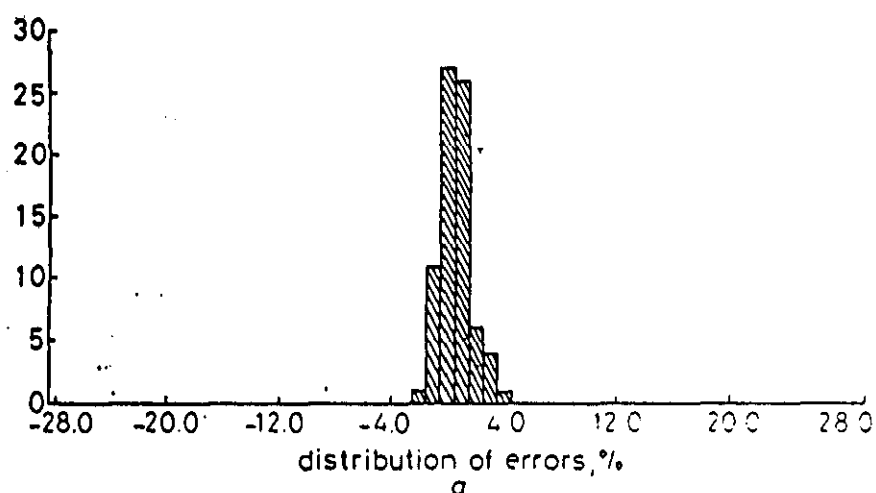
5.9 CHAPTER SUMMARY

- The prototype coil group assembly method and electronic hardware design have been described.
- Systematic and random assessment of the accuracy of the three models are compared.



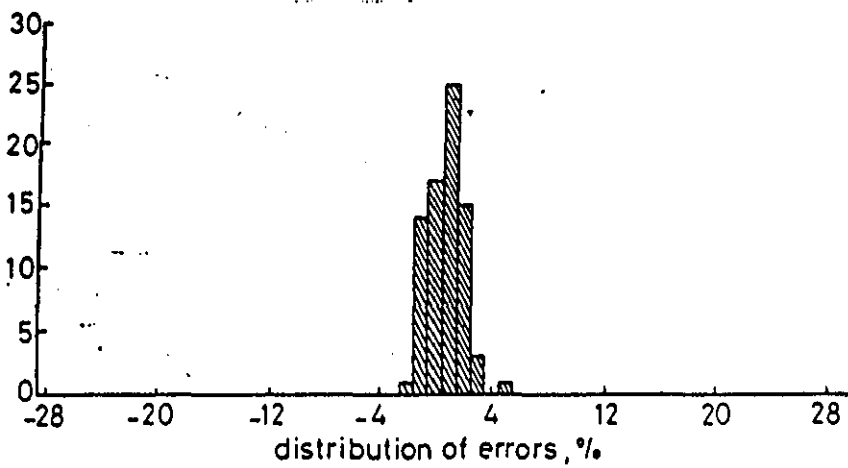
a Look-up table method	mean = -0.3; σ = 1.36; range = 7
b Model 2	mean = -1.22; σ = 3.18; range = 12
c Model 1	mean = -2.26; σ = 19.78; range = 97

Figure 5-12 Distribution of errors in x

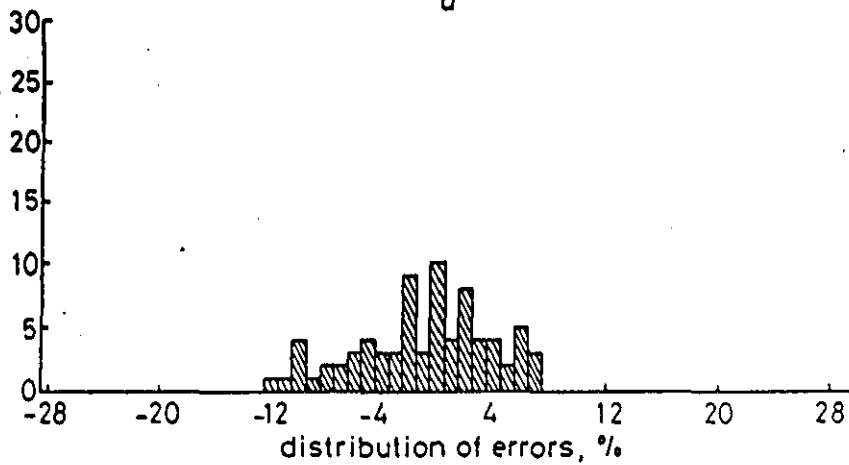


a Look-up table method	mean = 0.53; σ = 1.12; range = 6
b Model 2	mean = 0.07; σ = 5.37; range = 20
c Model 1	mean = -2.07; σ = 13.10; range = 60

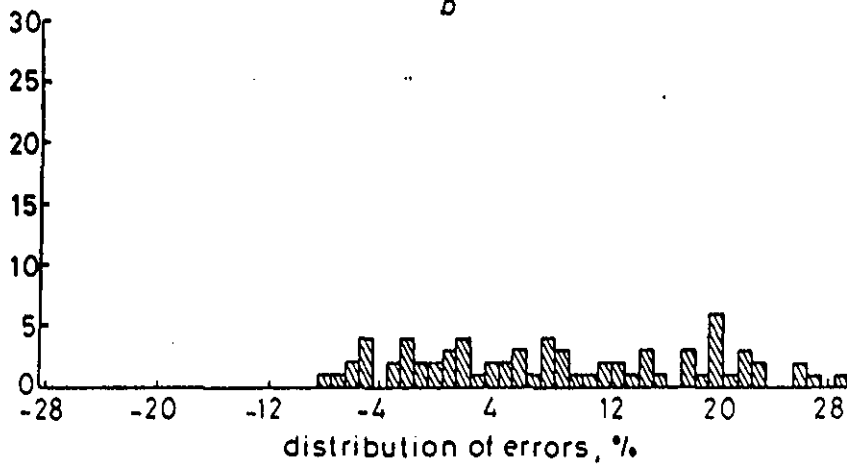
Figure 5-13 Distribution of errors in y



a



b



a Look-up table method

b Model 2

c Model 1

mean = 0.66; σ = 1.21; range = 7.0

mean = -0.95; σ = 4.87; range = 19.0

mean = 14.15; σ = 10.18; range = 38.0

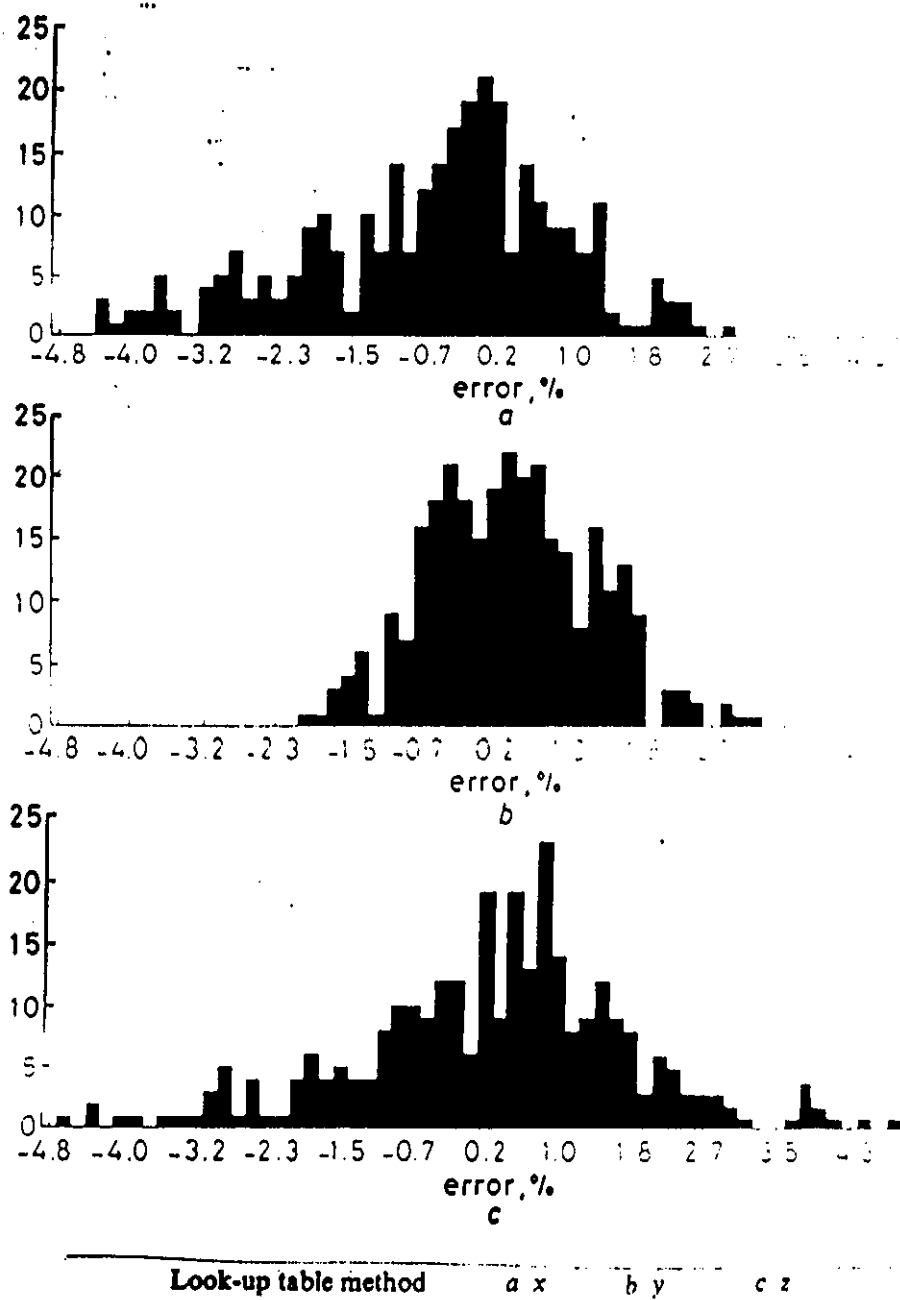


Figure 5-15 Distribution of errors for 300 random points - Look-up table method

6. TOWARDS A FORCE TRANSDUCER

6.1 MATERIAL FOR THE MECHANICAL ELEMENT OF TRANSDUCER

6.1.1 General considerations of material selection

When searching for a suitable material to provide the mechanical element of the transducer, materials used routinely for insole manufacture were obvious candidates. Somewhat surprisingly it was found that there was little or no information available on the mechanical properties of such materials.

One of the main problems with polymeric materials used for insoles is that of “compression set” or permanent deformation due to repeated or continuous loading. This problem would obviously lead to an instability if such materials were used in a transducer. This may also be linked to the dynamic performance of the material. Permanent deformation under load may be interpreted in terms of the visco-elastic behaviour of the material. This type of loading rate dependent behaviour is one end of the spectrum whilst the dynamic performance of the material in terms of its mechanical response to high frequency forces will also determine the frequency response of the transducer.

Perhaps more importantly, such materials tend to be selected for their apparent property of redistributing mechanical forces. Whilst it may be desirable to assess this at a later stage, it is more desirable to be able to measure the mechanical forces seen at the foot-shoe interface in a conventional shoe with relatively firm underfoot conditions.

In general it is clear then that the mechanical properties of the chosen material need to be stable within the temperature and humidity seen within the shoe and over a large number of cyclic loading patterns.

Assembly and integration within the prototype transducer was also a large factor in material choice. Many of the materials routinely used for insole material are thermoset materials. Such materials may be machined (with difficulty) and the coils bonded to them. Nevertheless a material into which the coils could be moulded (figure 3.2) was the ideal solution.

6.1.2 Mechanical properties required

Manufactures of rubbers and rubber like materials tend to quote only the 'Shore Hardness' score or the IRHD (International Rubber Hardness Degree) rather than more conventional engineering properties such as Young's modulus. For rubber, hardness is a measurement of the reversible, elastic deformation produced by a specifically shaped indenter under a specified load. A number of different standards for measuring rubber hardness have been used. Readings in IRHD, British Hardness Degrees (°BS) or Shore Durometer A Scale are approximately the same (Lindley, 1967). For elastic isotropic materials the hardness bears a known relationship to Young's modulus (BS 903 Part A26: 1969). Natural rubbers have a very high bulk modulus of elasticity, being essentially incompressible. Their modulus of elasticity in compression is thus very dependent on any restriction on space for the material to deform into. Such restriction could be a straight forward containment with a fixed volume or in a more subtle containment. For instance, rubber between and bonded to two plates will have a different compression modulus to that of the same rubber compressed between two plates to which it is not bonded. In the transducer we require the 'plates' (the coils) to be bonded to the rubber-like material and so this situation is worth examining in more depth:

The stiffness of rubber in compression, when the loaded surfaces are prevented from slipping (by bonding or other means), depends upon the 'shape factor', S , defined as the ratio of the loaded area to the total force-free area. This dependence is expressed by

$$E_c = E_o(1 + 2.k.S^2) \quad (6.1)$$

where E_c = compression modulus, E_o = Young's modulus, S = shape factor and k is a numerical factor given in tabulated form by Lindley, 1967.

For a particular application we may wish to think in terms of an overall spring constant, k_c , that is obviously dependent upon the size of the rubber block used (figure 6.1):

$$k_c = \frac{F}{d} = \frac{E_c \cdot A}{h} \quad (6.2)$$

where F is the compressive force applied, d the compression caused, A the area of the rubber block over which the compression is applied and h the uncompressed thickness of the block.

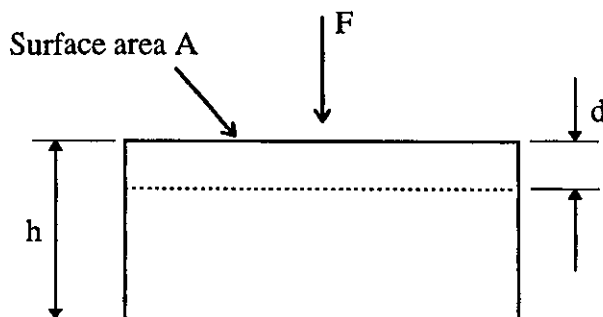


Figure 6-1 Rubber block under compression

The shear modulus, G , is also related to the 'hardness' scores and is again provided by Lindley, 1967 in tabulated form. Then a shear spring constant, k_s , may be calculated from:

$$k_s = \frac{F}{d} = \frac{G \cdot A}{h} \quad (6.3)$$

where F is the applied shear force, d the displacement of the upper face of a block of cross sectional area A and height, h :

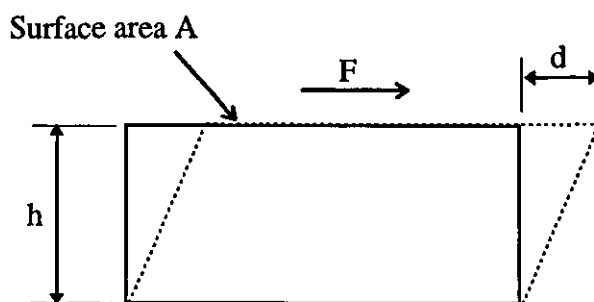


Figure 6-2 Rubber block under shear

It should be noted that these relations apply to isolated blocks of rubber and would be modified if the block was part of a continuous sheet of material. However the option of isolating the transducer material from the rest of the insole of which it will form part has not been ruled out. Also these formulae, together with the relation of Shore Hardness or IRHD.

to both Young's and the Shear modulus, provide a means of identifying a suitable material for the transducer core.

Using the design specification derived in section 3.1.5 and assuming a classic Newtonian material whose compression is to be less than 3 mm (since from chapter 5 it was shown that reasonable accuracy could be obtained with axial displacements of +/- 1.5mm) we can calculate a desired compression modulus of:

$$E_c = \frac{\text{stress}}{\text{strain}} = \frac{1.5 \times 10^6}{\frac{3}{5}} = 2.5 \text{MPa} \quad (6.4)$$

which, using equation 6.1 and data from Lindley (1967) gives an IRHD of between 70-75. Similarly, from section 3.1.5, a shear stress measurement range of +/- 180kPa is required and for a displacement range of +/- 3.0mm (using equation 6.3):

$$k_s = \frac{180.A}{15} = \frac{G.A}{5} \Rightarrow G = 300 \text{kPa} \quad (6.5)$$

Using data from Lindley (1967), this requires a rubber with an IRHD greater than 75. Clearly there is some conflict between the shear and compressive requirements. However selection of a rubber with an intermediate hardness and careful selection of the range of displacements should allow an appropriate compromise.

In terms of dynamic performance, the mechanical properties defined above should be stable for loading frequencies from 0 to perhaps 200Hz (50Hz is usually considered an adequate sampling frequency for biomechanical studies of walking). Whilst information on the frequency response of insole materials is not generally available such materials have been shown to perform a shock absorbing (frequency selective) role in footwear (Johnson, 1986). It was noted however that the mechanical performance of natural rubber was felt to be "substantially independent of frequency below 1000 cycles per second (at an ambient temperature of 0-50 °C)" (Lindley, 1967) although this situation was less true of rubbers with an IRHD above 60.

6.1.3 Material selection

Silicon rubber was identified as a material that could be found in various grades possessing different mechanical properties. Two particular grades were identified as candidates for use in the prototype transducer, Dow Corning Q3-3481 and Dow Corning E RTV silicone rubbers. These came in liquid form with a curing agent. The mixture of these two needed vacuum treatment prior to a curing time of around 24 hours.

The mechanical data given on these materials is presented below in table 6.1:

Material	Tensile Strength (Mpa)	Hardness (Shore A)
Q3-3481	4.2	19
E RTV	4.8	40

Table 6.1 Mechanical properties of rubbers

Clearly, these do not appear to offer the hardness required in the final transducer (see section 6.12). However rubbers of higher hardness that could be readily moulded without complex moulding systems could not be identified. It was therefore decided to use each of these to manufacture the prototype transducer. Obviously this prototype would only be able to cope with a smaller range of forces than that desired, but, the full principle of the force transducer could at least be explored.

6.2 FORCE TRANSDUCER ASSEMBLY

The assembly process had to achieve three critical objectives: to ensure that the longitudinal axis of the excitation coil was aligned with the centroid of the receiving coil group; that the planes in which the coils lay were parallel and that the coils lay as near to the ends of the transducer as possible whilst being adequately covered by the silicon rubber to provide added electrical insulation and mechanical protection. It was also necessary to provide some means of temporarily holding the transducer for the calibration process that allowed dismounting from the calibration rig without damaging the transducer.

Perhaps the one drawback of using silicon rubber is that there are very few bonding agents that will adhere to it. Indeed, even when allowed to cure from the liquid form, it does not

adhere to many surfaces. However surface priming agents are available which improve adhesion and these were used to ensure adhesion of the rubber to the coils.

Assembly of the prototype transducer proved to be a three stage operation. The first stage was to embed the coils (the excitation coil and separately the group of three receiving coils) into a thin sheet of silicon rubber.

The method that was used to temporarily mount the transducer is shown in figure 6.3. A layer of cardboard is bonded to each of the plastic plugs which in turn is bonded to the rubber. This bond was made at the time the coils were cast into the sheet of rubber. The coils were located over the centre of each of the plates shown in figure 6.4. These plates formed the floor of moulds into which a small amount of liquid rubber was poured. Care was taken to ensure that the rubber ran between the coils and the floor of the mould. The thickness of the rubber sheet formed when the lid of the mould was pressed in place was controlled by small raised areas on the corners of the lid (figure 6.5).

The second stage of the production process involved casting of a plug of rubber, which formed the core of the transducer, using a simple mould.

The final stage of transducer assembly was carried out with the aid of the assembly jig shown in figure 6.6. The thin sheets of rubber, into which the coils are embedded, were bonded to the plug of rubber forming the core of the transducer using liquid silicone rubber.

The mould was separated (figure 6.7) leaving the assembled transducer with the calibration mounting blocks attached. Following calibration, these blocks were removed by splitting the cardboard into two thin layers, one attached to the calibration mounting blocks and the other to the transducer. All but a very thin layer of paper fibres was then removed by wetting the transducer faces and gently rubbing.

6.3 FORCE CALIBRATION

6.3.1 The problem

The problem faced was to introduce and measure forces applied in three orthogonal directions to the surface of the assembled transducer - i.e. a three dimensional force production and measurement system was required to enable calibration and assessment. The

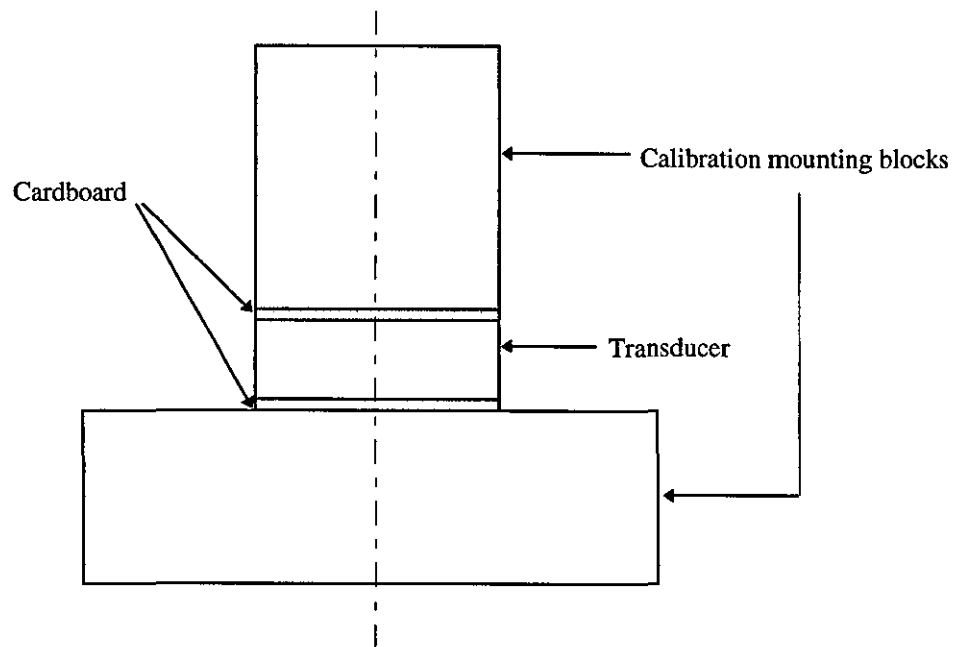


Figure 6-3 Mounting of transducer for calibration

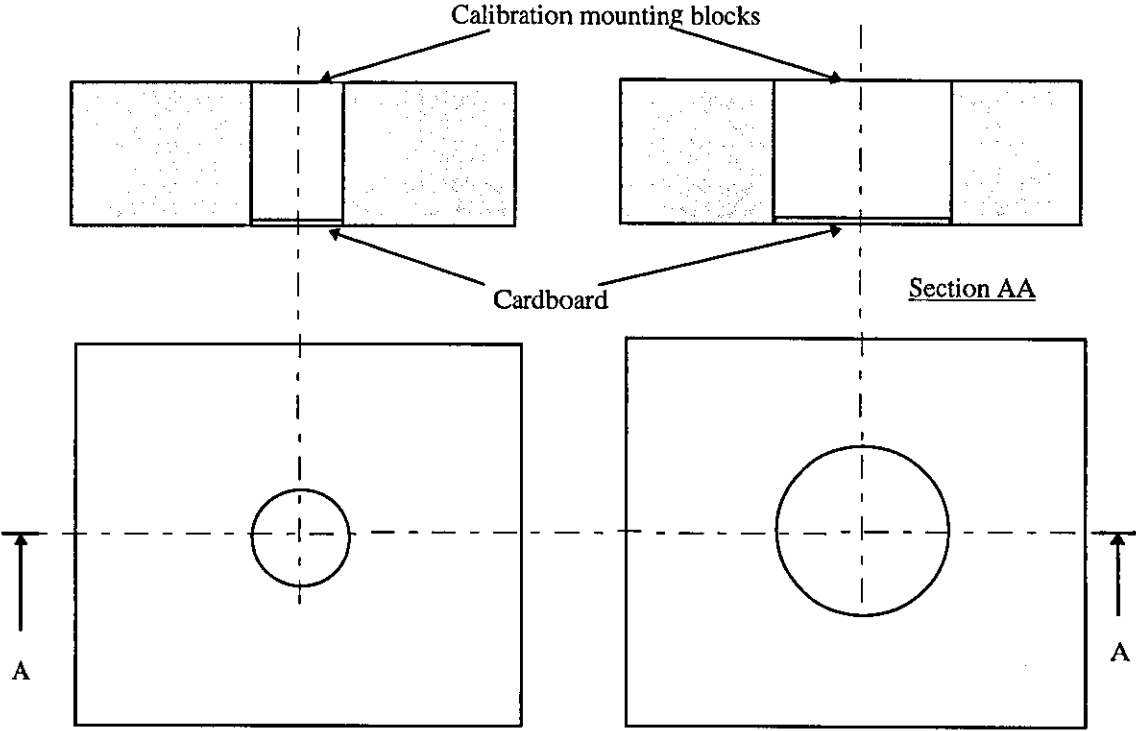


Figure 6-4 Moulding plates

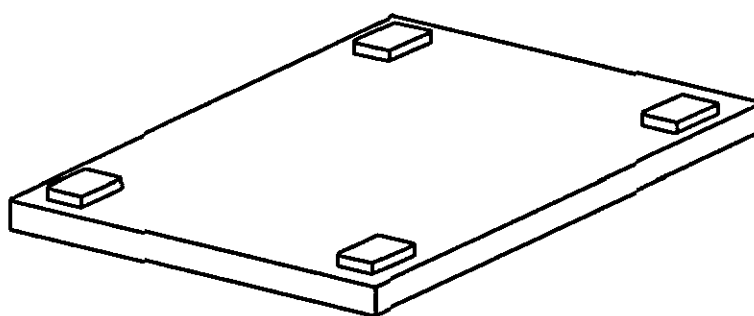


Figure 6-5 Lid with raised sections

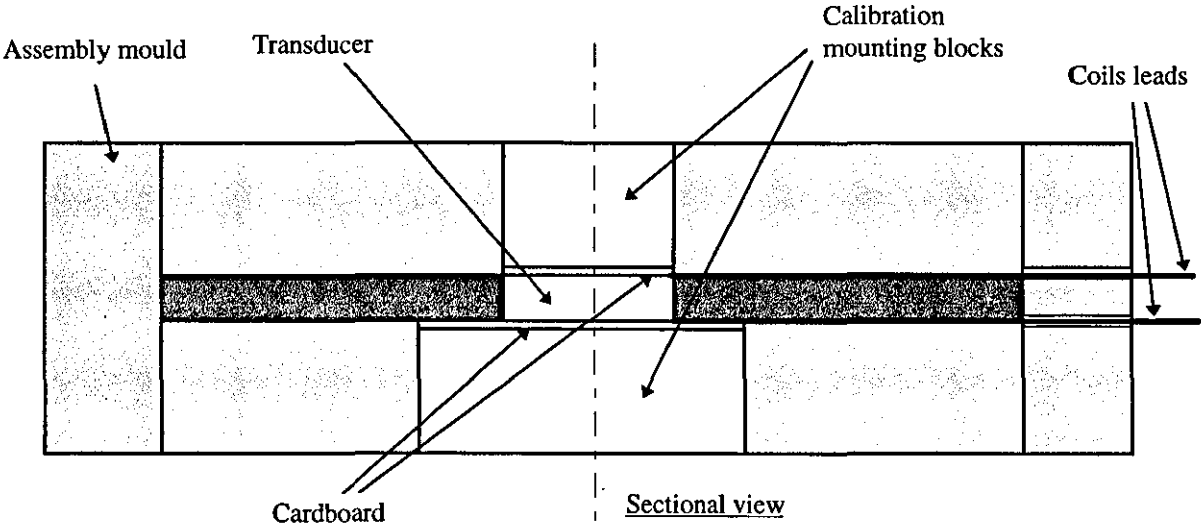


Figure 6-6 Transducer assembly mould

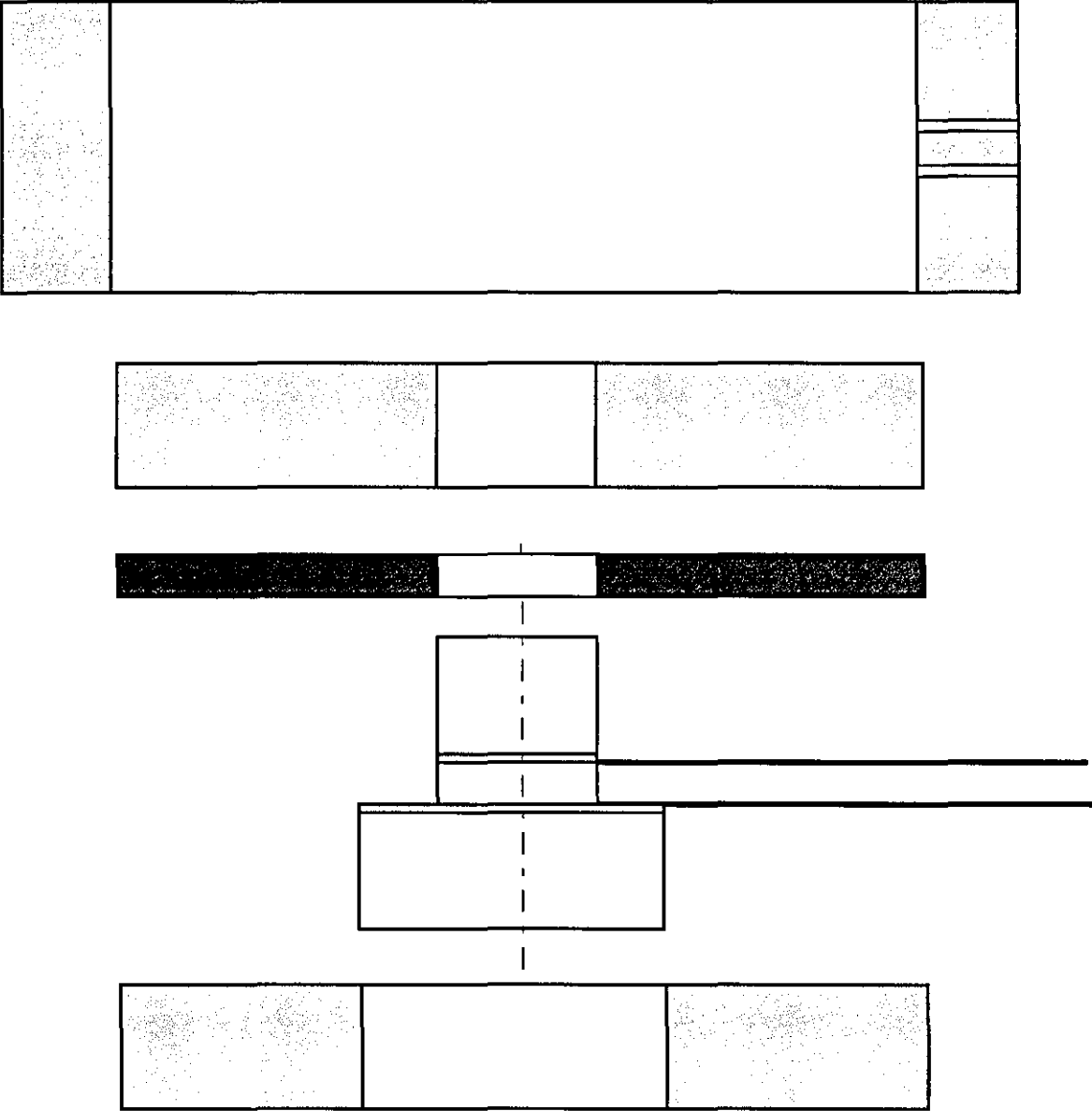


Figure 6-7 Removal of assembled transducer from the mould

testing rig was designed primarily to assess the induced voltage-displacement characteristics (section 3.5.4.1) was also designed to enable force application along three orthogonal axes. In practice problems were found with the design when force calibration on a prototype force transducer was attempted. The problems arose because of the use of proprietary linear bearings which, when loaded, exhibited relatively high friction and sticking points. The bearing system was designed and manufactured in various high density plastics to avoid the use of metallic components (used in commercial bearings) in the vicinity of the coil sets. It was the use of these materials (which are in fact somewhat visco-elastic and subsequently more difficult to machine accurately) that reduced the performance of the design. The system might have been usable had there been a direct measure of the forces being applied to the transducer. However the design relied upon calibrated masses being loaded onto the various cable and pulley systems. The cables were attached to the table and piston system and the cables run over pulleys to enable controlled directional force application to the transducer, described in chapter 3. The motion of the table and piston system however relied upon the flawed bearing system. The frictional forces introduced were found not to be repeatable or predictable and hence a new approach to force calibration had to be sought.

Clearly typical materials mechanical testing machines produce and measure force along one axis only. No system capable of measuring three dimensional forces could be identified. In view of this it was clear that new apparatus needed to be designed and built specifically for the purpose of force calibration.

6.3.2 Design objectives

1. To be able to apply accurately defined forces along the three orthogonal axes of the transducer to enable a look-up table, of the force against voltage combination, to be constructed.
2. A minimum of 1.5MPa direct stress and 180kPa shear stress are required to be applied to the transducer.
3. The system needs to enable the application of the forces in fine increments such that the maximum force is achieved in 20-50 steps.

4. The accuracy of the calibration obviously depends directly upon the calibration rig - a target of 2% maximum error was assumed as a target.
5. The force application system must be such as to ensure that no bending moment is applied along the longitudinal axis of the transducer.
6. The force application system must be such as to ensure that no torque is applied around the longitudinal axis of the transducer.
7. Since the transducer is “air-cored” it is sensitive to the presence of magnetic materials close to its surfaces, it is therefore essential to avoid this in the calibration rig.
8. Mechanised and automated calibration is highly desirable.
9. Dynamic performance assessment of the transducer using the rig is also desirable.

6.3.3 Design solution

The calibration system was designed to apply a resultant force composed of two components, a force along the longitudinal axis of the transducer (the vertical force) and a radial force perpendicular to the longitudinal axis (shear force). The direction of application of the shear force could be varied by rotating the mounting on which the transducer was held. Hence the calibration would be in terms of shear force, shear force angle and direct force (r, θ, z) rather than the forces along the conventional (x, y, z) orthogonal axes. Figure 6.8 shows the force application scheme. This approach offers two advantages: firstly it requires only two force transducers, and secondly the radial force calibration should lead to more uniform results. This should be the case since the induced voltage-displacement characteristics have been shown to be a function of radial displacement, and therefore, in the force transducer case, a function of radial force. This should enable an appropriately spaced mesh of points to be selected for the look-up table such that the estimate of $\partial V / \partial r$ at each point in the mesh is more accurately represented.

In order to overcome the problem experienced with the first rig of providing relatively friction free guided motion of one end of a transducer with respect to the other (ensuring defined loading during calibration) two options were considered. The obvious approach was to use high quality commercial linear roller bearings integrated into a rig designed and

manufactured to high precision such that the required accuracy of motion could be maintained even whilst under the loads required for calibration. Such precision has a high cost attached to it and because of this, a cheaper alternative was proposed. This was based on the idea of a table suspended below a mounting structure by four bars, each having universal joints at each end. Depending upon the length of the four bars, small displacements of the table lie in a plane. Figure 6.9 shows a schematic drawing of this arrangement and of how the freedom of motions are used to guide direct and radial force application to the transducer. The forces are again most conveniently applied through a series of wire and pulley wheels. Appendix 3 contains working drawings of this design which was manufactured. It should be noted that the force application and measurement system is not specified in the drawings. In order to avoid high cost on a limited budget an arrangement utilising a spring balance and screw thread retraction was used. Figure 6.10 shows a diagram of this. As the adjustment nut is turned clockwise along the threaded bar a stretch is applied to the spring which has its other end attached via the metal cable to the moving table of the calibration rig. Since the extension of the spring is calibrated it gives a direct measurement of the force applied via the cable to the moving table and hence to the transducer.

Manufacture and assembly of this rig was completed towards the end of this research project. The results were again disappointing particularly in terms of force application. Firstly the tolerances in the rotational freedom achieved were not as small as was hoped for, primarily due to slack in each of the universal joints. However larger, higher specification universal joints might improve this. In any case with well aligned force application this did not appear to cause a problem. Most significant was the problem of smooth force application. The tension in the springs appeared to magnify mechanical shocks introduced into the system when the spring tensioning nuts were adjusted. This problem made defined increments of force along each of the two axes impossible and thus led to the failure of the second approach to three dimensional force calibration of the prototype transducer. It was then felt that only a highly accurate precision built automated dynamic calibration system using electromechanical force actuators and transducers would enable 3D force calibration and assessment. Such a design and build exercise was considered to be beyond the scope of this project.

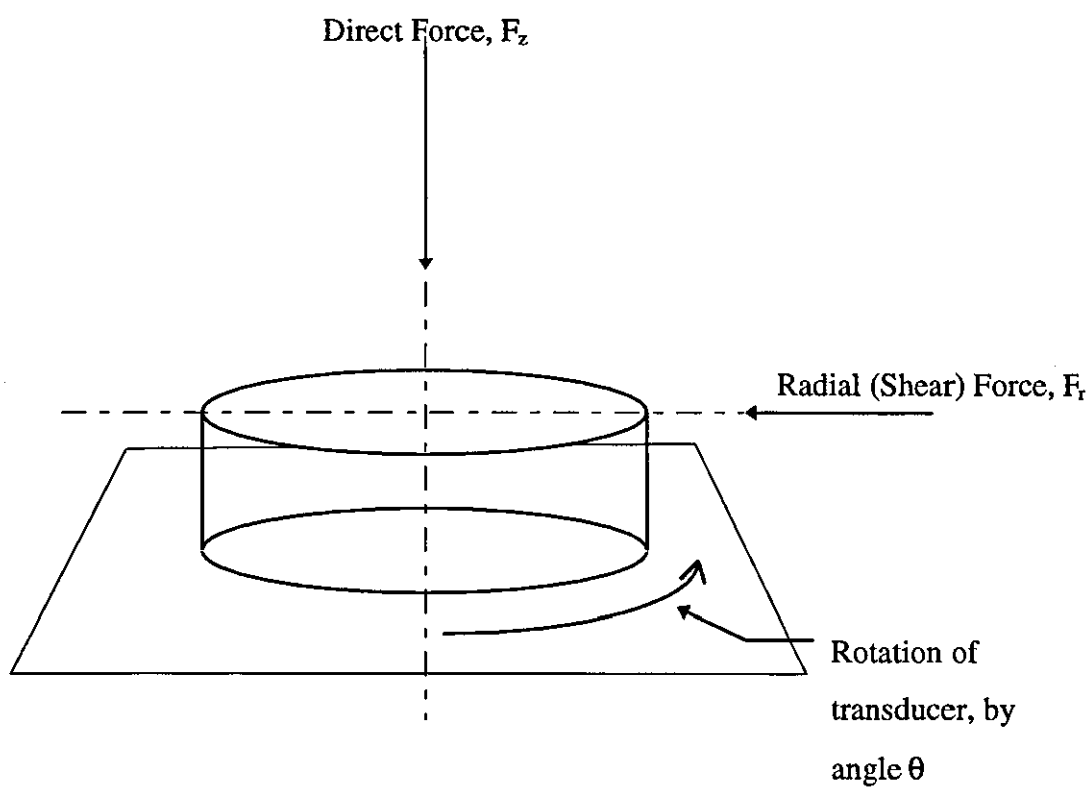


Figure 6-8 Force calibration scheme

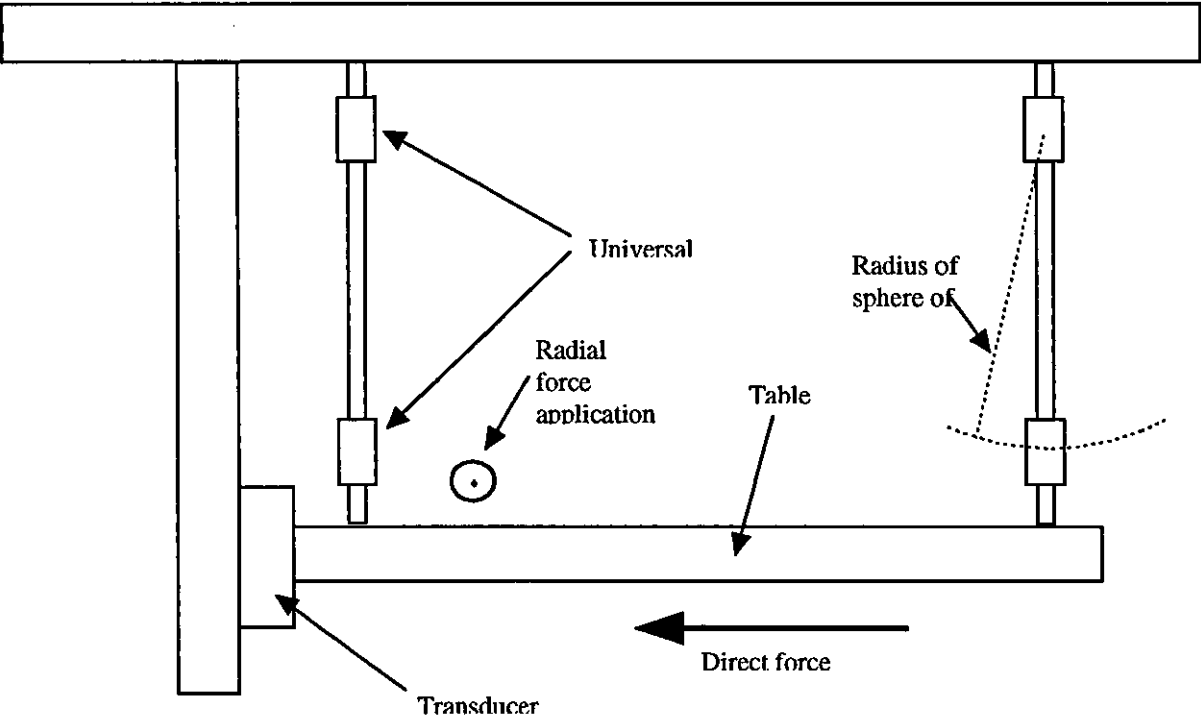


Figure 6-9 Force application guidance

Extension proportional to force applied

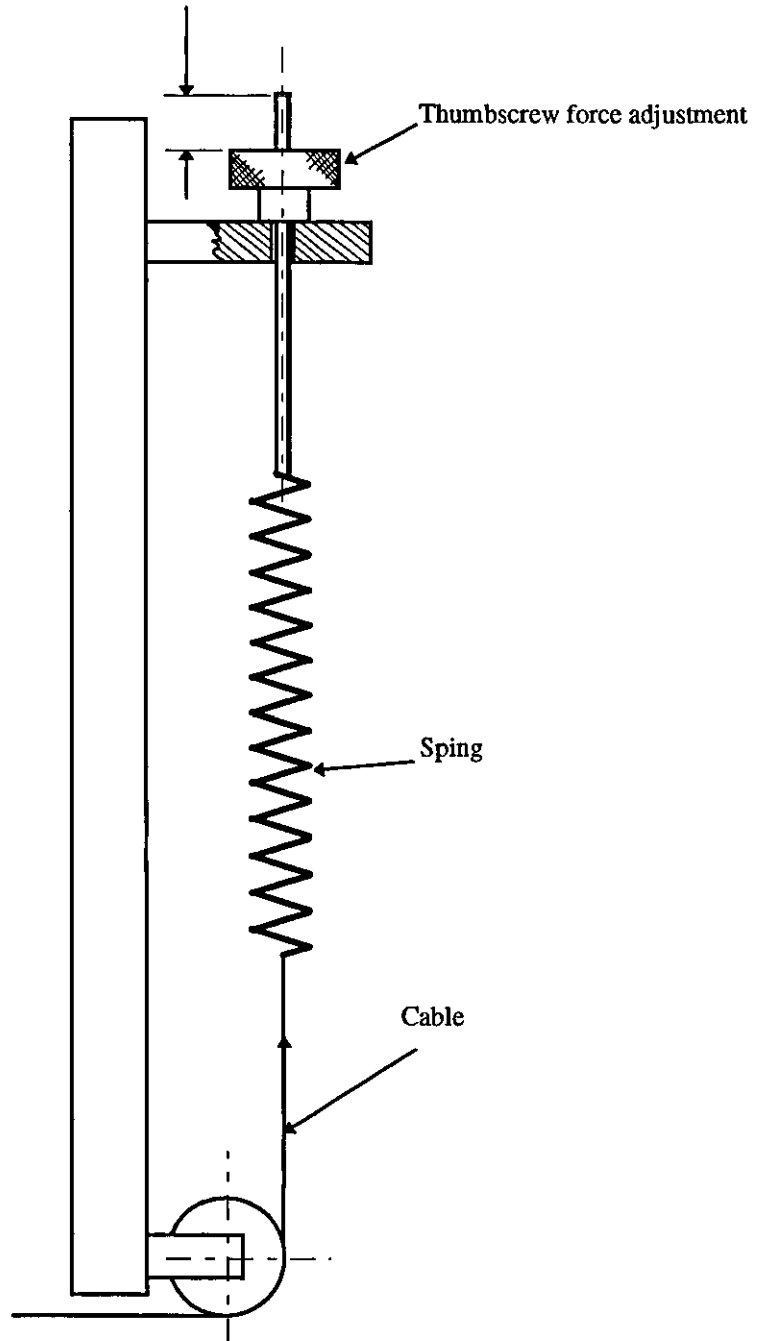


Figure 6-10 Force application and measurement system

7. CONCLUSIONS AND SUGGESTIONS FOR FURTHER WORK

The review of literature on transducers for mapping force distribution across the foot during gait reveals the varied methods/principles used for such transducers. Most distinctly it reveals the lack of in-shoe transducers for mapping 3D force distributions. Neither could any examples be found of principles that might be appropriately applied to the task of 3D force measurement in this environment.

Having concluded that a new approach was required for a force transducer, a method was proposed based upon the phenomena of electromagnetic induction. The task of researching the proposed force transducer was broken down into sections.

Firstly an examination of the practicality of the proposal, in terms of its use in a transducer small enough for the in-shoe application, was carried out. This was expanded on by an identification of the induced voltage - displacement characteristics of pairs of coils.

Following the encouraging results of the coil pair test, the mathematical basis of a 3D displacement transducer was explored and proven.

Whilst the ultimate objective of the research, the production of an in-shoe force transducer, was not achieved a good deal of progress from the 3D displacement transducer towards this end was made.

Firstly, various aspects of material selection were examined and a material suitable for prototype manufacture was identified.

Manufacturing/assembly techniques for the prototype transducers were then developed.

Attempts at force calibration failed because of the need for a much higher specification calibration rig. Time and financial constraints did not permit such a design and build exercise to be embarked upon. However an approach to the force calibration problem was suggested.

7.1 SUMMARY OF ACHIEVEMENTS

The following summarise the major achievements of this project:

- A force transducer specification was derived which consisted of: Maximum transducer height of 5mm, maximum transducer diameter of 10mm, vertical stress (compression) measurement range up to 1.5MPa and shear stress range up to 190kPa.
- A proposal was put forward for a new design principle for an in-shoe transducer based on electromagnetic induction between miniature coils held within a rubber material.
- The 3D force/displacement transducer principle proposed was to utilise a grouping of three receiving coils together with a single excitation coil. The voltages induced in the receiving coils, it was hypothesised, would allow determination of the position (in terms of x,y,z spatial co-ordinates) of the excitation coils with respect to the receiving coils. It was further hypothesised that with a mechanical restraining element mounted between the coils the system would be able to be calibrated as a three dimensional force transducer. To prove the approach proposed it was decided to explore development of a 3D displacement transducer in the first instance
- Miniature 'pancake' coils of 0.5mm height and diameters ranging from 3.5mm to 10mm (as required by to fit within transducer dimensions) were manufactured from 0.04 mm diameter wire.
- Useful flux linkage between miniature coils spaced within the constraints of the transducer was observed without the need to use current so large as to cause significant heating of the excitation coil. For example, the induced voltage in a 0.48mm long 100 turn, 4.54mm diameter coil when positioned at 4mm distance from a 180 turn excitation coil of 8 mm diameter and 0.48mm length carrying 30mA, 10kHz current was around 5mV
- Appropriate sensitivity of the induced voltage between miniature coils spaced within the constraints of the transducer was demonstrated. For example, the induced voltage in a 0.48mm long 100 turn, 4.54mm diameter coil when positioned at distances varying from

0.5 to 4mm from a 180 turn excitation coil of 8mm diameter and 0.48mm length carrying 30mA, 10kHz current varied from 5mV to 45mV

- In order to properly explore the induced voltage - displacement characteristics of the excitation coil - receiving coil pair and eventually enable transducer calibration and evaluation, a calibration/testing rig was designed and built. This was to be used, initially for the displacement transducer and eventually for the force transducer.
- The induced voltage - displacement characteristics of various pairs of excitation - receiving coils pairs were examined and analysed. Curve fitting techniques were used to describe the characteristics.
- Various mathematical algorithms for extracting the displacement of the excitation coil with respect to the receiving coils from voltages induced in the three coils were proposed. (These voltages varied in a non-linear way with displacement.)
- The mathematical approaches proposed for the transducer were developed, implemented in software and tested using the calibration rig. The most successful approach was shown to lead to position determination within an accuracy of $\pm 5\%$. The limitations and implementation cost of each method was examined.
- The materials selection criterion for the mechanical element of the force transducer were explored and a silicone rubber compound was identified as suitable for prototyping purposes.
- A force transducer assembly process was developed and solutions to various transducer manufacturing problems were suggested.
- The first calibration rig proved unsuitable for force calibration and after an unsuccessful attempt to identify any commercial three dimensional force transducer calibration system a revised force calibration rig was designed. This was based on a novel "frame mounting" system utilising universal joints.
- Further problems were identified with the second force calibration rig, particularly with the force application system and solutions suggested.

7.2 SUGGESTIONS FOR FURTHER WORK

The primary question of whether silicon rubber's mechanical non-linearities affect the mathematics needed to extract the forces from the voltages should be addressed

Sourcing of other materials for the transducer core should lead to an optimised force transducer for a particular range of forces is required.

An examination of how these materials perform under repeated dynamic loading is required to ensure that their force displacement characteristics remain constant with repeated loading. Quantification of their dynamic performance and hence the bandwidth of frequencies of forces that the transducer may be used to measure is also required.

More work is needed to ensure that the leads from the coils are robust enough since this is the most likely area for failure of the transducer in routine use.

The transducer design utilising rubber as the mechanical element leads to the scenario of electromagnetic induction across, what is essentially, an air-gap. This leads to the sensitivity of the system to the presence of magnetic material in the vicinity of the transducer. Identification of a rubber-like material with a higher magnetic permeability would improve this situation.

These in a sense are practical problems. However a number of other more fundamental questions need addressing following successful force calibration of a prototype.

Most fundamental, are questions that arise from "imperfect transducer loading conditions" that confound the basic assumptions that only evenly distributed direct forces are applied to the transducer face. In such a situation, the planes in which the coils lie, would no longer be parallel. In effect, this would imply a fourth degree of freedom within the system and perhaps could be resolved by adding a fourth receiving coil.

The effect of torque around the longitudinal axis of the transducer also needs to be considered. If the excitation coil is perfectly circular and has evenly distributed windings, then, in terms of displacement rotation of it would not be detectable. Clearly torque applied to a rubber matrix will affect its subsequent force displacement characteristics and we would therefore need to be able to measure a fifth degree of freedom. Manufacture of a

non-circular excitation coil may perhaps provide a solution. Likewise the use of a second excitation coil, mounted alongside the first and driven with a different excitation current frequency may offer an alternative.

Less fundamental, but of equal importance, the question of the need for isolated transducers as opposed to a transducer manufactured as a part of a continuous insole needs addressing. In particular the effects of forces, on the adjoining material of a continuous insole, upon the output of a transducer need to be evaluated. Related to this is the problem of the flexing of the insole as the shoe is flexed during walking.

It is clear that the majority of these goals could only be reached with the use of a precision engineered robust calibration and testing rig utilising actuators to enable rapid accurate automated calibration and testing, in particular dynamic testing.

In-shoe force measurement is a very difficult problem as is evidenced by the dearth of literature and problems outlined in the research reported in this thesis. A perfect solution would perhaps have been unlikely.

Despite the difficulty, an approach has been identified that actually offers a potential solution. Further, work has been described which proves the principle of the approach and begins to examine and offer solutions to the practical problems of future development.

The concept proposed in this thesis was awarded the annual IEE Measurements Prize (1990).

This work was published in the IEE Proceedings and this paper is included in Appendix D

References

- Assente, R., Ferrigno, G. et al. (1985), "Distributed multiplexing architecture for PVDF multitransducer platform scanning: a theoretical and practical approach". Proceedings of 5th Symposium of Electrets Heidelberg, Germany 674-684
- Bauman, J.H., Girling, J.P. and Brand, P.W. (1963), "Plantar Pressures and Trophic Ulceration". The Journal of Bone and Joint Surgery, 45 B, No 4, November
- Bennet, L., Kavner, D., Lee, B.K. and Trainor, F.A. (1979), "Shear vs Pressure as Causative Factors in Skin Blood Flow Occlusion". Archives of Physics in Medicine and Rehabilitation, 60, July, 309-314
- Betts, R. P. and Duckworth, T. (1978), "A device for measuring pressures under the sole of the foot". Engineering in Medicine 7 No 4, 223-228
- Betts, R. P., Franks, C. I., Duckworth, T. and Burke, J. (1980), "Static and dynamic foot pressure measurements in clinical orthopaedics". Medical & Biological Engineering & Computing, 18 No 5, 674-684
- Clot, J., Rabischong, P., Péruchon, E. and Faulpou J. (1975), "Principle and applications of the artificial sensitive skin". Proceedings of the 5th International Symposium on external control of human extremities Etan, Dubrovnik, 211-220
- Cobb J. and Claremont D.J. (1995), "Transducers for foot pressure measurement: survey of recent developments". Medical & Biological Engineering & Computing 33, 525-532
- Ctercteko, G.C., Dhanendran, M., Hutton, W.C. and Le Quesne, L.P. (1981), "Vertical forces acting on the feet of diabetic patients with neuropathic ulceration". British Journal of Surgery, 68, 608-614
- Davis, B.L. (1992), "Foot Ulceration: Hypotheses Concerning Shear and Vertical Forces Acting on Adjacent Regions of the Skin". Medical Hypotheses, 40, 44-47
- Dhanendran, M., Hutton, W. C. and Parker, Y. (1978), "The distribution of forces under the human foot: An on-line measuring system". Measurement Control, 11, July, 261-264
- Duckworth, T., Boulton, A.J.M., Betts, R.P., Franks, C.I. and Ward, J.D. (1985), "Plantar pressure measurements and the prevention of ulceration in the diabetic foot". The Journal of Bone and Joint Surgery, 67-B, 1, 79-85
- Elftman, H. (1934), "A cinematic study of the distribution of pressure in the human foot". The Anatomical Record, 59, 481-491
- Franks, C.I, Betts, R. P. and Duckworth, T. (1983), "Microprocessor based image processing system, for dynamic foot pressure studies". Medical & Biological Engineering & Computing, 21 No 5, 566-572
- Franks, C. I. and Betts, R. P. (1988), "Selection of transducer material for use with optical foot pressure systems". Journal of Biomedical Engineering 10 (4), 365-367

- Grover, F.W. (1946), "Calculation of self and mutual inductance". Dover Publications,
- Gross, T.S. and Bunch, R.P. (1988), "Measurement of discrete vertical in-shoe stress with piezoelectric transducers" . Journal Biomedical Engineering May; 10 (3): 261-5
- Hellebrandt, F.A. and Braun, G.L. (1938), "The influence of sex and age on the postural sway of man" . American Journal of Physical Anthropology XXIV, No 3 January-March
- Hennig, E.M., Cavanagh, P.R. and Macmillan, N.H.(1981), "High resolution in-shoe pressure measurements by piezoelectric transducers". Human Locomotion I(Canadian Society for Biomechanics, Ottawa), 120-121
- Hennig, E.M., Cavanagh, P.R., Albert, H.T.and Macmillan, N.H.(1982), "A piezoelectric method of measuring the vertical contact stress beneath the human foot". Journal of Biomedical Engineering 04-Jul
- Hermans, H. J., Waal, C. A., Burke, J. and Zivold, G. (1986), "A new gait analysis system for clinical use in a rehabilitation centre". Orthopaedics, 9, 1679-1675
- Johnson, G.R. (1986), "The use of spectral analysis to assess the performance of shock absorbing footwear" . Engineering in Medicine 15, 3, 117-122
- Lim, K. K. (1966), "The Fundamentals of Inductance Calculations". Journal of Department of Engineering University of Malaya 5, June, 29-45
- Lindley, P.B. (1967), "Engineering Design with Natural Rubber". NR Technical Bulletin
- Lord, M. (1981), "Foot pressure measurements: a review of methodology". Journal of Biomedical Engineering 3 , 91-99
- Lord, M.,Hosein, R. and Williams, R.B.(1992), "Method for in-shoe shear stress measurement" . Journal of Biomedical Engineering 14, May, 181-186
- Maalej, N and Webster, J. G. (1988), "A miniature electropotential force transducer". IEEE Transactions, BME-35 , 93-99
- Marey, E. J. (1873), "De La Locomotion terrestre chez les bipedes et les quadrupedes". Journal D' Anatomie et Physiologie 9 , 42-80
- May, M.T. (1968), "On the Usefulness of the Parts of the Body (a translation of Galen's work, 'De Usu Partium')". Cornell University Press, Ithaca, New York,
- McArdle, W.D., Katch, F.I. and Katch, V.L. (1991), "Exercise Physiology:Energy, nutrition and human performance" (3rd edition). Lea & Febiger, Philadelphia p569
- Murgatroyd, P. (1990), "Winding inductors using wire length measurement". Electrical Manufacturing & Coil Winding p238-241
- Nevill, A.J. (1991), "A foot pressure measurement system, utilising PVDF & co-polymer piezoelectric transducers" . PhD Thesis. University of Canterbury

- Nevill, A.J., Pepper, M.G. and Whiting, M. (1995), "In-shoe foot pressure measurement system utilising piezoelectric film transducers". *Medical & Biological Engineering & Computing*, 33 (1): 76-81
- Vines, G. (1985), "Measuring the weight on your feet". *New Scientist*, 13 June p 24
- Nicol, K. and Hennig, E.M. (1978), "Measurement of pressure distribution by means of a flexible large surface mat". *Biomechanics* (University Park Press, Baltimore USA) I-A , 374-380
- Pedotti, A., Assante, R., Fusi, G., Derossi, D., Dario, P. and Domenci C. (1984), "Multi-sensor piezoelectric polymer insole for pedobarography". *Ferroelectrics*, 60 , 163-174
- Perry, J. (1992), "Gait Analysis". McGraw Hill, New York,
- Peruchon, E., Jullian, J.M. and Rabischong P. (1989), "Wearable unrestraining footprint analysis system. Applications to human gait study". *Medical & Biological Engineering & Computing*, 27, 557-585
- Pollard, J.P., Le Quesne, L.P. and Tappin, J.W. (1983), "Forces under the foot" . *Journal of Biomedical Engineering* 5, Jan
- Rabischong, P., Aubriot, H., Peruchon, E., Guibal, C. and Domenici, C. (1967), "L'electropodographie: une methode nouvelle de mesure des forces plantaires". *Revue de Pédiatrie*, 44 , 9-24
- Rhodes, A. and Sherk, H. (1988), "High resolution analysis of foot ground reaction forces". *Foot Ankle*, 9 , 135-138
- Soames, R.W., Stott, J.R.R., Goodbody, A., Blake, C.D and Brewerton, D.A. (1982), "Measurement of pressure under the foot during function". *Medical & Biological Engineering & Computing* 20, 489-495
- Tappin, J.W., Pollard, J. and Beckett, E.A. (1980), "Method of measuring 'shearing' forces on the sole of the foot" . *Clinical Physics & Physiological Measurement* 1, No 1 , 83-85
- Terman, F.E. (1943), "Radio Engineers Handbook" . McGraw Hill, New York,
- Warren-Forward, M.J., Goodall, R.M. and Pratt, D.J. (1992), "Three-dimensional displacement and force transducer". *IEE Proceedings-A*, Jan, 139, 1, 21-29
- Williams, R.B., Porter, D. and Roberts, V.C. (1992), "Triaxial force transducer for investigating the stresses at the stump/socket interface". *Medical & Biological Engineering & Computing* Jan, 89-96
- Yu Dingan and Han, K.S (1987), "Self Inductance of Air-Cored Circular Coils with Rectangular Cross Section" . *IEE Transactions on Magnetics*, Nov, Mag-23 No 6

Bibliography

- Akhlaghi, F., Pepper, M. et al. (1993), "Assessment of in-shoe foot pressure patterns over multiple footsteps". Proceedings of IPSM/HPA 49th Annual. Conference. Lincoln, UK p68
- Akhlaghi, F., Daw, J. et al. (1994), "In-shoe, step-to-step pressure variations". Foot, 4, 62-68
- Appoldt, F.A., Bennett, L. and Contini, R. (1968), "Stump socket pressure in lower extremity prosthesis". Journal of Biomechanics 1, 247-257
- Barnett, C. H. (1956), "The phases of human gait". Lancet, ii, 617-621
- Bauman, J. H. and Brand, P. W. (1963), "Measurement of Pressure between foot and shoe". The Lancet, i, , 629-632, March 23
- Bennett, L., Lee, B. Y. and Boulton A. J. M. (1988), "Vertical shear existence in animal pressure threshold experiments". Journal of Decubitus, 1, 18-24
- Betts, R. P., Duckworth, T. and Austin, I.G. (1980), "Critical light reflection at a plastic/glass interface and its application to foot pressure measurements". Journal of Medical Engineering & Technology 4 No 3 ,136-142
- Cavanagh, P.R., Simoneau, G.G. and Ulbrecht, J.S. (1993), "Ulceration, unsteadiness, and uncertainty: the biomechanical consequences of diabetes mellitus". Journal of Biomechanics 26 Suppl 1 23-40
- Chodera, J. D. (1974), "Analysis of gait from foot prints". Physiotherapy, 60, 179-181
- Dinsdale, S. M. (1974), "Decubitus ulcers: role of pressure and friction in causation". Archives Physical Medicine & Rehabilitation 55: 147-152
- Ferguson, P. (1980), "Design criteria for the measurement of pressure at body/support interfaces". Engineering in Medicine 9 (4) , 209-213
- Franks, C. I., Betts, R. P. et al. (1983), "Microprocessor based image processing system, for dynamic foot pressure studies". Biological Engineering & Computing 21 (5) , 566-572
- Gross, T.S. and Bunch, R.P. (1989), "Material moderation of plantar impact stress". Medical Science of Sports Exercise, Oct; 21 (5): 619-24
- Hennacy, R.A. and Gunther, R. (1975), "A piezoelectric crystal method for measuring static and dynamic pressure distributions in the feet". Journal of the American Podiatric Association, 65, 444-449
- Khan, J.S. (1939), "Treatment of Leprous Trophic Ulcers". Leprosy in India, 11,19
- Meijer, J. H., Schut, G. L., Ribbe, M. W., Goovaerts, H. G., Nieuwenhuys, R., Reulen, J. P. and Schneider, H. (1989), "Method for the measurement of ulcer formation". Medical & Biological Engineering & Computing 27(5) 502-506

- Minns, R. J. (1982), "Two simple plantar pressure recording devices in clinical use: evaluation using a pedobarograph". *Journal of Engineering in Medicine* 11 (3) , 117-120
- Naylor, P. F. (1955), "The skin surface and friction". *British Journal of Dermatology*, 67, 239
- Roaf, R. (1976), "Causation and prevention of bedsores". *Bedsore Biomechanics*, Ed Kenedi R., Cowden J.M., Scales J.T. Baltimore Univ Park Press
- Sensors (1991), "A pressure mapping system for gait analysis" p21-23
- Spence, W. R. and Shields, M. N. (1968), "A new insole for the prevention of athletic blisters". *Journal Sports Medicine*, 0.45625
- Spence, W.R. and Shields, M.N. (1968), "Prevention of blisters, callosities and ulcers by absorption of shearing force". *Journal of American Podiatric Association* 58, 428
- Treves, F. (1884), "Treatment of perforating ulcer of the foot". *Lancet*, ii, 949-51

Appendix 1

Inductance Formulae

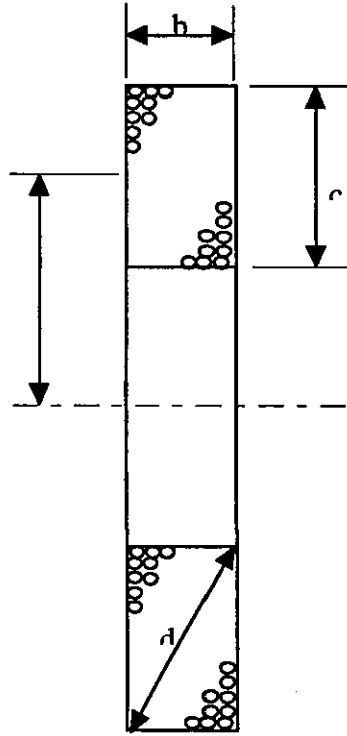


Figure A1.1 Coil cross sectional dimensions

Figure A1.1 shows the cross sectional dimensions of a short multi-layer coil. Three alternative formulae were used to calculate coil inductances and these are presented below:

Wheeler's approximate (cited by Terman, 1955) formulae for a short multi-layer inductance of solenoidal form:-

$$L_o = \frac{0.8a^2n^2}{(6a + 9b + 10c)} [\mu H]$$

where the dimensions (a-c) are in inches and n is the number of turns on the coil.

Terman (1955) gives a more accurate formulae:-

(for $b > c$ in figure A1.1)

$$L_o = 0.03193an^2[2.303(1 + \frac{b^2}{32a^2} + \frac{d^2}{96a^2})\log_{10}(\frac{8a}{d}) - y_1 + \frac{b^2}{16a^2}y_2][\mu H]$$

where n is the number of turns on the coil, a, b and c are the dimensions of the coil (in inches) as described in figure A1.1 whilst y1 and y2 are constants depending upon the value of b/c and are given in the table 1 below.

Gover (1946) gives the following formula for the self inductance of a circular coil of rectangular cross section of any proportions:-

$$L_o = 0.019739(\frac{2a}{b})n^2 a (K - k) [\mu H]$$

where a and b are the dimensions as defined in figure A1.1 and (in cm), K is dependent upon 2a/b and may be obtained using the table in figure A1.2. k varies as a function of c/2a and c/b and may be obtained from the table in figure A1.3.

TABLE 16.—VALUES OF y_1 , y_2 , AND y_3 FOR USE IN Eqs. (53) AND (54)

b/c or c/b	y_1	Differ- ence	c/b	y_2	Differ- ence	b/c	y_3	Differ- ence
0	0.5000	0.0253	0	0.125	0.002	0	0.597	0.002
0.025	0.5253	0.0237						
0.05	0.5490	0.0434	0.05	0.127	0.005	0.05	0.599	0.003
0.10	0.5924	0.0386	0.10	0.132	0.010	0.10	0.602	0.006
0.15	0.6310	0.0342	0.15	0.142	0.013	0.15	0.608	0.007
0.20	0.6652	0.0301	0.20	0.155	0.016	0.20	0.615	0.009
0.25	0.6953	0.0266	0.25	0.171	0.020	0.25	0.624	0.009
0.30	0.7217	0.0230	0.30	0.192	0.023	0.30	0.633	0.010
0.35	0.7447	0.0198	0.35	0.215	0.027	0.35	0.643	0.011
0.40	0.7645	0.0171	0.40	0.242	0.031	0.40	0.654	0.011
0.45	0.7816	0.0144	0.45	0.273	0.034	0.45	0.665	0.012
0.50	0.7960	0.0121	0.50	0.307	0.037	0.50	0.667	0.013
0.55	0.8081	0.0101	0.55	0.344	0.040	0.55	0.690	0.012
0.60	0.8182	0.0083	0.60	0.384	0.043	0.60	0.702	0.013
0.65	0.8265	0.0066	0.65	0.427	0.047	0.65	0.715	0.014
0.70	0.8331	0.0052	0.70	0.474	0.049	0.70	0.729	0.013
0.75	0.8383	0.0039	0.75	0.523	0.053	0.75	0.742	0.014
0.80	0.8422	0.0029	0.80	0.576	0.056	0.80	0.756	0.015
0.85	0.8451	0.0019	0.85	0.632	0.059	0.85	0.771	0.015
0.90	0.8470	0.0010	0.90	0.690	0.062	0.90	0.786	0.015
0.95	0.8480	0.0003	0.95	0.752	0.064	0.95	0.801	0.015
1.00	0.8483	1.00	0.816	1.00	0.816	

Figure A1.1 (From Terman, 1955)

TABLE 36. VALUES OF K FOR SHORT SINGLE-LAYER COILS, FORMULA (118) (Concluded)

$b/2a$	K	d_1	d_2	$b/2a$	K	d_1	d_2
0.50	0.525510	4800		0.75	0.623011	3111	
.51	.530310	4708	-92	.76	.626122	3063	-48
.52	.535018	4619	-89	.77	.629185	3016	-48
.53	.539637	4534	-86	.78	.632200	2970	-46
.54	.544170	4450	-84	.79	.635170	2924	-46
0.55	0.548620	4368	-81	0.80	0.638094	2880	-44
.56	.552988	4290	-78	.81	.640974	2837	-43
.57	.557278	4212	-77	.82	.643811	2794	-43
.58	.561491	4137	-76	.83	.646605	2753	-41
.59	.565628	4063	-74	.84	.649358	2712	-41
0.60	0.569691	3992	-71	0.85	0.652070	2673	-39
.61	.573683	3923	-68	.86	.654743	2634	-39
.62	.577606	3856	-68	.87	.657376	2596	-38
.63	.581462	3790	-66	.88	.659972	2560	-37
.64	.585252	3724	-65	.89	.662532	2522	-37
0.65	0.588976	3662	-63	0.90	0.665054	2486	-36
.66	.592638	3601	-61	.91	.667540	2452	-34
.67	.596239	3541	-60	.92	.669991	2417	-34
.68	.599780	3483	-58	.93	.672408	2384	-33
.69	.603263	3426	-57	.94	.674792	2350	-33
0.70	0.606689	3370	-56	0.95	0.677142	2318	-32
.71	.610060	3316	-54	.96	.679460	2286	-32
.72	.613376	3263	-54	.97	.681747	2256	-31
.73	.616639	3211	-52	.98	.684003	2225	-31
.74	.619850	3161	-50	0.99	.686228	2195	-30
0.75	0.623011		-50	1.00	0.688423		

TABLE 36. VALUES OF K FOR SHORT SINGLE-LAYER COILS, FORMULA (118)

$b/2a$	K	d_1	d_2	$b/2a$	K	d_1	d_2
0	0	34960		0.25	0.365432	8386	
0.01	0.034960	26138	-8822	.26	.373818	8168	-219
.02	.061098	22809	-3329	.27	.381986	7958	-209
.03	.083907	20655	-2154	.28	.389944	7758	-200
.04	.104562	19053	-1602	.29	.397703	7566	-192
0.05	0.123615	17780	-1273	0.30	0.405269	7382	-184
.06	.141395	16724	-1056	.31	.412650	7205	-176
.07	.158119	15823	-901	.32	.419856	7035	-170
.08	.173942	15038	-784	.33	.426890	6871	-164
.09	.188980	14343	-696	.34	.433762	6713	-158
0.10	0.203324	13720	-623	0.35	0.440474	6562	-152
.11	.217044	13156	-564	.36	.447036	6414	-147
.12	.230200	12642	-514	.37	.453450	6274	-141
.13	.242842	12169	-473	.38	.459724	6136	-137
.14	.255011	11732	-436	.39	.465860	6004	-132
0.15	0.266744	11327	-406	0.40	0.471865	5877	-128
.16	.278070	10948	-378	.41	.477742	5754	-124
.17	.289019	10595	-354	.42	.483496	5634	-120
.18	.299614	10262	-333	.43	.489129	5518	-116
.19	.309876	9949	-313	.44	.494646	5405	-112
0.20	0.319825	9654	-295	0.45	0.500052	5296	-108
.21	.329479	9374	-280	.46	.505348	5191	-105
.22	.338852	9108	-266	.47	.510539	5089	-102
.23	.347960	8856	-252	.48	.515628	4989	-100
.24	.356816	8616	-240	.49	.520617	4893	-96
0.25	0.365432		-229	0.50	0.525510		-93

Figure A1.2 Table for K (From Grover, 1946)

b/c		c/2a										b/c
		0	0.05	0.10	0.15	0.20	0.25	0.30	0.35	0.40	0.45	
0	1	1	1	1	1	1	1	1	1	1	1	0
0.05	1	0.9871	0.9843	0.9821	0.9801	0.9782	0.9763	0.9745	0.9728	0.9712	0.9696	0.05
0.10	1	.9749	.9695	.9651	.9612	.9575	.9541	.9507	.9474	.9442	.9412	0.10
0.15	1	.9634	.9555	.9491	.9434	.9381	.9332	.9283	.9237	.9189	.9145	0.15
0.20	1	.9524	.9422	.9339	.9266	.9197	.9133	.9070	.9010	.8951	.8894	0.20
0.25	1	.9419	.9294	.9194	.9105	.9021	.8943	.8868	.8795	.8725	.8656	0.25
0.30	1	.9318	.9172	.9059	.8950	.8853	.8762	.8675	.8591	.8510	.8431	0.30
0.35	1	.9221	.9054	.8920	.8802	.8692	.8589	.8491	.8396	.8305	.8217	0.35
0.40	1	.9128	.8941	.8792	.8660	.8537	.8423	.8314	.8210	.8110	.8013	0.40
0.45	1	.9038	.8832	.8668	.8523	.8389	.8264	.8145	.8032	.7923	.7819	0.45
0.50	1	.8951	.8727	.8548	.8391	.8246	.8111	.7983	.7861	.7744	.7632	0.50
0.55	1	.8867	.8625	.8434	.8264	.8108	.7964	.7827	.7697	.7573	.7454	0.55
0.60	1	.8786	.8527	.8322	.8141	.7975	.7822	.7677	.7540	.7409	.7284	0.60
0.65	1	.8707	.8432	.8214	.8022	.7847	.7686	.7533	.7389	.7251	.7121	0.65
0.70	1	.8630	.8339	.8109	.7907	.7723	.7554	.7394	.7243	.7100	.6963	0.70
0.75	1	.8556	.8249	.8007	.7796	.7603	.7426	.7260	.7103	.6955	.6816	0.75
0.80	1	.8484	.8162	.7908	.7688	.7487	.7303	.7130	.6968	.6810	.6672	0.80
0.85	1	.8413	.8077	.7813	.7584	.7374	.7184	.7005	.6838	.6681	.6533	0.85
0.90	1	.8345	.7995	.7720	.7482	.7265	.7068	.6884	.6712	.6551	.6399	0.90
0.95	1	.8279	.7914	.7629	.7383	.7159	.6956	.6767	.6591	.6426	.6271	0.95
1.00	1	.8214	.7837	.7548	.7287	.7056	.6848	.6656	.6474	.6306	.6148	1.00

	c/2a											
b/c	0.50	0.55	0.60	0.65	0.70	0.75	0.80	0.85	0.90	0.95	1.00	b/c
0	1	1	1	1	1	1	1	1	1	1	1	0
0.05	0.9696	0.9679	0.9663	0.9648	0.9633	0.9618	0.9604	0.9591	0.9577	0.9562	0.9547	0.05
0.10	.9412	.9381	.9351	.9322	.9293	.9265	.9238	.9212	.9187	.9161	.9136	0.10
0.15	.9145	.9102	.9059	.9017	.8977	.8938	.8900	.8863	.8820	.8794	.8763	0.15
0.20	.8894	.8839	.8785	.8732	.8683	.8634	.8586	.8540	.8497	.8457	.8421	0.20
0.25	.8656	.8590	.8526	.8463	.8405	.8347	.8292	.8239	.8190	.8144	.8103	0.25
0.30	.8431	.8355	.8282	.8210	.8143	.8078	.8017	.7959	.7905	.7854	.7807	0.30
0.35	.8217	.8132	.8051	.7971	.7897	.7825	.7759	.7697	.7638	.7583	.7532	0.35
0.40	.8013	.7920	.7831	.7745	.7664	.7587	.7515	.7450	.7388	.7329	.7274	0.40
0.45	.7819	.7718	.7622	.7531	.7443	.7360	.7285	.7217	.7152	.7090	.7032	0.45
0.50	.7632	.7526	.7424	.7327	.7234	.7146	.7068	.6996	.6920	.6865	.6805	0.50
0.55	.7454	.7342	.7235	.7132	.7036	.6945	.6862	.6787	.6717	.6651	.6590	0.55
0.60	.7284	.7160	.7054	.6947	.6847	.6754	.6668	.6589	.6516	.6448	.6386	0.60
0.65	.7121	.6998	.6882	.6771	.6668	.6572	.6484	.6402	.6326	.6266	.6194	0.65
0.70	.6965	.6837	.6717	.6603	.6497	.6399	.6308	.6224	.6146	.6075	.6012	0.70
0.75	.6816	.6683	.6560	.6443	.6334	.6234	.6140	.6055	.5976	.5904	.5839	0.75
0.80	.6672	.6530	.6409	.6290	.6179	.6076	.5981	.5894	.5815	.5742	.5676	0.80
0.85	.6533	.6394	.6264	.6143	.6030	.5926	.5829	.5742	.5662	.5589	.5521	0.85
0.90	.6399	.6257	.6124	.6002	.5888	.5782	.5684	.5597	.5517	.5443	.5375	0.90
0.95	.6271	.6126	.5991	.5867	.5752	.5644	.5545	.5459	.5378	.5303	.5236	0.95
1.00	0.6148	0.6001	0.5865	0.5738	0.5621	0.5512	0.6413	0.5324	0.5244	0.5170	0.5102	1.00

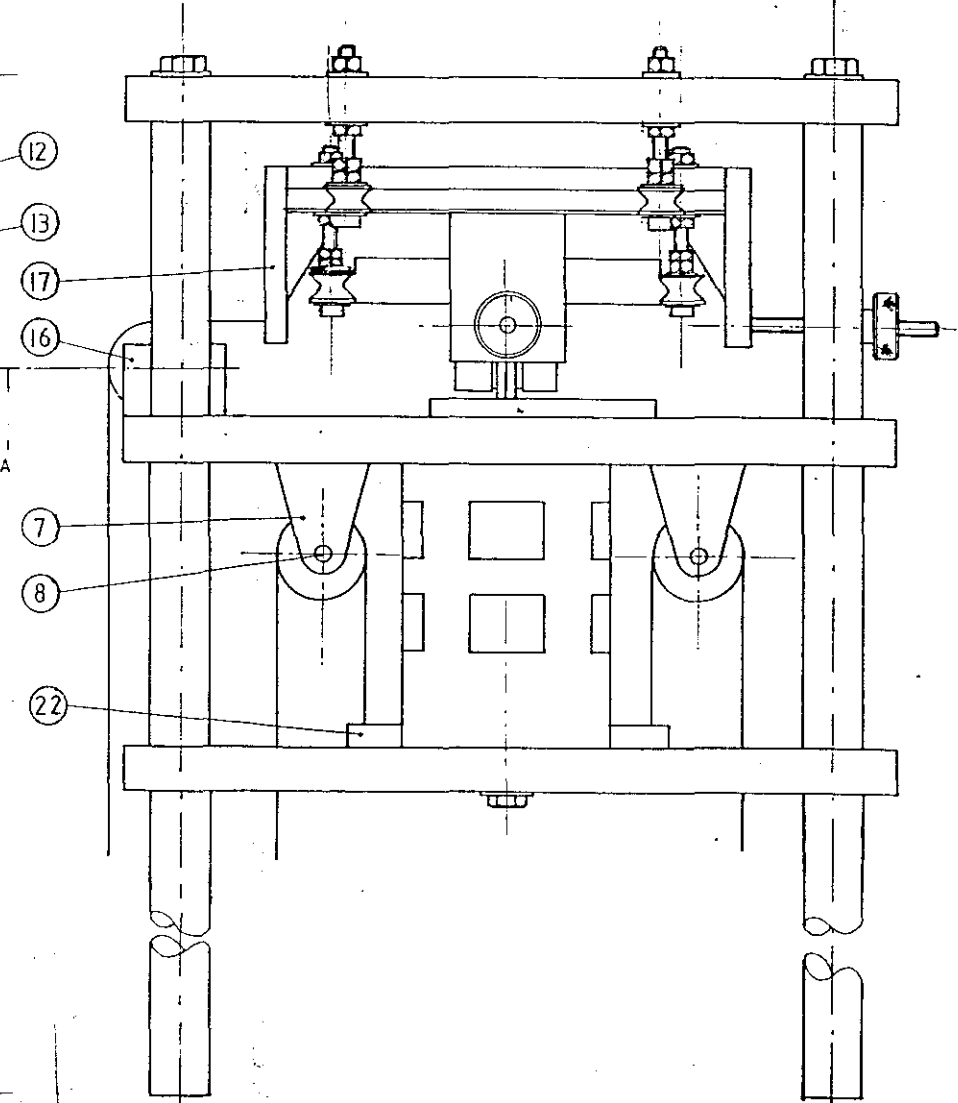
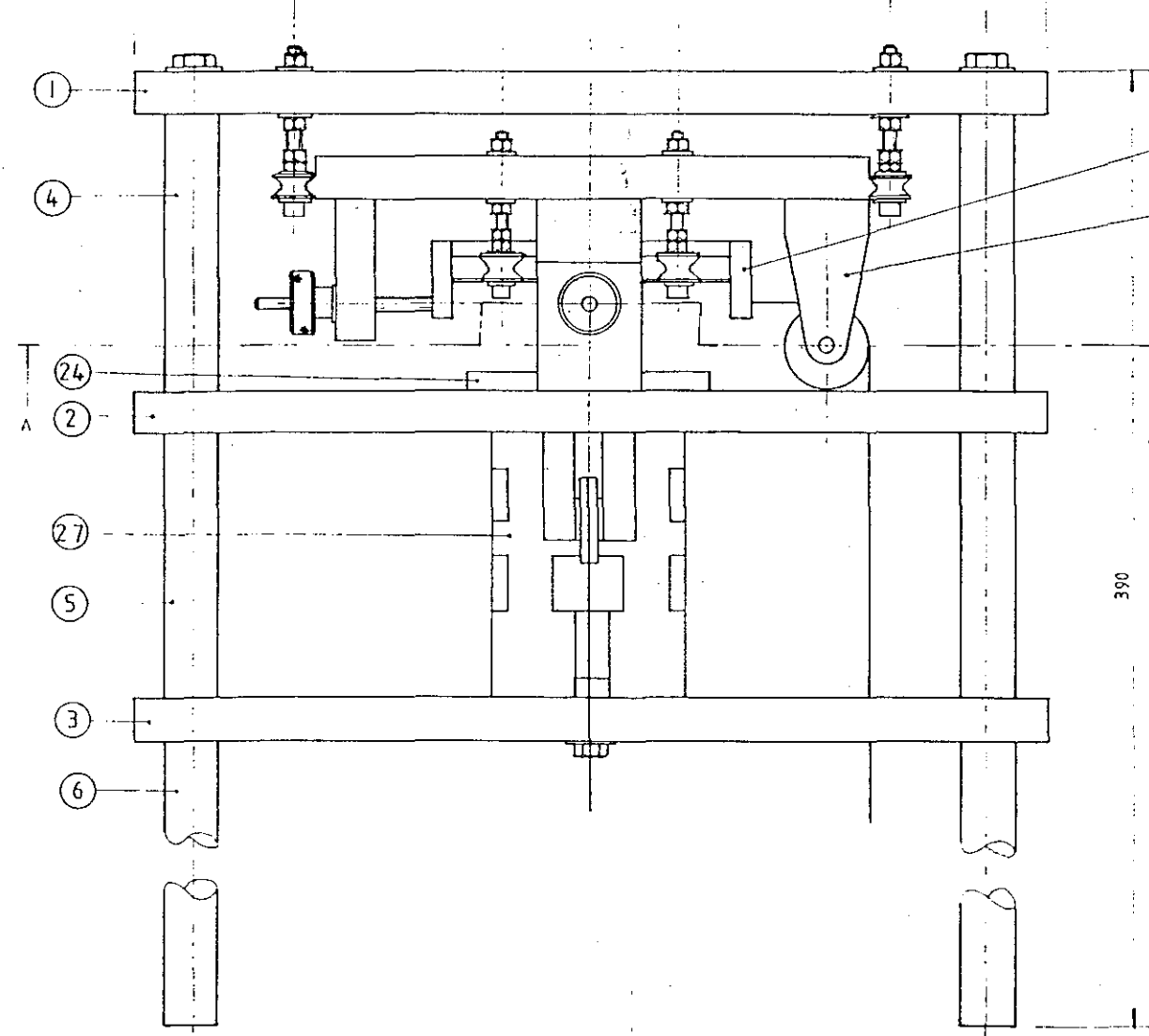
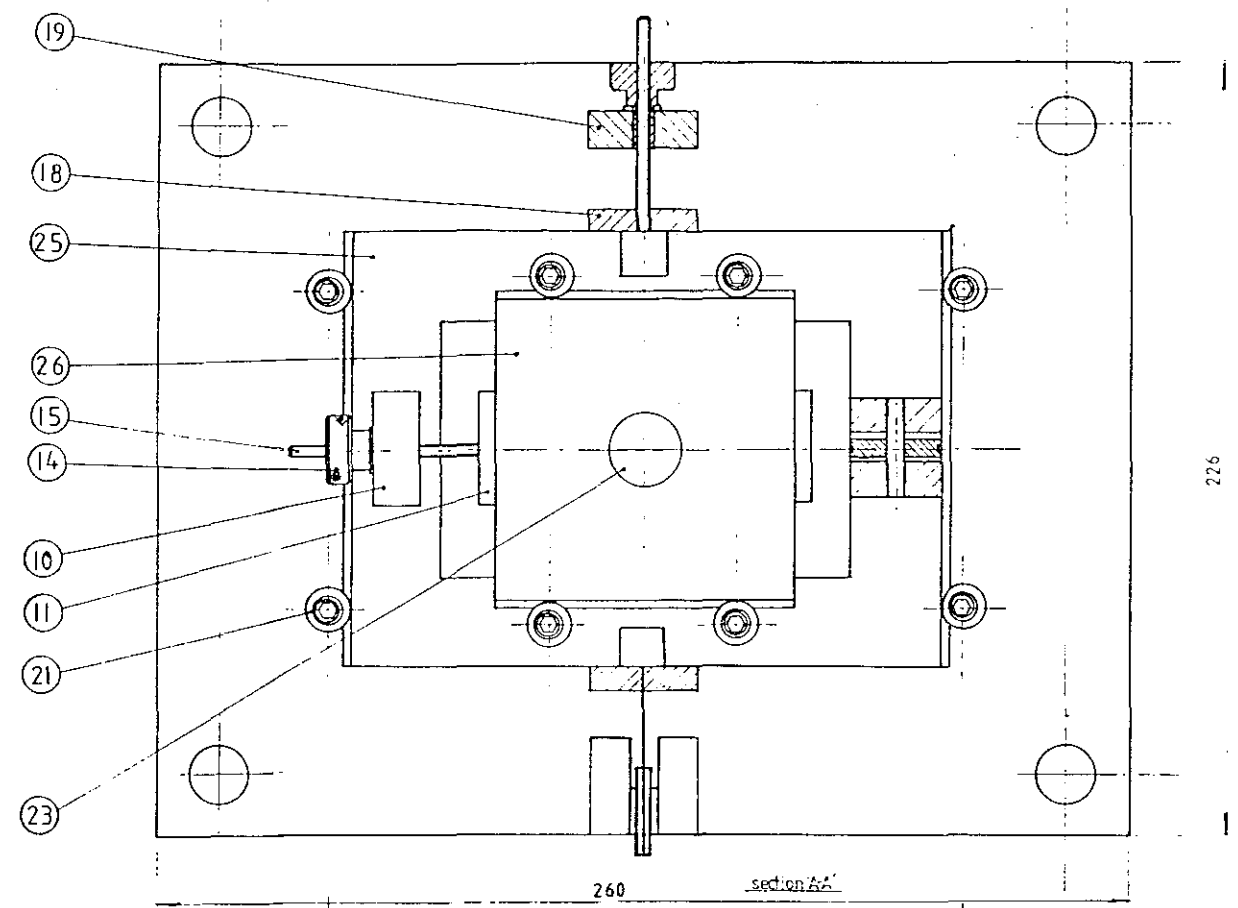
		c/2a											
b/c		0	0.05	0.10	0.15	0.20	0.25	0.30	0.35	0.40	0.45	0.50	b/c
0	0	0	0	0	0	0	0	0	0	0	0	0	0
0.05	0	0.0045	0.0090	0.0134	0.0178	0.0226	0.0269	0.0314	0.0359	0.0398	0.0436	0.05	0.05
0.10	0	.0077	.0153	.0229	.0304	.0379	.0453	.0527	.0601	.0674	.0745	0.10	0.10
0.15	0	.0098	.0194	.0291	.0387	.0482	.0576	.0669	.0763	.0855	.0944	0.15	0.15
0.20	0	.0114	.0228	.0341	.0454	.0566	.0677	.0786	.0894	.1000	.1105	0.20	0.20
0.25	0	.0128	.0256	.0383	.0510	.0635	.0759	.0881	.1001	.1120	.1237	0.25	0.25
0.30	0	.0140	.0280	.0419	.0557	.0694	.0829	.0962	.1093	.1221	.1347	0.30	0.30
0.35	0	.0151	.0301	.0451	.0598	.0745	.0889	.1031	.1172	.1309	.1443	0.35	0.35
0.40	0	.0160	.0319	.0478	.0634	.0789	.0942	.1092	.1240	.1385	.1526	0.40	0.40
0.45	0	.0168	.0335	.0501	.0666	.0828	.0988	.1146	.1300	.1452	.1599	0.45	0.45
0.50	0	.0175	.0349	.0522	.0694	.0863	.1030	.1194	.1354	.1511	.1663	0.50	0.50
0.55	0	.0182	.0362	.0541	.0720	.0895	.1068	.1237	.1403	.1563	.1720	0.55	0.55
0.60	0	.0188	.0374	.0559	.0743	.0924	.1102	.1276	.1446	.1611	.1772	0.60	0.60
0.65	0	.0193	.0385	.0576	.0764	.0950	.1132	.1311	.1485	.1655	.1819	0.65	0.65
0.70	0	.0198	.0395	.0591	.0784	.0974	.1160	.1343	.1521	.1694	.1861	0.70	0.70
0.75	0	.0203	.0404	.0605	.0802	.0996	.1186	.1373	.1554	.1729	.1899	0.75	0.75
0.80	0	.0207	.0413	.0617	.0818	.1016	.1210	.1400	.1584	.1762	.1934	0.80	0.80
0.85	0	.0211	.0421	.0629	.0833	.1036	.1232	.1424	.1611	.1792	.1966	0.85	0.85
0.90	0	.0215	.0428	.0639	.0847	.1052	.1252	.1447	.1637	.1820	.1995	0.90	0.90
0.95	0	.0218	.0435	.0649	.0860	.1068	.1271	.1469	.1661	.1846	.2022	0.95	0.95
1.00	0	.0221	.0441	.0658	.0872	.1082	.1288	.1489	.1683	.1869	.2047	1.00	1.00

b/c	c/2a											b/c
	0.50	0.55	0.60	0.65	0.70	0.75	0.80	0.85	0.90	0.95	1.00	
0	0	0	0	0	0	0	0	0	0	0	0	0
0.05	0.0436	0.0484	0.0529	0.0572	0.0613	0.0653	0.0692	0.0730	0.0767	0.0803	0.0839	0.05
0.10	.0745	.0816	.0885	.0953	.1020	.1085	.1149	.1211	.1272	.1331	.1388	0.10
0.15	.0944	.1023	.1100	.1176	.1250	.1321	.1390	.1457	.1523	.1587	.1648	0.15
0.20	.1105	.1208	.1308	.1406	.1501	.1594	.1684	.1771	.1854	.1933	.2009	0.20
0.25	.1237	.1350	.1460	.1568	.1673	.1775	.1874	.1968	.2058	.2144	.2224	0.25
0.30	.1347	.1471	.1590	.1706	.1819	.1928	.2032	.2132	.2226	.2315	.2399	0.30
0.35	.1443	.1574	.1701	.1823	.1942	.2057	.2166	.2269	.2366	.2458	.2544	0.35
0.40	.1526	.1663	.1796	.1924	.2048	.2167	.2279	.2384	.2484	.2577	.2664	0.40
0.45	.1599	.1742	.1880	.2012	.2140	.2262	.2377	.2484	.2585	.2679	.2766	0.45
0.50	.1663	.1811	.1953	.2089	.2220	.2345	.2462	.2571	.2672	.2766	.2852	0.50
0.55	.1720	.1872	.2018	.2157	.2291	.2418	.2536	.2645	.2748	.2842	.2926	0.55
0.60	.1772	.1927	.2076	.2218	.2354	.2482	.2601	.2712	.2814	.2907	.2990	0.60
0.65	.1819	.1977	.2128	.2272	.2409	.2539	.2659	.2770	.2872	.2964	.3046	0.65
0.70	.1861	.2022	.2175	.2321	.2459	.2589	.2710	.2821	.2923	.3014	.3095	0.70
0.75	.1899	.2062	.2217	.2365	.2504	.2634	.2755	.2866	.2968	.3068	.3137	0.75
0.80	.1934	.2098	.2255	.2404	.2544	.2675	.2796	.2907	.3007	.3096	.3174	0.80
0.85	.1966	.2132	.2291	.2440	.2581	.2712	.2833	.2943	.3042	.3130	.3206	0.85
0.90	.1995	.2163	.2323	.2473	.2614	.2745	.2866	.2976	.3074	.3160	.3234	0.90
0.95	.2022	.2191	.2352	.2503	.2644	.2776	.2896	.3005	.3102	.3186	.3259	0.95
1.00	.2047	.2217	.2378	.2530	.2672	.2804	.2924	.3031	.3126	.3209	.3281	1.00

Figure A1.3 Table for k (From Grover , 1946)

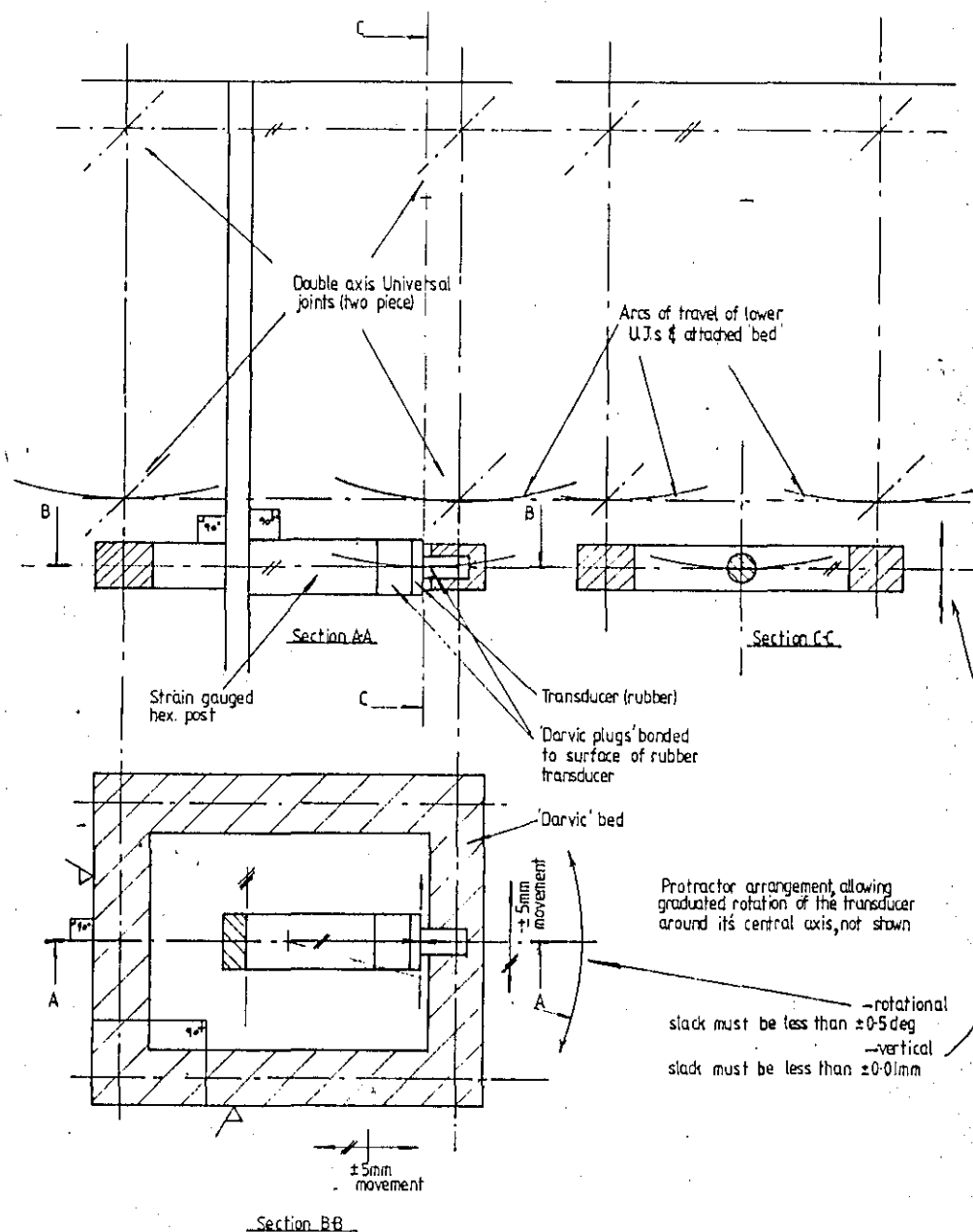
Appendix 2

Displacement Calibration Rig Design

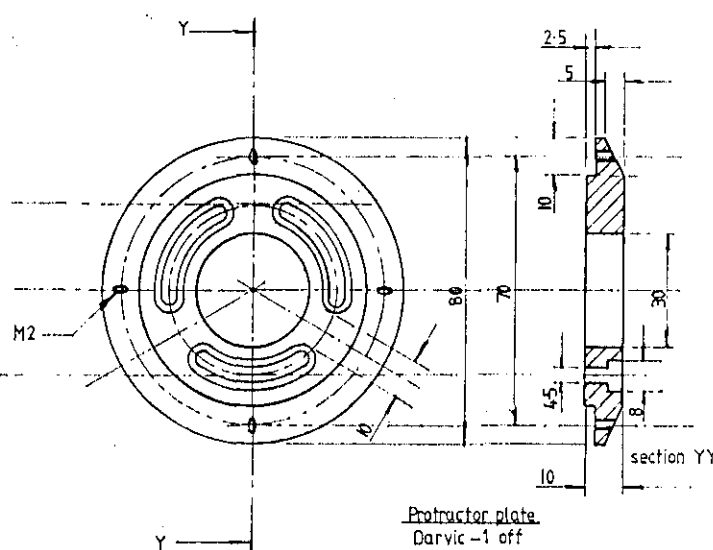


Appendix 3

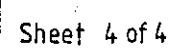
Force Calibration Rig Design

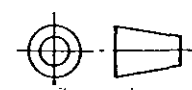
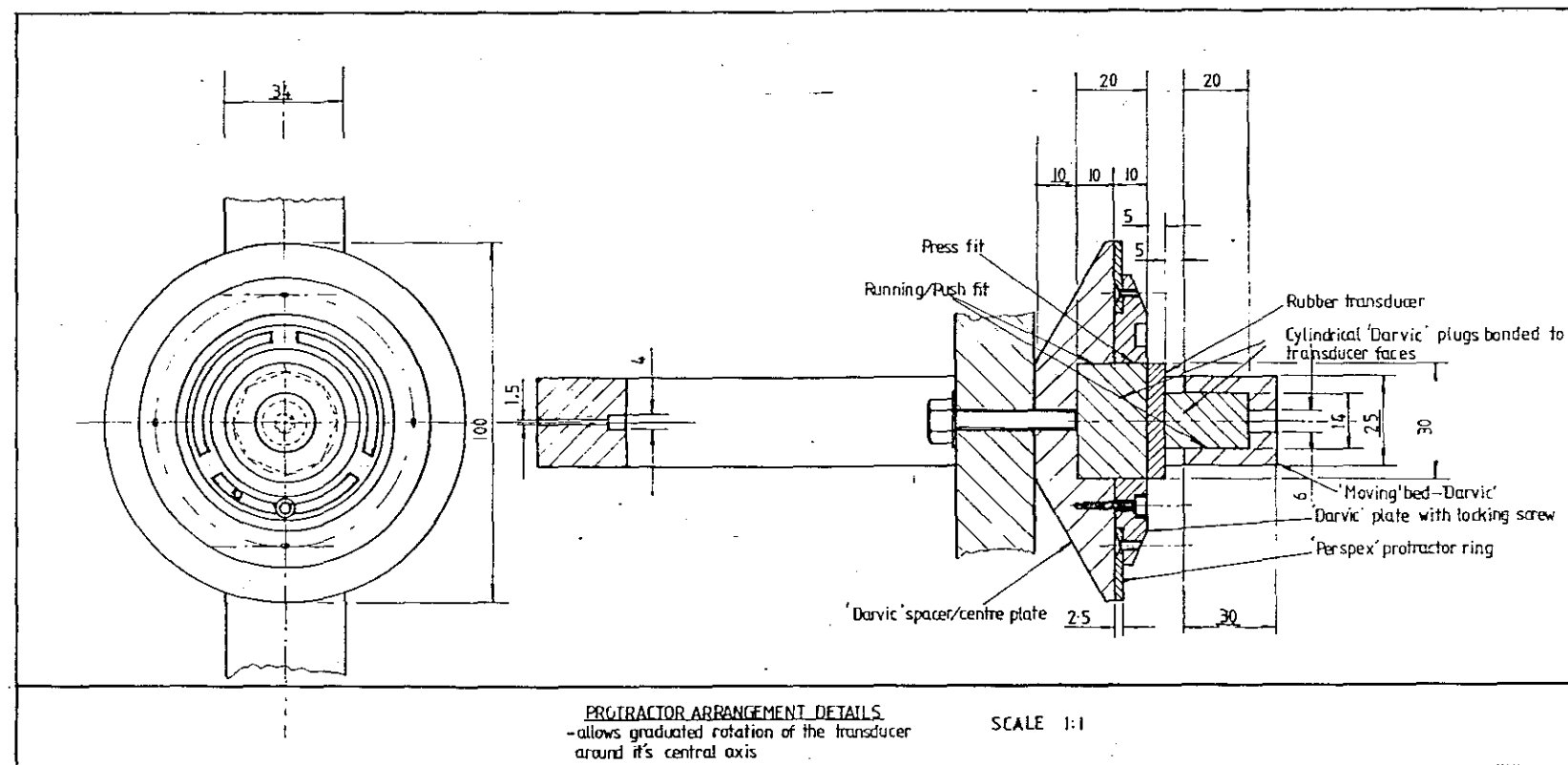
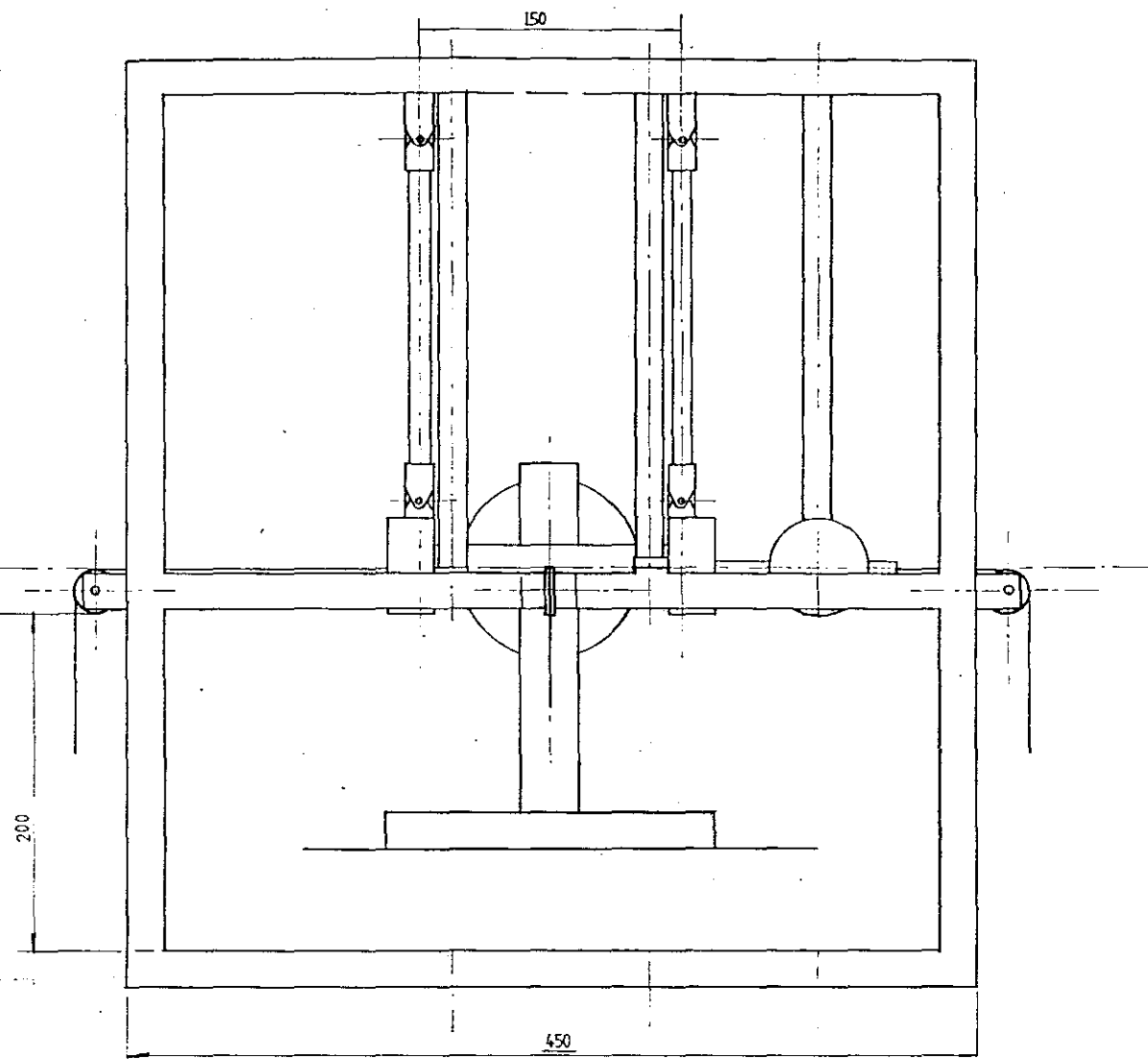
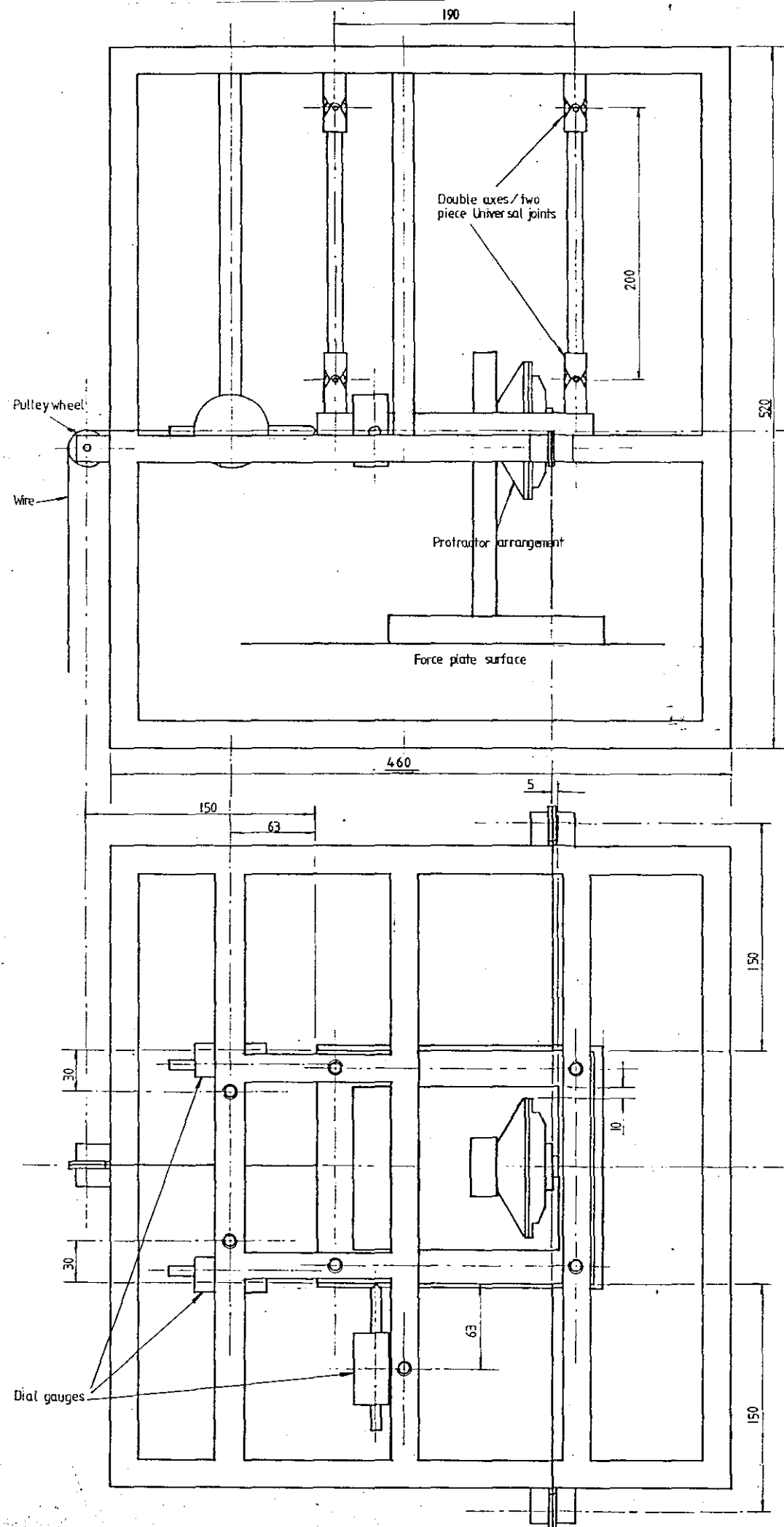


M.J. Warren-Forward

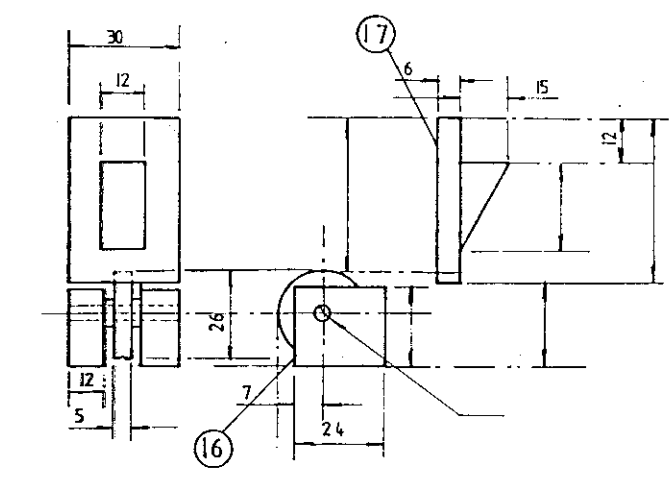
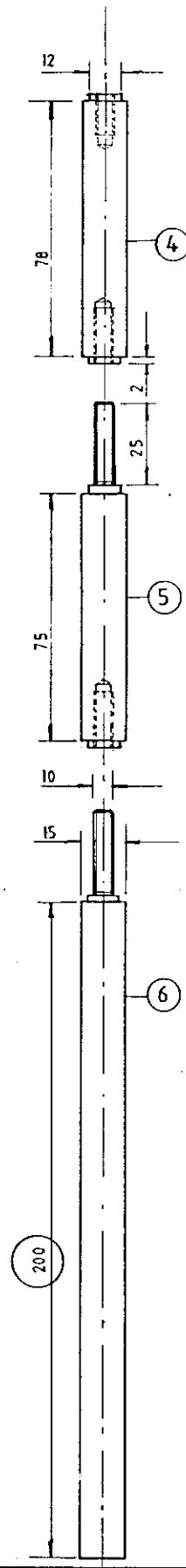
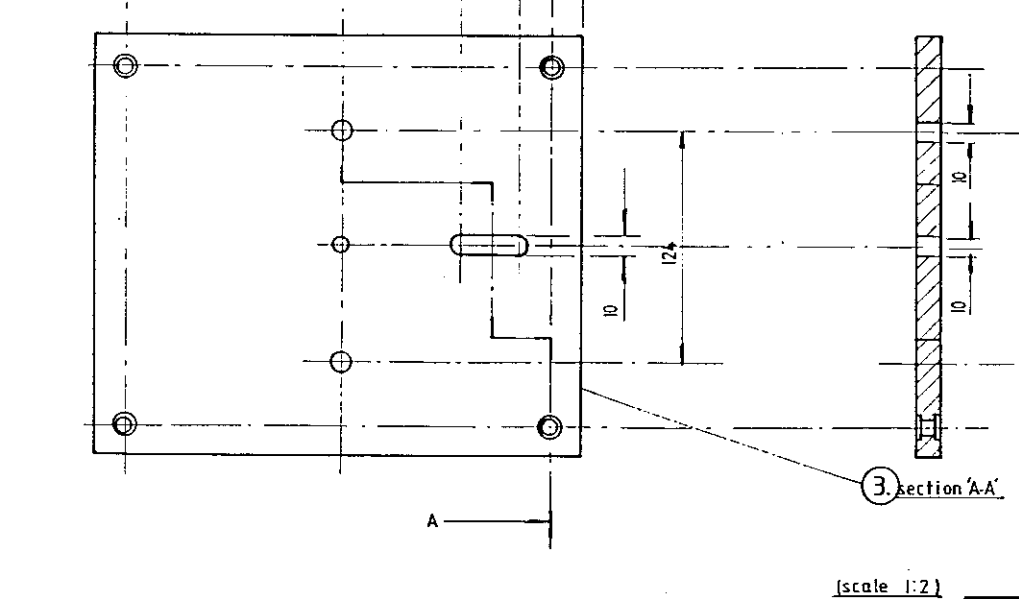


Technical drawing of a protractor ring assembly. The drawing shows a circular protractor ring with four mounting holes. Dimensions include a total diameter of 100, a hole diameter of 25, and a hole spacing of 60. A section line Z-Z is indicated. A note specifies "clearance for M2 csk" for the mounting holes. The assembly is labeled "Protractor ring Perspex -1 off".

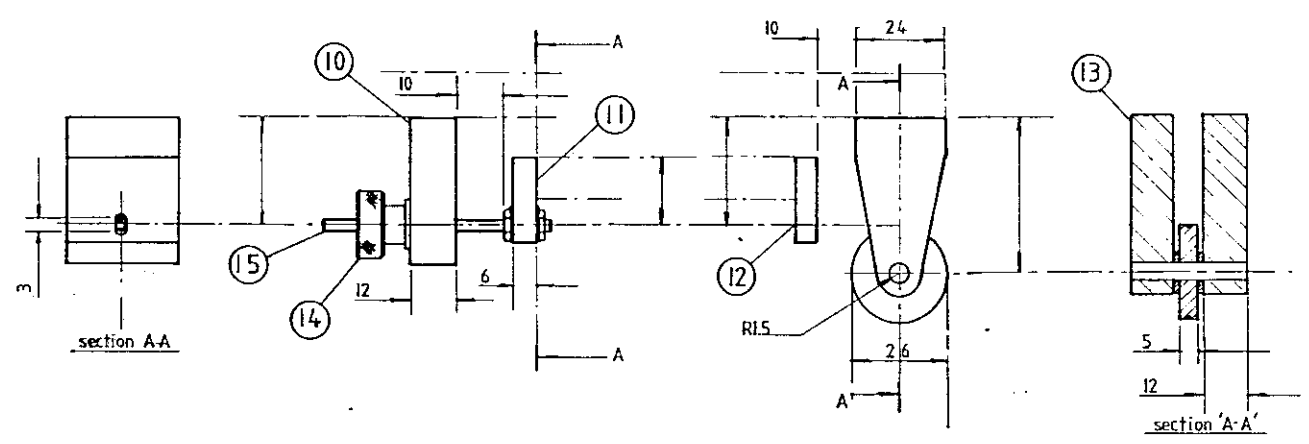
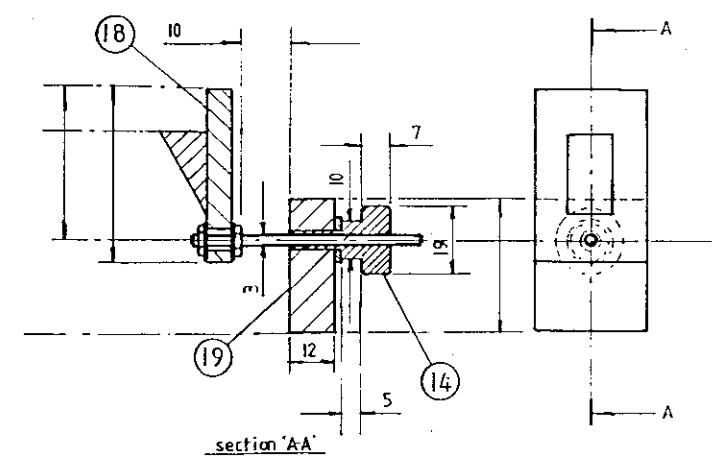




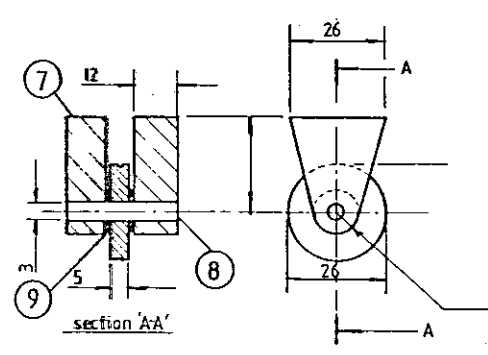
Scale 1:1 Unless otherwise stated	Dimensions in mm	1st angle proj ^a Unless otherwise stated	Drw no 4 of 4	15-11-88	DETAILS OF TEST RIG	Drn by M. FORWARD	PART NO	DESCRIPTION	MATL	NO OFF
---	------------------	---	------------------	----------	---------------------	----------------------	------------	-------------	------	-----------



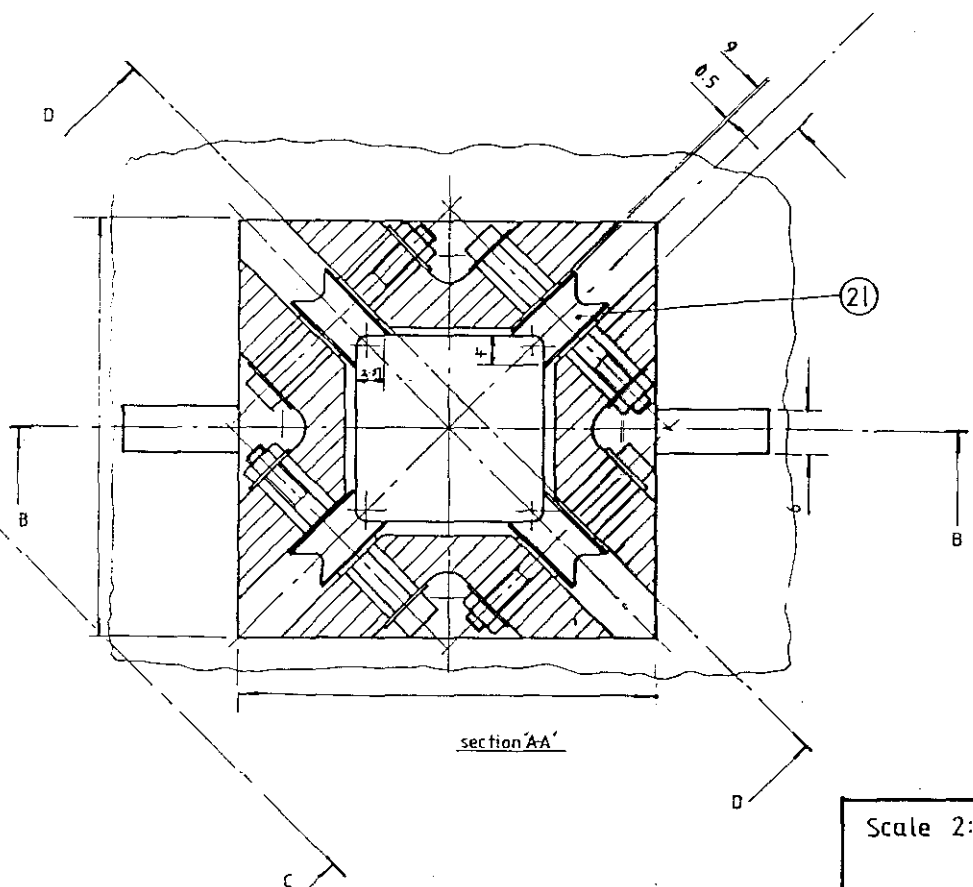
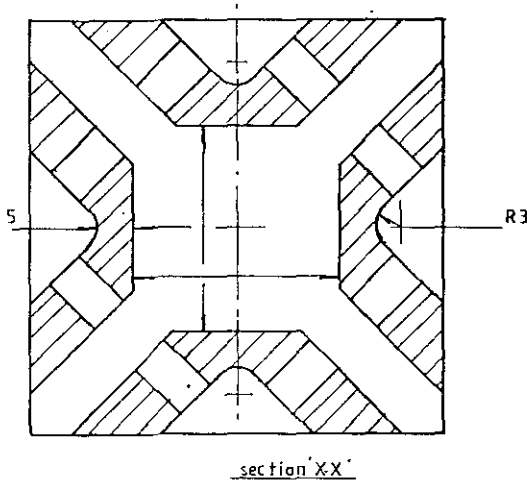
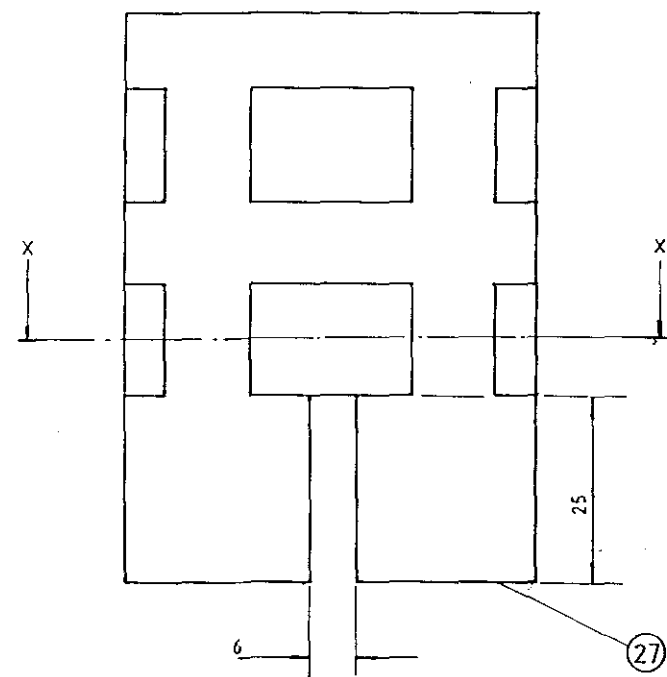
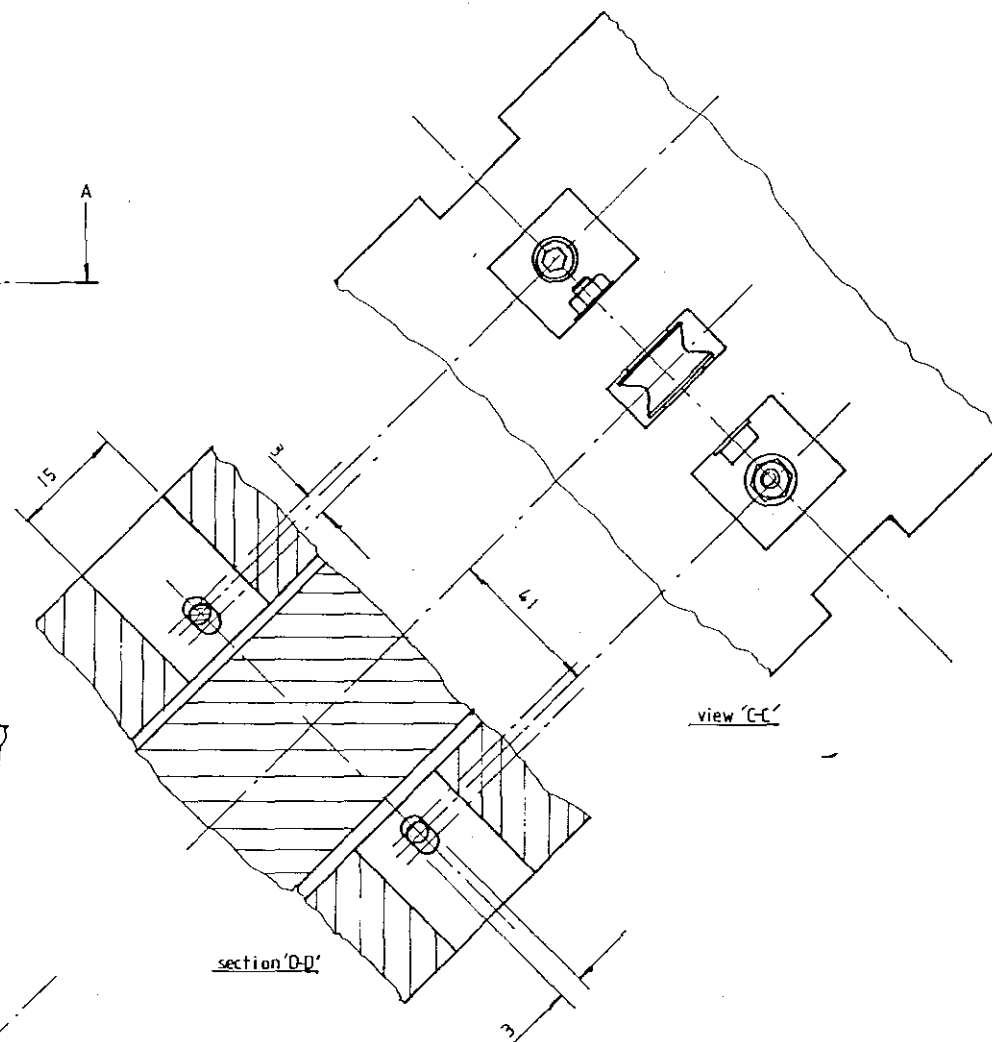
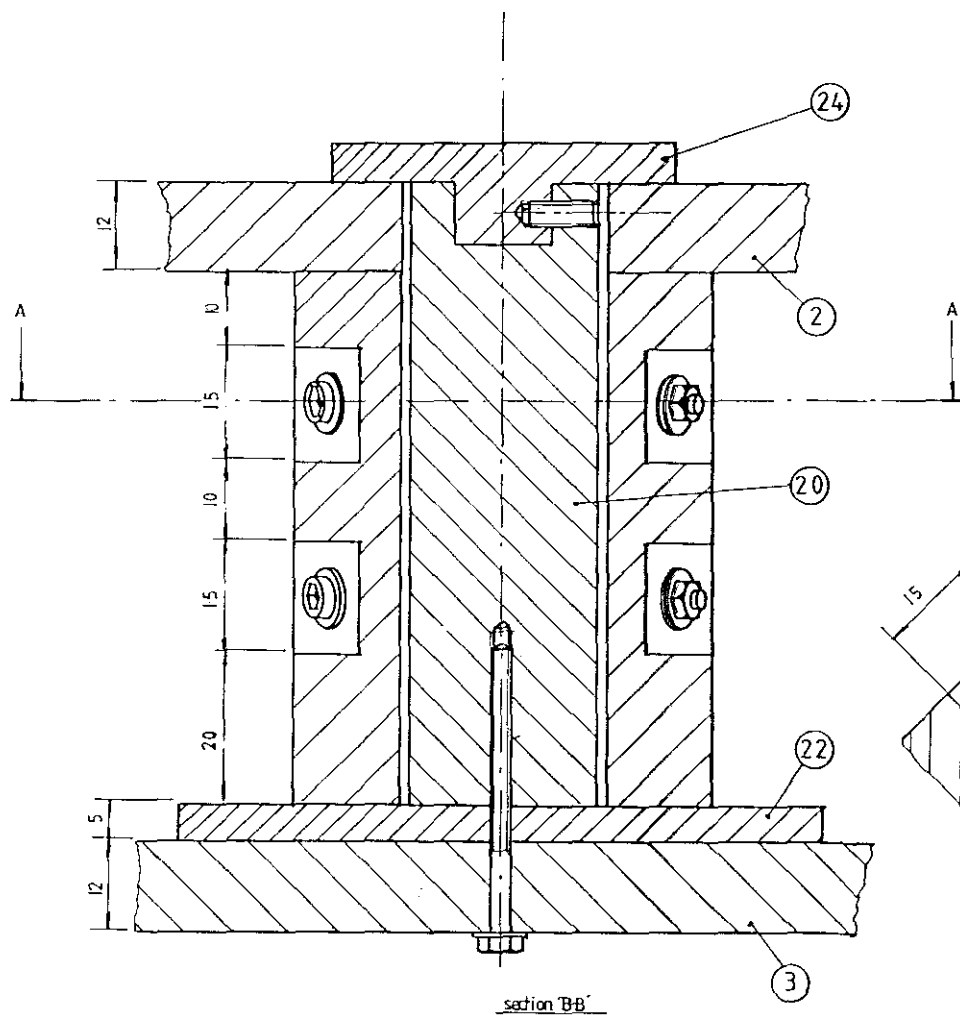
UPPER BED DISPLACEMENT CONTROL APPARATUS



LOWER BED DISPLACENT CONTROL APPARATUS



19	SCREW ADJUSTMENT BRACKET(U.BED)		1
18	BRACKET (U.BED SREW THREAD)		1
17	BRACKET (U.BED.PULLEY)		2
16	PULLEY MOUNTING(U.BED)		2
15	SCREW THREAD		2
14	KNURLED NUT		2
13	PULLEY MOUNTING (L.BED)		2
12	BRACKET(L.BED.PULLEY)		1
11	BRACKET (L.BED.SCREW THREAD)		1
10	SCREW ADJUSTMENT BRACKET(L.BED)		1
9	WASHER/SHIM		8
8	PULLEY SHAFT		4
7	PULLEY MOUNTING		2
6	LOWER SUPPORT POST	STEEL	4
5	MIDDLE SUPPORT POST	STEEL	4
4	UPPER SUPPORT POST	STEEL	4
3	LOWER MOUNTING PLATE		1
2	MIDDLE MOUNTING PLATE		1
1	UPPER MOUNTING PLATE	DARVIC	1
PART NO.	DESCRIPTION	MATL	NO OFF



27	Vertical pillar bearing support		1
Part No.	Description	Matl	No off

Scale 2:1	Dimensions in mm	1st angle prj ⁿ	Dwg no. 2 of 4	15.11.88	ASSEMBLY DETAIL OF VERTICAL DISPLACEMENT APPARATUS	Drn by M.FORWARD
-----------	------------------	----------------------------	----------------	----------	--	------------------

Appendix 4

Publication of research

Three-dimensional displacement and force transducer

M.J. Warren-Forward
R.M. Goodall
D.J. Pratt

Indexing terms: Transducers, Measurement and measuring

Abstract: A nonintrusive method which has been developed for measuring triaxial forces within footwear, developed particularly for use in the design of footwear for diabetics, is described. The technique uses four coils, one for excitation and the other three for sensing, embedded into a rubber insole. The voltages induced in the sensing coils can be processed to give displacements in three orthogonal directions. Given an appropriate material for the insole, forces can also be measured using the technique. The coils and electronic processing are briefly described, but the emphasis is on the computer processing which is used to extract the normal and shear displacement components from the voltage measurements. A number of approaches are proposed and analysed, and their performance contrasted by a comprehensive set of experimental results.

1 Introduction

The project, which was instigated by and carried out in collaboration with colleagues at the Orthotics and Disability Research Centre at the Derbyshire Royal Infirmary, has been funded by the British Diabetic Association. The primary aim was to improve the design of footwear for patients with diabetes, who frequently suffer from ulceration of the foot surface. This is caused by a combination of ailments suffered progressively with age in diabetics; loss of sensation and failing blood circulation in the extremities of the body. The latter of these problems also has the effect of vastly increasing the healing period and the susceptibility to infections such as gangrene. It is known that a redistribution of the forces imposed on the foot during walking aids healing and helps prevent further ulceration. The design of a prescription shoe is currently a subjective trial-and-error process because no method of measuring the triaxial forces exerted over small areas of the foot surface during normal activity exists. The first stage of the project, carried out at Loughborough University, has been to develop such a system. There are two important require-

ments of the system: first, that it measures triaxial forces i.e. direct forces (pressure) and the forces applied tangentially to the foot surface (shear forces), and secondly that it must be nonintrusive such that it does not disturb the distribution which would exist without the sensing element. The second stage of the project will be carried out at the hospital, and will involve clinical trials, initially to validate the measurements, but later to analyse existing footwear and hence guide the design and manufacture of prescription footwear.

The literature includes a number of papers describing the measurement of vertical forces on the sole of the foot, some attempting to measure in-shoe pressures [1-3]. Reports of measuring shearing forces on the sole of the foot, particularly in-shoe measurements, are rather less frequent and the results are limited. A device has been briefly described [4] which measures shear force along one axis. Various additional clinical results have been reported by the same group [5] but the fact that the most recent report [6] is based on the timing of such forces along one axis seems to emphasise the lack of published information on the calibration and bench testing of the device. The simultaneous in-shoe measurement of triaxial forces described clearly represents a significant advance on current measurement practice in this field.

The transducer concept is based upon determining the variations in flux linkage between an AC excitation coil embedded in one surface of a carefully chosen rubber-like material, and a set of receiving coils in the other surface (Fig. 1). The rubber material forms the insole fitted within

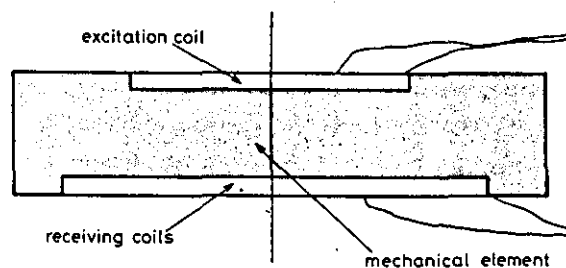


Fig. 1 Transducer construction
Side elevation

the shoe, and will have a number of sets of coils, each set forming a sensing element, spread across its area. Just one sensing element is discussed here, a thin circular pad of material with coils in its top and bottom surfaces.

The physical design of the sensing element is covered, followed by an outline of the electronics. The way in which the triaxial position measurements are extracted from voltage outputs of the three receiving coils is dis-

Paper 8329A (S4), first received 25th February and in revised form 12th July 1991

M.J. Warren-Forward and R.M. Goodall are with the Department of Electronic and Electrical Engineering, Loughborough University of Technology, Loughborough, Leicestershire LE11 3TU, United Kingdom. D.J. Pratt is with the Orthotics and Disability Research Centre, Derbyshire Royal Infirmary, London Road, Derby DE1 2QY, United Kingdom.

cussed in the following section, and in particular two alternative methods are examined. Experimental results for the measurement techniques are also presented.

2 Physical design

The requirement of nonintrusiveness, together with the desirability of measuring over a reasonably small area of the foot surface, severely limit the maximum physical size of the device. An overall thickness of rubber material of no more than 5 mm together with a measurement area having 10 mm diameter or less were required. To maximise the thickness of rubber material between the coils (and hence the range of movement) they needed to be thin, and a coil thickness of 0.5 mm was chosen. Fig. 2 shows the dimensions of a single coil, for which a special method of manufacturing was developed. Fig. 3 shows the positioning of the coils in a single sensing element, in which the three receiving coils are symmetrically arranged about the centre of the excitation coil. Note that the use of four receiving coils may have simplified the subsequent processing of the signals, but would have markedly increased the overall size.

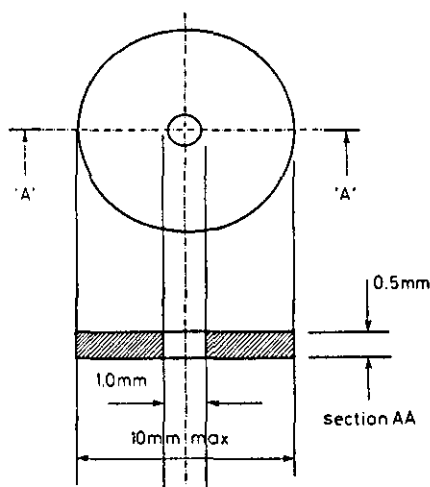


Fig. 2 Typical coil dimensions

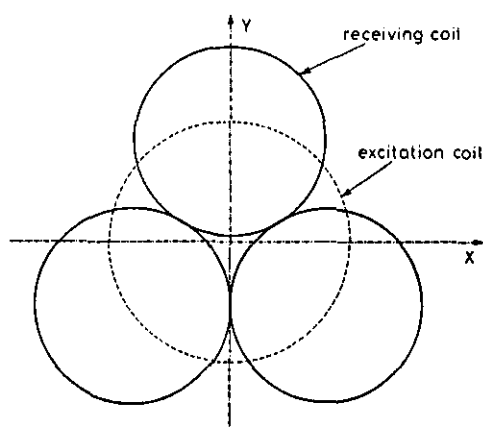


Fig. 3 Positioning of coils

Tests were first carried out on a single pair of coils without the rubber, partly to assess the flux linkage which could be obtained without causing significant heating effects in the excitation coil, but also to measure the basic characteristics as a function of displacement. It

was discovered that coils consisting of about 100 turns of 0.063 mm diameter wire and with an overall diameter of around 10 mm and thickness of 0.5 mm provided reasonable flux linkage when current-driven with 40 mA at 20 kHz. This creates a maximum flux density of around 1 mT, and induced voltages of typically 50–100 mV are obtained with 3–4 mm separation between the two coils. Each coil has a resistance of 16 Ω and an inductance 0.15 mH. The size and relative positioning of the coils has much bearing on both the range of movement, and the applicable methods of extracting the position from the voltage outputs of the coils.

Fig. 4 shows typical induced voltage-displacement characteristics of a pair of coils of such dimensions. These were measured using a specially designed test rig by which one coil can be moved in the three directions, with the planes in which the two coils lie being kept parallel to one another throughout the displacements. The diagram shows the induced voltage as a function of radial displacement at three different vertical distances (curves A, B and C at 0, 4 and 6 mm, respectively). Curve D shows the induced voltage as a function of vertical displacement along the central axis of the coils (at a radial displacement of zero). Fig. 5 shows the general shape of the induced voltage 'surface' for displacements in the x-y plane about the central axes of the coils and at some fixed vertical displacement z. The whole of this surface is scaled up or down as a function of the vertical displacement of the coil pair. These characteristics are typically polynomial functions with an order of about 4. Fig. 4 also shows the limitations imposed on any device utilising these characteristics in terms of the range within

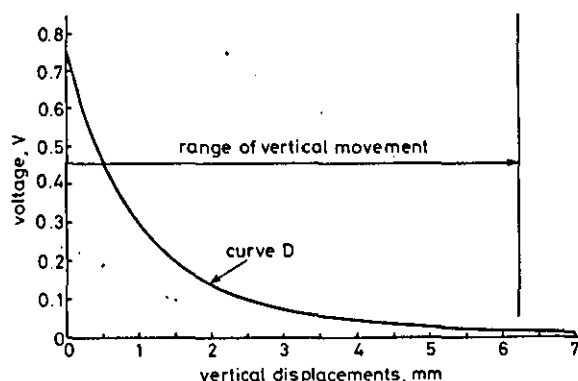
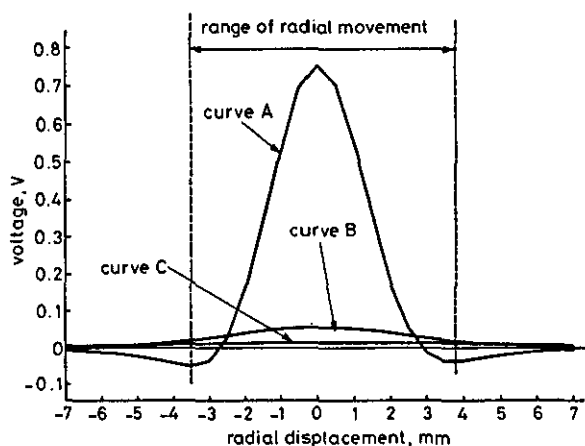


Fig. 4 Typical induced voltage-displacement characteristics

which a reasonable induced voltage is measurable. There are relatively linear portions to the radial displacement characteristics. There are no such linear portions to the vertical characteristic, but large sections may be approximated well by a quadratic fit.

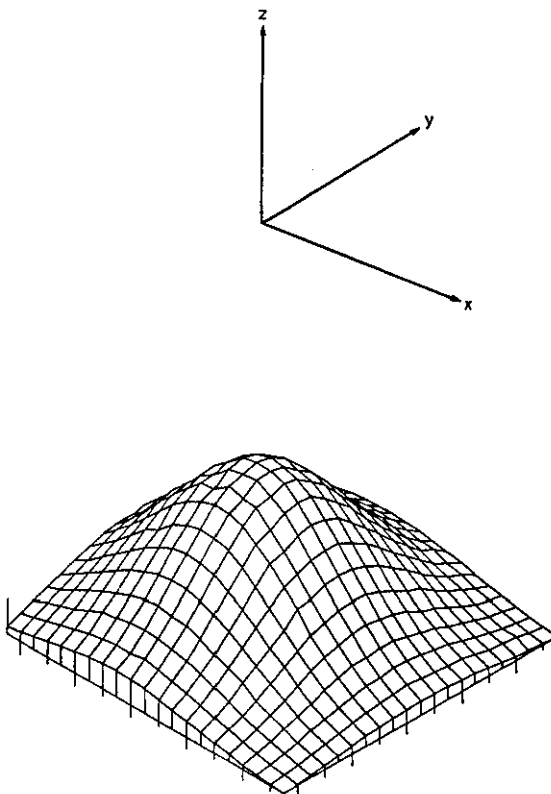


Fig. 5 Surface of induced voltage for movements in horizontal x - y plane

Factors in the selection of a suitable rubber element were

- (a) suitability of its force-displacement characteristics compared with the range of the sensing element
- (b) insensitivity of the mechanical characteristics to repeated or sustained loading within the environment of the shoe
- (c) feasibility of manufacture

A silicon rubber material was used in the prototype devices. Although this was not particularly easy to use, the stability of the material and its mechanical characteristics are close to that desired. However, it may suffer some undesirable characteristics with larger values of compression.

3 Electronic processing

Fig. 6 shows the electronics used. A number of features of the design attempt to minimise the effects of temperature variations by making the measurements independent of the coil resistances. The drive stage creates a substantially constant current irrespective of the resistance of the excitation coil, with a voltage of around 1.1 V necessary to sustain the coil current of 40 mA. The induced voltage will be 90° phase-shifted with respect to the excitation current, which is allowed for prior to demodulation. An

input buffer amplifier with an input impedance well in excess of $1\text{ M}\Omega$ ensures that the receiving coil current is

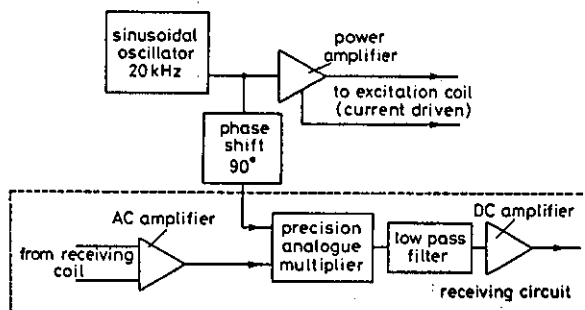


Fig. 6 Electronic processing scheme

negligible, which would otherwise affect the measured voltage (phase sensitive detection helps to eliminate any residual effect). A high precision multiplier is used to provide accurate synchronous demodulation of the induced AC voltage, but various potentiometers allow fine adjustment of the phase shift, the excitation current level, and the range of movement which corresponds to maximum range of voltage at the input to the multiplier. The frequency of 20 kHz was chosen as a compromise: the higher the frequency the greater the induced voltage, but the performance of the operational amplifier must be increased to ensure sufficiently small deviations in the phase response.

The receiving circuit is repeated three times per sensing element, thereby giving DC output voltages in proportion to each coil's coupling with the excitation coil. These are then captured by a personal computer, through suitable interfacing, and all subsequent processing is carried out by the computer.

4 Extraction of position information

The electronic circuit provides three DC voltages which need to be converted into x , y and z displacements (forces). It is easy to calibrate the transducer to determine sets of voltages V_1 , V_2 and V_3 for different positions x , y and z , but the reverse process of deducing x , y and z from the three voltages is by no means straightforward.

Two options have been investigated. The first involves constructing a model of the displacement-voltage characteristics, and then using calibration data to determine 'best fit' parameters for the model's equations, from which the displacements can then be calculated. The other employs a look-up table technique. Although the former method was found to have limitations, its theoretical and practical appraisal are presented here, together with the latter method which suited the requirement and constraints better.

4.1 Mathematical model approach

4.1.1 Coil pair characteristics

Referring to Fig. 4 and the comments made earlier, it would be expected that the voltage-displacement characteristics could be represented by a function such as

$$V(r, z) = J(z)F(r)$$

in which V is the induced voltage, r is the radial displacement from the central axis, z the vertical distance between the coils; $J(z)$ and $F(r)$ are general functions which can be considered to take the form of polynomial approximations.

4.1.2 Three dimensional analysis: Model 1

It may be seen that, using only one coil pair, the uniqueness of any induced voltage is not assured unless movement is restricted to one axis. Intuitively the addition of two or more receiving coils at suitable positions should enable unique position determination in three dimensions. Using the minimum of three coils placed at the corners of an equilateral triangle lying in the horizontal plane, three functions are expected:

$$V_i(r, z) = J(z)F_i(r) \quad i = 1, \dots, 3 \quad (1)$$

or in terms of the Cartesian co-ordinates x , y and z using a linear approximation for the function $F_i(r)$ and a quadratic approximation for $J(z)$, as postulated at the end of Section 2

$$\begin{aligned} V_1(x, y, z) &= J(z)[V_1(0, 0, 0) + a_1x_1 + b_1y_1] \\ V_2(x, y, z) &= J(z)[V_2(0, 0, 0) + a_2x_2 + b_2y_2] \\ V_3(x, y, z) &= J(z)[V_3(0, 0, 0) + a_3x_3 + b_3y_3] \end{aligned} \quad (2)$$

where

$$J(z) = 1 + k_1z + k_2z^2 \quad (3)$$

Note that the expressions for V_i in terms of x and y approximate the characteristics onto a plane, modified of course by the value of z .

The coils may either be considered to lie in the same horizontal plane but at different x and y co-ordinates, or they may be represented by three different co-ordinate systems. The co-ordinate systems of the coils are identical except that the horizontal x - y plane of each coil's co-ordinate system is rotated by 120° to match the corner of the equilateral triangle at which the coil lies. For systems with axes x , y and z and x' , y' and z , in which x' , y' and z is obtained from x , y and z by rotation of ϕ° of the x - y plane about the z -axis, the transformation required to translate co-ordinates in system x' , y' , z to express them in system x , y , z is

$$\begin{bmatrix} x \\ y \end{bmatrix} = \begin{bmatrix} \cos \phi & -\sin \phi \\ \sin \phi & \cos \phi \end{bmatrix} \begin{bmatrix} x' \\ y' \end{bmatrix} \quad (4)$$

Thus if the axes of coil 1 are made to be the reference, and those of coils 2 and 3 are obtained by rotations of $+120^\circ$ and -120° , respectively, then

$$\begin{aligned} x_1 &= x \\ y_1 &= y \\ x_2 &= -x/2 - [\sqrt{3}/2]y \\ y_2 &= [\sqrt{3}/2]x - y/2 \\ x_3 &= -x/2 + [\sqrt{3}/2]y \\ y_3 &= -[\sqrt{3}/2]x - y/2 \end{aligned} \quad (5)$$

Assuming that the coefficients a_i and b_i for each of the coils are the same, the sum of the three voltages will be independent of x and y and dependent only on the initial

voltages at the reference origin, and of course the function $J(z)$. That is

$$\sum_{i=1}^3 V_i(x, y, z) = J(z) \sum_{i=1}^3 V_i(0, 0, 0) \quad (6)$$

Thus the process of calibrating the coil set consists of choosing an origin, bearing in mind the coil pair characteristics, and selecting convenient calibration points to enable solution of the coefficients in eqns. 2 and 3. A movement purely in the z -direction, for instance using voltages at the points $(0, 0, 1)$ and $(0, 0, -1)$, will enable k_1 and k_2 in $J(z)$ to be determined (eqns. 3 and 6). The voltages at the point $(1, 0, 0)$ may be used in eqn. 2 to determine a_1 , a_2 and a_3 although in practice we used an average from $(1, 0, 0)$ and $(-1, 0, 0)$. Similarly the points $(0, 1, 0)$ and $(0, -1, 0)$ are used to determine the coefficients b_1 , b_2 and b_3 .

The converse process of converting a set of voltages into x , y and z is as follows:

First calculate

$$J(z) = \frac{\sum_{i=1}^3 V_i(x, y, z)}{\sum_{i=1}^3 V_i(0, 0, 0)} \quad (7)$$

This immediately enables the quadratic eqn. 3 to be solved to give two values for z , one of which can readily be eliminated on the basis of being out of range. The value for $J(z)$ can also be substituted into eqn. 2, and solved for x and y using the relationships given in eqn. 5.

The essential requirements for accuracy of this method are reasonably obvious: throughout the range of operation the assumed functions are representative (linear for x and y , quadratic for z); the coefficients (a_i , b_i , k_1 and k_2) in the expressions are the same for each coil, and the coils are positioned accurately; the planes in which the coils lie must also be kept parallel.

4.1.3 Three dimensional analysis: Model 2

The limitation with the first model occurs in representing the function $F(r)$ as a linear function of (x, y) because strictly it is a function of the radial displacement between the central axes of the excitation and receiving coils. The plane which is represented by the linear function in x and y will be tangential to the actual surface of the characteristics, which means that the greater the movement away from the central point, expressed as a fraction of the pitch circle radius of the centres of the coils, the greater the error.

A better model is to represent the characteristics of each coil by a portion of a cone, rather than by a plane, although the mathematics is more complicated.

More correctly then the model

$$V(r_i, z) = J(z)F(r_i) \quad (8)$$

may be used with some appropriate approximations for $J(z)$ and $F(r)$, and where each of the receiving coils has its own expression for r_i (Fig. 7)

$$\begin{aligned} r_1 &= \sqrt{y^2 + (x + R)^2} \\ r_2 &= \sqrt{[(y - R\sqrt{3}/2)^2 + (x - R/2)^2]} \\ r_3 &= \sqrt{[(y + R\sqrt{3}/2)^2 + (x - R/2)^2]} \end{aligned} \quad (9)$$

The use of eqn. 9 with a linear approximation for $F(r)$ and a quadratic for $J(z)$ leads to some improvements, but the results presented will show that the inaccuracies are

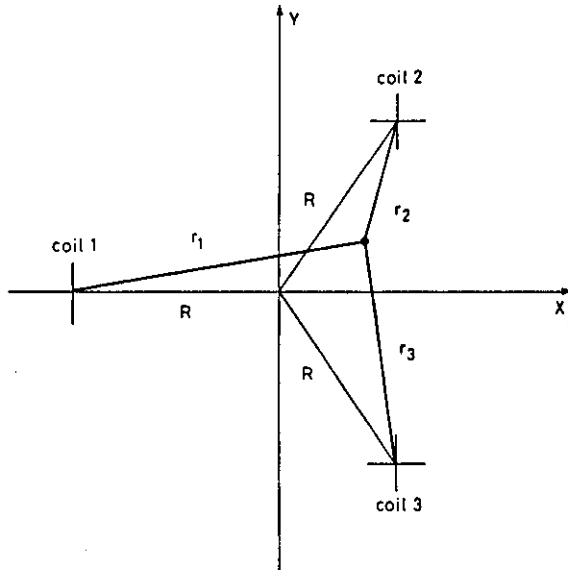


Fig. 7 Geometry for radii calculations used in model 2

still quite large. It is felt that these errors arise because of over-simplified expressions for $J(z)$ and $F(r)$. Given that the look-up table method described avoids the necessity of solving high order polynomials, a combination of the approaches of mathematical model involving limited calibration (and high order polynomial approximations) together with the look-up table technique using data generated by such a model was developed.

A series of radial sweeps passing through the longitudinal axis of each receiving coil in turn were made at different vertical separations (of receiving and excitation coils), i.e. a series of characteristics such as that in Fig. 4 (upper) were collected. A fourth order least squares approximation (in radius) was made to each of these and then in turn a third order approximation (in vertical separation) was made to each of the coefficients of the radial functions. This then allowed generation of a set of data representing V_1, V_2, V_3 at x, y, z which was to be used with the look-up table method described below.

4.2 Look-up table method

Again four coils are used, one excitation coil and three receiving coils placed (conveniently) at the corners of an equilateral triangle in the horizontal plane as in the previous method. The first stage involves the collection (by means of calibration) of three-dimensional data to create three matrices containing the induced voltages at a three-dimensional network of positions. The converse process of extracting the position information (x, y, z) from the actual voltages (V_{1a}, V_{2a}, V_{3a}) then involves location of the nearest point in the matrices, followed by linear interpolation about that point, as follows:

Select the nearest point P_n from the matrices for which

$$[(V_{1a} - V_{1n})^2 + (V_{2a} - V_{2n})^2 + (V_{3a} - V_{3n})^2] \text{ min} \quad (10)$$

where (V_{1n}, V_{2n}, V_{3n}) are the voltages at point P_n in the matrix.

The exact functions which give the voltage against

positions are written for each coil as functions f_i where

$$V_i = f_i(x, y, z) \quad i = 1, \dots, 3 \quad (11)$$

Now at any point (x, y, z) a small change in V_i may be expressed as

$$\delta V_i = (\partial f_i / \partial x) \delta x + (\partial f_i / \partial y) \delta y + (\partial f_i / \partial z) \delta z$$

$$\begin{bmatrix} \delta V_1 \\ \delta V_2 \\ \delta V_3 \end{bmatrix} = \begin{bmatrix} \partial V_1 / \partial x & \partial V_1 / \partial y & \partial V_1 / \partial z \\ \partial V_2 / \partial x & \partial V_2 / \partial y & \partial V_2 / \partial z \\ \partial V_3 / \partial x & \partial V_3 / \partial y & \partial V_3 / \partial z \end{bmatrix} \begin{bmatrix} \delta x \\ \delta y \\ \delta z \end{bmatrix} \quad (12)$$

or

$$\delta V = \Delta V \delta P$$

and so

$$\delta P = (\Delta V)^{-1} \delta V \quad (13)$$

δV can be calculated by taking the nearest voltages V_n from the actual voltages

$$\delta V = V_a - V_n \quad (14)$$

δP can now be calculated from eqn. 13 using $(\Delta V)^{-1}$, and then the actual position is

$$P_a = P_n + \delta P \quad (15)$$

in which P_n are the values of x, y and z for the nearest point identified in eqn. 10.

From each matrix of voltages it is possible to determine a range to correspond to the maximum movement in x, y and z . The processing described may be performed offline to produce matrices of positions x, y and z at evenly spaced voltages (V_1, V_2, V_3) over the defined range.

The process of position determination may then be initiated, first, by reading the set of voltages V_n , finding the nearest voltage V_n using least squares, then identifying the point x_n, y_n, z_n as a first approximation to the actual position.

The partial derivatives in three dimensions can readily be deduced from the adjacent values in the matrices. It is then necessary to linearly interpolate between the evenly spaced voltages

$$\begin{bmatrix} \delta x \\ \delta y \\ \delta z \end{bmatrix} = \begin{bmatrix} \partial x / \partial V_1 & \partial x / \partial V_2 & \partial x / \partial V_3 \\ \partial y / \partial V_1 & \partial y / \partial V_2 & \partial y / \partial V_3 \\ \partial z / \partial V_1 & \partial z / \partial V_2 & \partial z / \partial V_3 \end{bmatrix} \begin{bmatrix} \delta V_1 \\ \delta V_2 \\ \delta V_3 \end{bmatrix} \quad (16)$$

The maximum range of displacements detectable with this approach is limited only by the range over which a reasonable level of induced voltage is achieved (Fig. 4 and Section 2). The accuracy obtainable is dependent on the number of points used in the calibration table and the nonlinearity of the induced voltage-displacement characteristics. For the results presented, a matrix of $13 \times 13 \times 7$ points was used in x, y and z , respectively, resulting in 1183 calibration points for each of V_1, V_2 and V_3 .

5 Assessment of mathematical model and look-up table techniques for the displacement transducer

Having calibrated a set of coils using both of the methods described, the following results demonstrate the accuracy and range of displacements obtainable with each method using the calibrated coil set. They are presented in terms of displacements in the x, y and z co-ordinate system, with the origin representing a point 3.5 mm from the receiving coils along the central axes of the equilateral

triangle on which the receiving coils are located (Fig. 8). The movements are of the excitation coil relative to this origin.

Displacements of ± 3 mm in x - y and ± 1.5 mm in z are taken as the maximum imposed by the induced voltage/displacement characteristics for the coil. A minimum (vertical) distance of 2.0 mm between the excitation and receiving coils was maintained throughout the tests and calibration. In the force transducer this gap corresponds to the maximum compression of the rubber element. Note that the mechanical characteristics of the rubber were chosen to give consistency with these displacements for the expected range of directional forces.

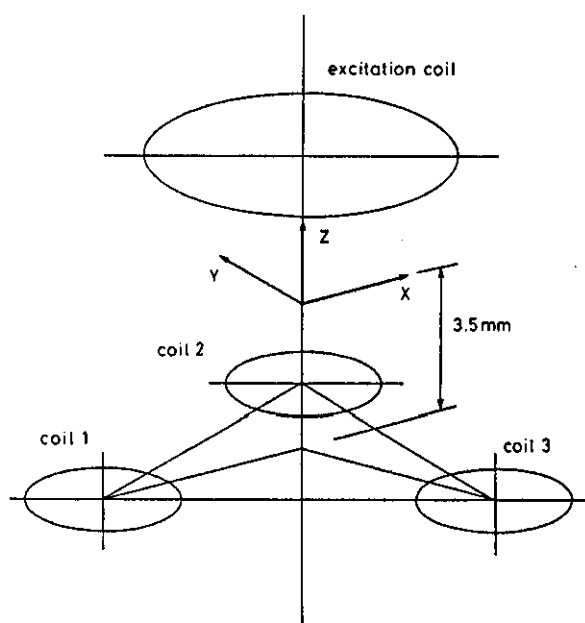


Fig. 8 Location of reference origin with respect to receiving coils

5.1 General assessment

Variation of the error in predicted measurements against actual measurements while varying the displacement along each of the co-ordinate axes in turn are shown in Figs. 9–11 for each of the methods, measured without the rubber element in place. Those for the look-up table method show a small error variation of around $\pm 3\%$ of the full maximum scale (half the range). There are some slight trends — the error in z seems to have a small constant imposed on it indicating perhaps some small offset in the electronics. The variation of errors in x and y , when each of their respective axes is traversed, shows a slight gradient. The reasons for this are unclear.

The results for the mathematical model methods show greater errors and, as would be expected, more significant trends. The seven calibration points used were the points ± 1 in x , y and z together with the origin as mentioned earlier. With the first model the curves for the displacement along the axes within the calibrated region show error fluctuations of the order of 20% (5–10% of the reduced region). Again z appears to have a somewhat constant component in its error characteristic. The results for the second modelling method show rather greater success — of the order of $\pm 10\%$ over the full range of movement of x , y and z , i.e. in comparison with the $\pm 3\%$ for the look-up table method.

5.2 Statistical approach

Three hundred random points (x, y, z) were generated, movements made to these points and predicted positions calculated using the look-up table method. The distributions of the errors are shown in Fig. 12.

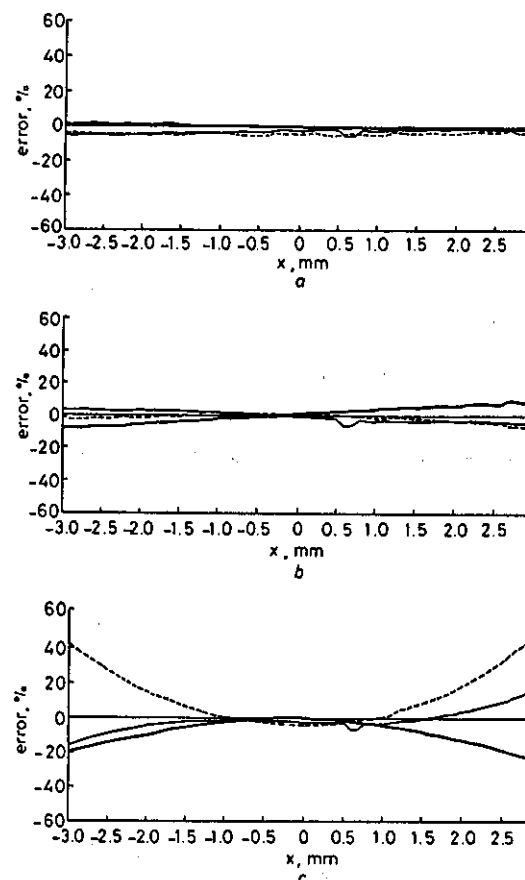


Fig. 9 Errors in x , y and z for displacements in x -direction

— x
 --- y
 ... z
 a Look-up table method
 b Model 2
 c Model 1

The same strategy was applied to each of the other methods using only 76 random points lying within a reduced volume of ± 2.50 mm in x and y and ± 1.125 mm in z , the resultant errors being expressed as a percentage of these full scale deflections (Figs. 13–15). It is apparent that the first model technique fails completely whereas the second model enjoys rather more success, showing errors less than 20%, which compares with 8% errors with the look-up table method. Given that the model method requires rather less calibration time, and may reduce to coil calibration as opposed to transducer calibration (with the subsequent effect on system assembly) it is felt worthwhile reserving judgement on a final strategy for calibration until the problems of coil and transducer manufacture have been ironed out. Confirmation is also needed that the transition to force measurement introduces no unexpected complications.

5.3 Comparison of processing requirements

The mathematical model technique required seven calibration points when used in obtaining the above results,

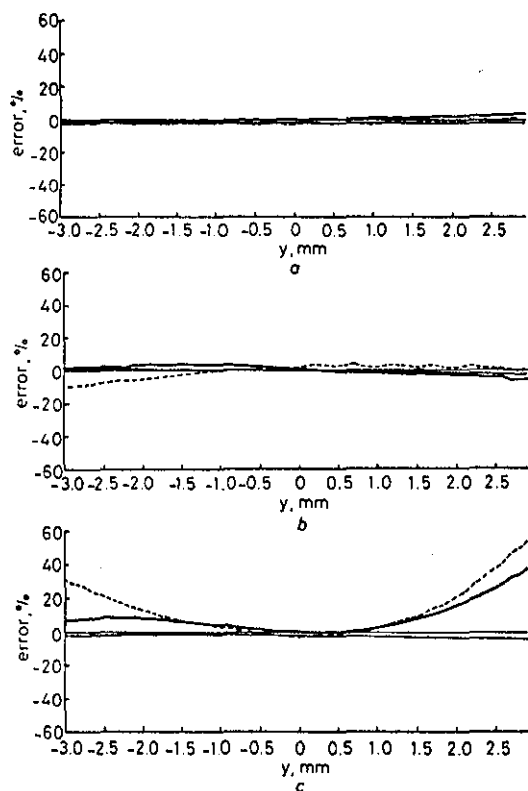


Fig. 10 Errors in x , y and z for displacements in y -direction
 — x a Look-up table method
 - - y b Model 2
 . . . z c Model 1

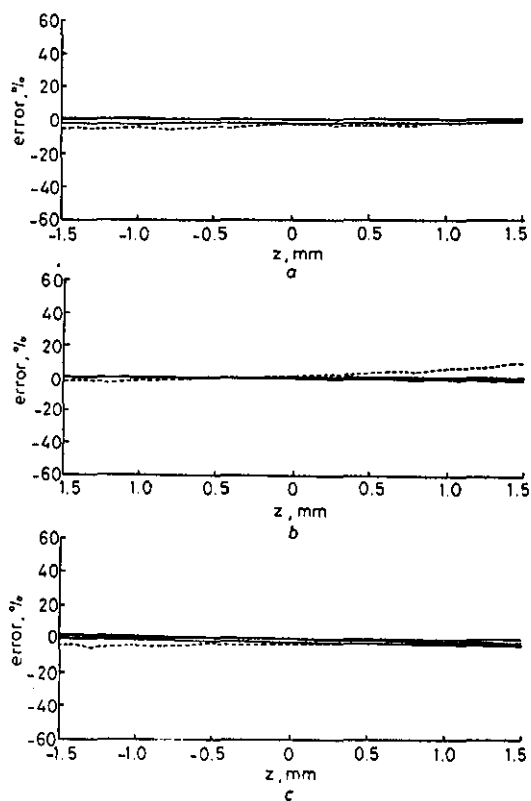


Fig. 11 Errors in x , y and z for displacements in z -direction
 — x a Look-up table method
 - - y b Model 2
 . . . z c Model 1

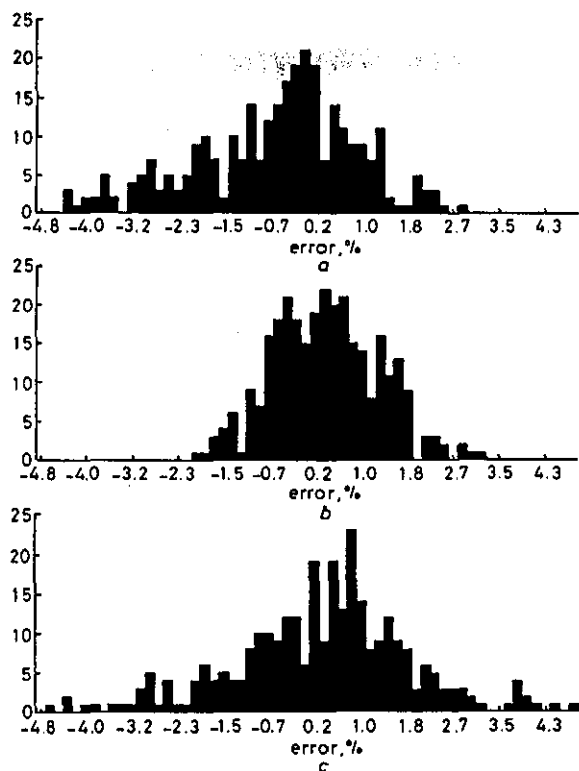


Fig. 12 Distribution of errors for 300 random points

Look-up table method

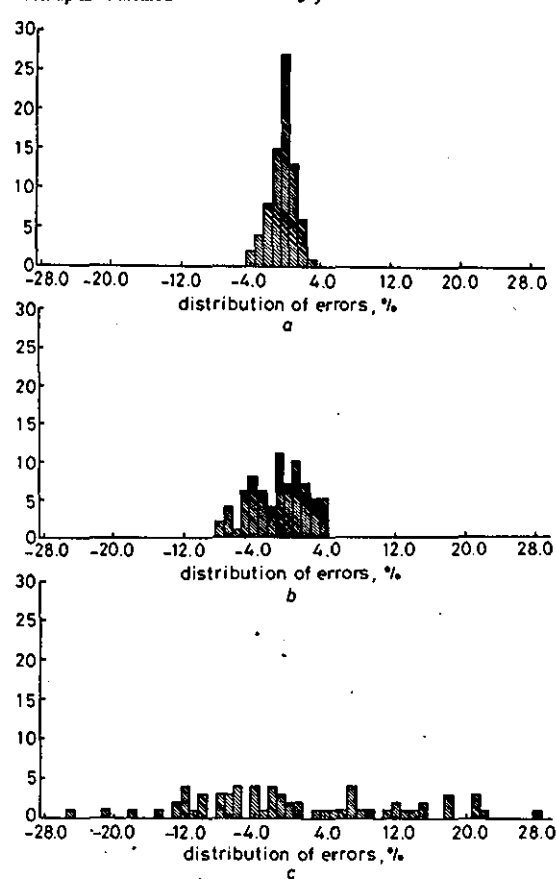


Fig. 13 Distribution of errors in x

Reduced volume

a Look-up table method mean = -0.3 ; $\sigma = 1.36$; range = 7
 b Model 2 mean = -1.22 ; $\sigma = 3.18$; range = 12
 c Model 1 mean = -2.26 ; $\sigma = 19.78$; range = 97

whereas the look-up table used here consisted of 1183 calibration points (and the accuracy obtained is obviously directly related to the number of points in the table for a given x - y - z space). Calibration is quite simple where

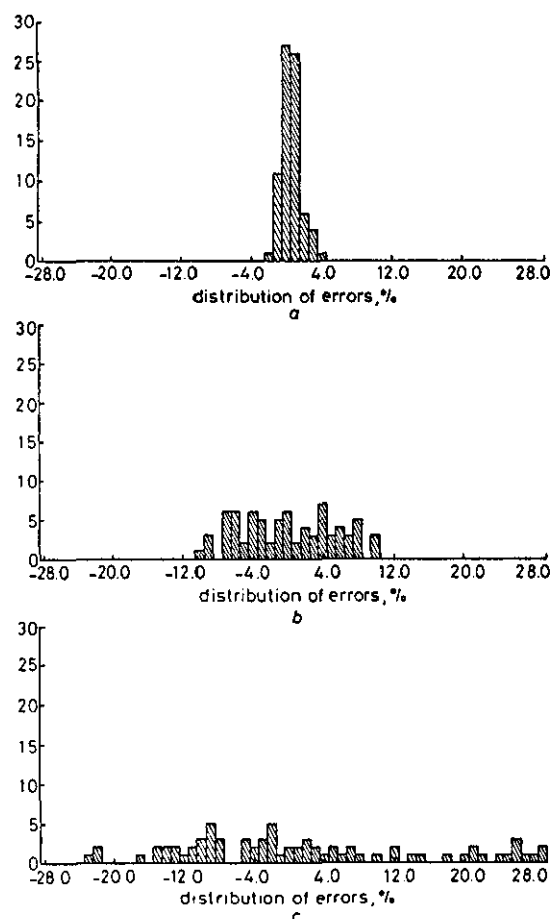


Fig. 14 Distribution of errors in y

Reduced volume	
a Look-up table method	mean = 0.53; σ = 1.12; range = 6
b Model 2	mean = 0.07; σ = 5.37; range = 20
c Model 1	mean = -2.07; σ = 13.10; range = 60

the mathematical model is to be used. However, great care must be taken in manufacturing the coils to ensure the accurate positioning of well matched (identical) coils. Characteristics for the combination of excitation and receiving coils also need to be examined to judge the best spacing of the coils and calibration points for a given range of movements. Although intelligent coil matching and spacing are required for the look-up table method it is by no means as critical. An indication of the processing and memory requirements is useful, and the figures quoted are based on a PC compatible computer with a 80386 processor. The look-up table method involves considerable offline processing, typically taking 10 mins for the number of calibration points referred to, but the online calculations are few and fast — a sampling frequency of 1 kHz is feasible. The look-up table itself can become quite large, particularly if higher accuracies are required. However, even with the values held as real data types, only in the region of 10 kbytes is necessary for the table generated from the 1183 calibration points. The offline processing for the model technique is very simple, but the online processing is more complex and takes about three times as long as the look-up table method;

memory requirements are, however, very small by comparison.

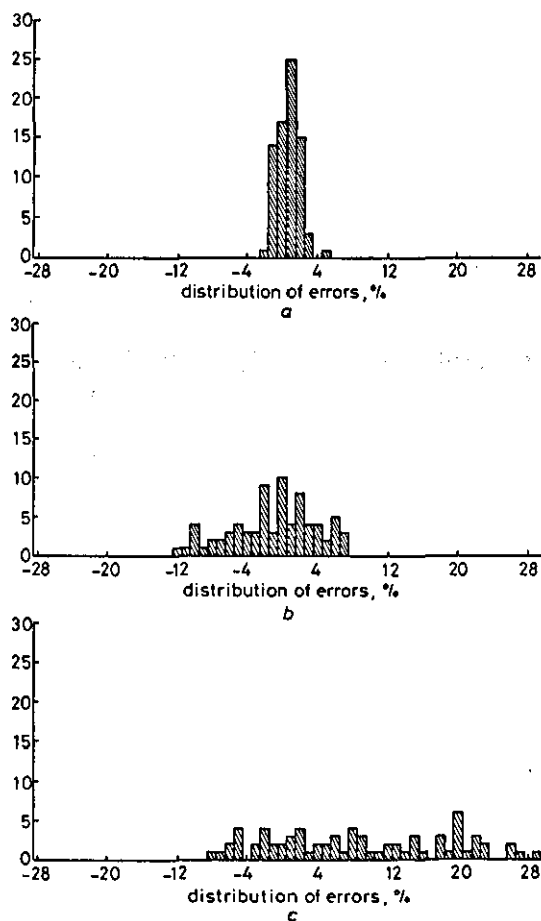


Fig. 15 Distribution of errors in z

reduced volume	
a Look-up table method	mean = 0.66; σ = 1.21; range = 7.0
b Model 2	mean = -0.95; σ = 4.87; range = 19.0
c Model 1	mean = 14.15; σ = 10.18; range = 38.0

6 Conclusion

The use of the device for three-dimensional displacement measurement has been considered, and it was found that accuracies in the region of 5% are achievable. Work is continuing on the force transducer, but the performance is expected to be similar, because both theoretical predictions and dynamic experimentation show that the silicon rubber material has consistent and relatively linear characteristics, subject of course to the range of corresponding movements being consistent with the operating range used for displacement measurement. The rubber will clearly induce some further nonlinearity, but the look-up table is likely to maintain its superior performance under these conditions. The effects of the coils not being parallel, as will happen to a certain extent within a shoe, are also being quantified, although preliminary results suggest this is not a major problem. If necessary an additional coil can be added to monitor the effects, and the general nature of the look-up table can be extended to include the extra coil.

The research programme described has been to develop the basic sensing element. The work is continuing to provide eight sensing elements in one insole with a view to embarking on clinical trials. The authors believe

the work to have been successful: a practical, inexpensive and robust transducer to meet the specification has been developed, and the underlying theoretical studies have added useful techniques to the science of measurement.

7 References

- 1 HENNIG, E.M., CAVANAGH, P.R. ALBERT, H.T., and MAC-MILLAN, N.H.: 'A piezoelectric method of measuring the vertical contact beneath the human foot', *J. Biomed. Eng.*, 1982, 4, pp. 213-222
- 2 PEDOTTI, A., ASSENTE, R., FUSI, G., DE ROSSI, D., DARIO, P., and DOMENICI, C.: 'Multisensor piezoelectric polymer sole for pedobarography', *Ferroelectrics*, 1984, 60, pp. 163-174
- 3 PERUCHON, E., JULLIAN, J.M., and RABISCHONG, P.: 'Wearable unrestraining footprint analysis system: applications to human gait study', *Med. Biol. Eng. Comput.*, 1989, 27, pp. 557-565
- 4 TAPPIN, J.W., POLLARD, J., and BECKETT, E.A.: 'Methods of measuring "shearing forces on the sole of the foot"', *Clin. Phys. Physiol. Meas.*, 1980, 1, (1), pp. 83-85
- 5 POLLARD, J.P., LE QUESNE, L.P., and TAPPIN, J.W.: 'Forces under the foot', *J. Biomed. Eng.*, 1983, 5, pp. 39-42
- 6 TAPPIN, J.W., and ROBERTSON, K.P.: 'Study of the relative timing of shear forces on the sole of the forefoot during walking', *J. Biomed. Eng.* 1991, 13, pp. 37-40

